TÉCNICO LISBOA

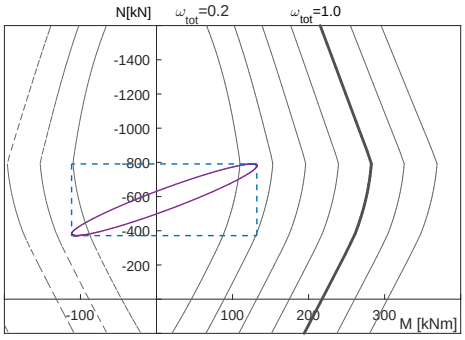

Seismic Analysis of Structures: Stress-resultant Interaction based on Response Spectra

Ana Rita Graça Tomaz

Thesis to obtain the Master of Science Degree in

Civil Engineering

Supervisor(s): Prof. Manuel da Cunha Ritto Corrêa
Prof. Luís Manuel Coelho Guerreiro

Examination Committee

Chairperson: Prof. António Manuel Figueiredo Pinto da Costa
Supervisor: Prof. Manuel da Cunha Ritto Corrêa
Member of the Committee: Jorge Miguel Silveira Filipe Mascarenhas Proença

June 2017

Acknowledgments

The author would like to thank her supervisors: Prof. Manuel Corrêa and Prof. Luís Guerreiro for their guidance and endless dedication during the development of this work.

She acknowledges the support of her parents during the past six years, in particular when changing her course, and sends a special thanks to her sister, to be delivered in Poland.

She would like to thank everyone that was part of her academic journey, in particular Samuel, Rafa, Vargas, my fellow civil girls: Rita, Sofia, Teresa and Carolina and finally my two best friends Isabel and Isabel.

Resumo

O propósito desta dissertação é explorar uma metodologia que caracterize a resposta das estruturas a excitações dinâmicas de forma mais precisa e menos conservativa que a presentemente utilizada na aplicação dos regulamentos em vigor.

Para dimensionar uma secção de betão armado é necessário quantificar um conjunto de variáveis como o esforço normal, momentos fletores ou deslocamentos. O método estudado determina a superfície de interação entre essas variáveis que pode ser sobreposta à superfície de capacidade resistente da secção, permitindo otimizar o seu dimensionamento.

A informação necessária para aplicar o método é calculada de forma rotineira nas usuais análises modais, as quais utilizam espectros de resposta para obter a resposta em cada modo de vibração e um critério de combinação modal para obter um valor final (máximo) de cada variável. Alternativamente a admitir a simultaneidade dos valores máximos é computacionalmente possível avaliar a correlação entre variáveis em cada modo, calculando a sua superfície de interação.

Para além de ser um problema teórico interessante, tem também claras aplicações no dimensionamento de pilares sujeitos a flexão composta ou desviada, podendo levar a reduções significativas das taxas de armadura, permitindo uma economia de materiais sem comprometer a segurança estrutural.

Acresce que o princípio de estabelecer correlações de variáveis em cada modo, construindo superfícies de interação finais, pode ser aplicado em diferentes contextos como o dimensionamento de sapatas conjuntas ou o estabelecimento de análises estáticas equivalentes. Estes exemplos serão estudados em detalhe por não serem usualmente abordados na literatura especializada.

Palavras-chave: Análise Sísmica, Métodos de Combinação Modal, Interação de Esforços, Fundações, Análise Estática Equivalente

Abstract

The focus of this dissertation is to explore a methodology that characterizes a structure response to a dynamic excitation more accurately and less conservatively than the one currently adopted in the application of design codes.

To design a reinforced concrete section requires a set of variables such as the axial force, bending moments or displacements. The studied method produces a surface that reproduces the interactions between those variables which can be superimposed to the capacity curve of that section to optimize its design.

The method input is routinely calculated in the typical modal analysis that resorts to response spectra to characterize each mode response and then uses a combination criteria to obtain the final (maximum) value of each variable. Instead of assuming the simultaneity of all the variables maximum values it is computationally possible to evaluate the correlation between variables, calculating their final interaction surface.

Besides being an interesting theoretical problem it has clear applications in the design of columns subjected to a combination of axial force with a single or two bending moments, leading to significant reductions of steel reinforcement ratios, allowing a material economy without compromising the structural safety.

Furthermore, the principle of establishing correlations of variables in each mode and constructing a final interaction surface can be applied in different contexts such as the design of combined footings or devising equivalent static analysis. These examples will be detailed as they are not commonly addressed in the specialized literature.

Keywords: Seismic Analysis, Modal Combination Methods, Stress-resultant Interaction, Foundations, Equivalent Static Analysis

Contents

List of Tables

List of Figures

Nomenclature

Greek symbols

α, β	Counterclockwise angles in a 3D domain.
$\mathbf{\Phi}$	Normalized vibration mode matrix.
χ	Curvature.
η	Damping correction factor.
γ_I	Importance factor of the structure.
μ	Reduced bending moment.
ν	Reduced axial force.
Φ	Normalized vibration mode.
ψ	Interpolation function.
σ	Material stress.
σ_{max}	Maximum soil stress.
θ	Counterclockwise angle in a 2D domain.
ε_{c2}	Compressive strain transition value in the parabolic-rectangle diagram of concrete.
ε_{cu2}	Compressive ultimate strain transition value in the parabolic-rectangle diagram of concrete.
ε_g	Strain at the section's geometrical center.
ε_{ud}	Design ultimate strain for steel.
ε_{yd}	Design yielding strain for steel.
ξ	Viscous damping coefficient.

Roman symbols

$\mathbf{1_k}$	Unitary vector of freedom degrees aligned with the earthquake direction k.
$\mathbf{P}$	Sub-part of the interaction matrix.

$\mathbf{V}$ Vibration mode shape matrix.

$\mathbf{X}$ Interaction matrix.

$\mathbf{x_f}$ Vector with the realization of each variable after the modal combination.

$\mathbf{x_i}$ Vector with the realization of each variable in mode i.

$\mathbf{Y}$ Interaction matrix defined in principal coordinates.

$\ddot{q}$ Acceleration.

$\dot{q}$ Velocity.

A Area of the cross-section.

E Young's modulus.

f Cyclic frequency.

f_{cd} Design value of concrete compressive strength .

f_{yd} Design yield strength of reinforcement.

G Shear Modulus.

h_c Auxiliary compressed concrete height.

I Inertia of the cross-section.

J Torsional constant of the cross-section.

L Length of the element

M Bending moment.

m_{eff} Effective modal mass.

N Axial force.

N Number of freedom degrees.

n Number of relevant modes.

P Modal participation factor.

p Angular frequency.

q Behavior factor.

q Relative soil-structure displacement.

q_s Soil displacement.

q_t Total displacement.

S_d Design spectral acceleration.

T Torsional moment.

T Vibration period.

V Shear force.

v Vibration mode shape.

w_{tot} Total percentage of reinforcement.

x_t Projection of $\mathbf{x_i}$ in a unit vector of generic orientation.

x_{NA} Position of the neutral axis.

$\mathbf{A}$ Transformation of coordinates matrix.

$\mathbf{C}$ Damping matrix.

$\mathbf{d}$ Displacement vector.

$\mathbf{f}$ Force vector.

$\mathbf{f_{ext}}$ Exterior force vector.

$\mathbf{f_{fix}}$ Equivalent node force vector.

$\mathbf{K}$ Stiffness matrix.

$\mathbf{M}$ Consistent-mass matrix.

$\mathbf{u}$ Deformed shape vector.

Subscripts

f Footing subdivision index.

i Mode index.

k Direction index.

x, y, z Earthquake directions.

G Normalized variable.

Superscripts

e Element referential.

g Global referential.

T Transpose.

Chapter 1

Introduction

The violence of seismic events, such as the one that devastated Lisbon in 1755, motivated the study of original structural mechanisms to resist such ground motions, as the "gaiola pombalina" system implemented at that date, and kept the scientific community interested ever since.

Nowadays, structural designers are assisted by computational programs that model structures, calculate stress-resultants and perform dynamic analysis in short periods of time. These programs simulate seismic events and its effects on structures with great detail, producing large amounts of data. The challenge is now to interpret all this data in physically coherent ways, allowing it to assist the design process. The motivation for this dissertation is to use the information normally calculated in dynamic analysis and use it to construct interaction envelopes, which is a less conservative approach than the one currently applied.

Considering the design of a column cross-section, it is common practice to perform modal analysis based on response spectra and then combine the modal response values to calculate the design value of any variable. These values are the maximum peak values of each variable, which typically are axial forces and bending moments.

Performing the cross-section design considering the most unfavorable combination is overly conservative as these stress-resultants are co-dependent. One way to express their correlation is through an interaction envelope: a geometrical representation of all the viable combinations of stress-resultants.

The increased computational effort to generate these envelopes is compensated with the resultant material economy, which does not compromise the structural safety.

Besides the application to the design of cross-sections, this idea of interaction envelopes can be applied in different design contexts. There is already some research that implements this with displacements to perform serviceability limit state verification. This dissertation will focus on yet two other applications: combined footings and devising equivalent static analysis. In both situations, interaction envelopes are constructed. The first correlates the stress-resultants of the two columns that share a combined footing. As for the second, the correlation of the shear forces and torsional moments is used to quantify a set of equivalent static forces.

1.1 Dissertation Outline

This dissertation is organized in seven Chapters with the following content:

Chapter 2 - Background: Brief presentation of the main publications written about the subjects: modal analysis, combination methods (ABS, SRSS and CQC), interaction surfaces.

Chapter 3 - Structural Analysis: Introduction of the methods used for the static and dynamic analysis. Definition of the earthquake properties according to the response spectra method. Description of the structural modeling.

Chapter 4 - Response Interaction Envelopes: Theoretical derivation of the interaction envelopes. Detailed explanation of three methods to construct the envelopes: Intersection, Divider and Equation methods. Application to simple 2D and 3D examples. Introduction to the equivalent static analysis.

Chapter 5 - Resistant Interaction Surfaces: Review on the construction of capacity surfaces for reinforced concrete cross-sections: the 2D and 3D case. Detailed explanation of the action and resistant interaction envelopes for combined footings.

Chapter 6 - Results and Discussion: Detailed analysis of three practical examples. The first approaches the design of a 2D structure and its static equivalent analysis. The second concerns a simple 3D structure with the purpose of studying the relevance of the CQC combination method. Finally, the last example focuses on the design of a few columns and a combined footing in a 3D structure. The equivalent static analysis is generalized to 3D.

Chapter 7 - Conclusion: Summarizes the main topics discussed previously and suggests possible further research.

Chapter 2

Background

The motivation for the present dissertation is the work developed by Menun and Der Kiureghian [1] and [2]: *Envelopes for seismic response vectors*, in which it is described a method for an accurate evaluation of interaction surfaces for earthquake-induced stress-resultants. The underlying idea is to properly consider the interactions between the stress-resultants in all the linear structural analysis made for a 3D structure: for the number n of relevant modes and for the $k = 3$ possible seismic directions. Each of these analyses applies the response spectra method which is largely used and recommended by the design codes, see Eurocode 8 [3]. This method provides the peak value of the desired response quantity such as a displacement, a bending moment, an axial force or even a normal stress, σ. However, for most design situations more than one quantity is necessary, for example: when a column is subjected to an axial force and bending moment (N and M) or bi-axial bending moments (N, M_2, M_3); or even when we want to control bi-directional inter-story drifts. The widely used approach in these cases is to combine the maximum value of each quantity, which can be overly conservative as the maximum values do not occur all at the same time. This motivated the study of the interactions between any set of variables necessary for design.

With the purpose of combining modal analyses, it is customary to use the CQC combination, developed by Der Kiureghian [4]. The principal advantage of this method is that it takes into account the relation between the modes frequencies. Thus, it is not necessary to choose one of the limit cases: equal frequencies (ABS combination) or well-separated ones (SRSS combination). The method is based on the statistic analysis of stationary Gaussian processes, through its auto-correlation function, see Azevedo [5]. Applying a Fourier transform to this function we obtain a power spectral density function and their related spectral moments. For multi-degree systems, we have both spectral moments and cross-spectral moments and from the relations of those, a correlation coefficient can be deduced. This is the theoretical base of the CQC combination.

For the combination of seismic directions, there is not an established method, but rather a series of possible ones permitted by the codes. Based on Penzien and Watabe [6] the seismic input during its strong motion phase can be considered as three ground motion components that are simultaneous, statistically non-correlated, and whose orientation remains stable over time. The system of principal

axes is defined with a vertical and two orthogonal horizontal ones, where the major principal axis is directed to the epicenter. This originates the idea of the percentage rules, that calculate each variable as a sum of 100% of that response resulting from the major direction and a percentage of the responses on the other two directions. The most common of these empirical rules are the 100-30 and the 100-40. However, this overlooks an important aspect: the orientation of the ground motion axes is, in general, different from the principal system of axes of the structure. Furthermore, the orientation θ of the ground motion axes is unknown. For this reason, Wilson et al. [7] (or [8]) arguments that an SRSS rule is preferable as it considers the totality of the response in both horizontal axes, producing a result that does not depend on the selected system of axes and has equal resistance to a seismic input from any direction. For the vertical component, it is common to use 2/3 of the horizontal ones. Further research on this topic has been conducted by Menun and Der Kiureghian [9] that developed a method called CQC3. This procedure takes into account the influence of orientation θ allowing to use relative intensities of the components of the ground motion, through the use of a constant $0 < \gamma < 1$ that multiplies the major principle direction when evaluating the others. It also provides an expression for the critical orientation, θ_{cr} that corresponds to the maximum value of a given variable. We remark that the previous methods are particular cases of this one, for example, the SRSS rule results of defining $\gamma = 1$. We reiterate that this is not a closed topic as some codes still enforce the use of simpler combinations and they find support among some researchers, see Hernandez and Lopez [10] and Menun and Der Kiureghian [11].

Returning to the main focus of this work, after choosing the combination methods for the modes and directions, we have evaluated several quantities and defining their maximum values. The next design phase is to plot the interaction surface involving those quantities (normally stress-resultants) and overlaying it to a resistant capacity surface for the cross-section. For reinforced concrete sections the design is based on axial force and bending interaction diagrams. We remark that the critical combination of a set of values on the interaction surface can not be determined without the knowledge of the resistant capacity surface. In fact, the critical combination does not necessarily include the maximum value of any of the variables, as it is the one closest to the capacity surface.

The work of Sessa et al. [12] follows this idea and focuses on calculating a parameter λ that multiplies each point of the interaction surface so that it becomes tangent to the capacity surface. If all the values λ are greater than the unity then the safety of the section is checked.

Gupta and Singh [13] (or Gupta [14]) detailed the nature of the interaction surfaces constructed for a chosen set of design variables. It is proven that for two variables, as N and M in a column section, the result is an ellipse. For $n > 2$ this entity is a hyper-ellipsoid in a n-coordinate space where each point represents a set of simultaneous seismic response values. As the structures are also subjected to static loads the center of these elliptical envelopes must be shifted to include this effect. Finally, the interaction surface is completely defined and can be used for design. Being completely inscribed in a resistant capacity surface guarantees the section safety.

We have been looking at design methods based on pairs of stress-resultants, nonetheless there are more possibilities. Leblond [15] addressed the problem from the axial stress point of view. The idea is to combine the modal values of $N = \sqrt{\sum {N_i}^2}$ and $M = \sqrt{\sum {M_i}^2}$ to calculate $\sigma = \frac{N}{S} + \frac{Mv}{I}$. However, this

is not equal to calculate $\sigma = \sqrt{\sum {\sigma_i}^2}$ with σ_i evaluated in each mode by $\sigma_i = \frac{N_i}{S} + \frac{M_i v}{I}$. Actually the first combination overestimates the possible combinations of $M - N$. So by leaving N and M as variables and equaling $\frac{N}{S} + \frac{Mv}{I} = \sqrt{\sum \left(\frac{N_i}{S} + \frac{M_i v}{I}\right)^2}$ we have the equation of the interaction surface.

Alternatively, Menun [16] focused on the Mohr's circle which is a representation of the normal and shear stresses that act on any inclined plane of an infinitesimal element in plane stress. Taking into account the relations between σ_x, σ_y and τ in every mode it is possible to construct a correlation matrix and plot an interaction surface. By doing this for every possible orientation of the inclined plane the result is the so-called E_{Mohr} envelope. This includes all possible Mohr's circles during an earthquake, with the correspondent changes of radius and center. This envelope is developed for a three-dimensional infinitesimal element in Menun [17] and compared to the existent Mohr rupture diagram for reinforced concrete.

Some research has been done in order to simplify the security checks by choosing a set of points of the interaction surface and not the totality of them to be subjected to verification. The work of Panetsos and Anastassiadis [18] studies four alternatives to chose the "most unfavorable" combinations of two variables (N and M). The first is the "extreme values of all forces" method which describes a rectangle in the coordinate space ($M - N$) and is a procedure commonly applied. The second is the "extreme force" method, which chooses one variable at its maximum and the corresponding value of the other variable in the interaction surface. This produces four combinations, as the maximums can be either positive or negative. The third is the "extreme stress" method where we defined a maximum axial stress σ and calculate the correspondent pairs of ($M - N$) which are four points of the interaction surface. Finally the fourth is Gupta's method [14] which describes an octagon tangent to the surface. In Panetsos' study, the differences in the reinforcement area can be as impressive as 54%, which reiterates the importance of such investigations. The authors continued the study to ground motion directions with different intensities in Panetsos and Anastassiadis [19]. A similar procedure is developed by Erlicher et al. [20] for combinations of 3 variables, which corresponds to a polyhedron in a 3D coordinate system that can have different shapes and number of vertices. Also in this paper is developed an equivalent static analysis as an alternative to the modal combination.

It should be noted that the response spectra method, discussed until this point, presents an approximation for the maximum peak values of displacements and forces but with some limitations. For instance, it can only be applied in linear elastic analyses, to four different soil types and with a poor estimation of the damping properties of the structure. It is possible to construct a response spectrum specific to a certain location, including the local soil conditions and the distance to the nearest faults. However, there is no adaptation to the method that makes it suitable to estimate the non-linear behavior of the structures. This is why Tokoro and Menum [21] developed a procedure to calculate the interaction surface based on a modal pushover analysis. Although not as accurate as the existing response spectra, this allows estimating an envelope for structural systems possessing material non-linearities. The accuracy of the results is compared to a time-history analysis, which is a common practice in these studies. Also, Ferreira [22] and Belejo [23] worked with linear dynamic analysis on the frequency domain.

It is apparent from this that vast research and study is being conducted in this field. The use of

interaction surfaces to describe the seismic action uses the same quantities needed to perform the regular calculations (stress-resultants and frequencies of each mode) and does not require any special computational power. Despite its advantages by allowing a considerable economy of material it is still not present in the codes, taught in universities or used in most design companies.

In this dissertation we intend to explore the construction of the interaction envelopes, using not only the method presented in [1] but also new ones that allow the display of the envelopes constructed with different mode combinations. This will be done for both 2D and 3D structures, and for the later envelopes, of complex visualization, will be developed auxiliary representation methods. At the same time, the capacity curves will be computed allowing an optimization of the design for a given element.

Chapter 3

Structural Analysis

This introductory chapter has the purpose of introducing the methods used to perform the static and dynamic analysis needed to evaluate displacements and stress-resultants. When calculating the interaction diagrams, both analyses are necessary as the dynamic response is centered at the static point. The main concepts of these methods will be presented and detailed here, for a more complete exposition see Clough and Penzien [24] and Freitas and Tiago [25].

Moreover, this chapter will address the modeling of the structure. It must be stressed out that all the computation work developed was implemented as a Matlab program [26].

3.1 Static Analysis

This introductory section has the purpose of introducing the Displacement Method for calculating stress-resultants and the type of elements used for modeling a structure.

Beginning with the latter, the 3D structures are discretized in linear elements, such as the one in Figure 3.1, to simulate columns and beams. The slabs will not be introduced as 2D elements, but rather as loads applied to the beams, simplifying the model.

The generalized displacements (translations or rotations) of each degree of freedom in the element own referential are grouped in a 12 element vector, $\boldsymbol{d^e}$.

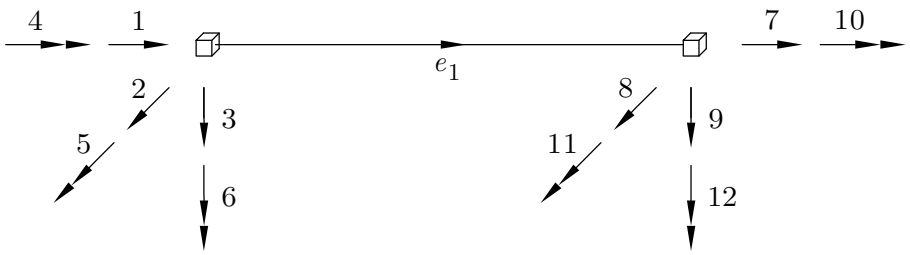

Figure 3.1: Numbering of the freedom degrees and sign convention of the 3D Element.

Each of these elements has an orientation in space defined by three unit vectors: e_1 parallel to the

bar, $\boldsymbol{e_2}$ defined by the user and $\boldsymbol{e_3}$ is calculated by $\boldsymbol{e_3} = \boldsymbol{e_1} \times \boldsymbol{e_2}$.

These unit vectors are illustrated in Figure 3.2 for common elements like columns and beams and are also presented the global unit vectors, $\boldsymbol{g_i}$.

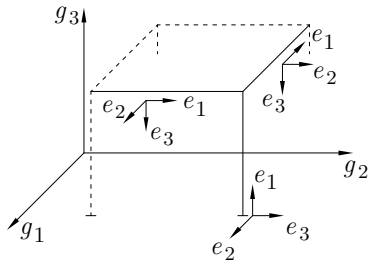

Figure 3.2: Unit vectors $\boldsymbol{e_i}$ and $\boldsymbol{g_i}$.

The relation between these unit vectors is described by a matrix $\boldsymbol{\Lambda}$:

$$\begin{bmatrix} \boldsymbol{e_1} \\ \boldsymbol{e_2} \\ \boldsymbol{e_3} \end{bmatrix} = \begin{bmatrix} \\ \boldsymbol{\Lambda} \\ \\ \end{bmatrix} \begin{bmatrix} \boldsymbol{g_1} \\ \boldsymbol{g_2} \\ \boldsymbol{g_3} \end{bmatrix} \quad \text{with,} \quad \Lambda_{ij} = \cos(\boldsymbol{e_i}, \boldsymbol{g_j}) \tag{3.1}$$

Any three-component vector, $\boldsymbol{v}$, can be written in the either form:

$$\boldsymbol{v} = \sum_{i=1}^{3} {v_i}^e \boldsymbol{e}_i = \sum_{i=1}^{3} {v_i}^g \boldsymbol{g}_i \tag{3.2}$$

Resorting to the matrix $\boldsymbol{\Lambda}$:

$$\begin{bmatrix} {v_1}^e & {v_2}^e & {v_3}^e \end{bmatrix} \begin{bmatrix} \boldsymbol{e_1} \\ \boldsymbol{e_2} \\ \boldsymbol{e_3} \end{bmatrix} = \begin{bmatrix} {v_1}^e & {v_2}^e & {v_3}^e \end{bmatrix} \begin{bmatrix} \\ \boldsymbol{\Lambda} \\ \\ \end{bmatrix} \begin{bmatrix} \boldsymbol{g_1} \\ \boldsymbol{g_2} \\ \boldsymbol{g_3} \end{bmatrix} = \begin{bmatrix} {v_1}^g & {v_2}^g & {v_3}^g \end{bmatrix} \begin{bmatrix} \boldsymbol{g_1} \\ \boldsymbol{g_2} \\ \boldsymbol{g_3} \end{bmatrix} \tag{3.3}$$

Finally, we get:

$$\begin{aligned} {v_i}^g &= \boldsymbol{\Lambda}^T {v_i}^e \\ {v_i}^e &= \boldsymbol{\Lambda}^{-T} {v_i}^g \quad \Leftrightarrow \quad {v_i}^e = \boldsymbol{\Lambda} {v_i}^g \end{aligned} \tag{3.4}$$

Equation (3.4) implies that the transpose matrix $\boldsymbol{\Lambda}$ is equal to its inverse ($\boldsymbol{\Lambda}^T = \boldsymbol{\Lambda}^{-1}$). The vector with the nodal displacements, $\boldsymbol{d}^e$, is formed by four individual ones with a similar behavior to $\boldsymbol{v}$. As such the referential transformations are ruled by a similar formula:

$$\boldsymbol{d}^e = \boldsymbol{A}^e \boldsymbol{d}^g \quad \Leftrightarrow \quad \begin{bmatrix} \\ \boldsymbol{d}^e \\ \\ \end{bmatrix} = \left[\begin{array}{cc|cc} \boldsymbol{\Lambda} & \boldsymbol{0} & \multicolumn{2}{c}{\multirow{2}{*}{$\boldsymbol{0}$}} \\ \boldsymbol{0} & \boldsymbol{\Lambda} & & \\ \hline \multicolumn{2}{c|}{\multirow{2}{*}{$\boldsymbol{0}$}} & \boldsymbol{\Lambda} & \boldsymbol{0} \\ & & \boldsymbol{0} & \boldsymbol{\Lambda} \end{array}\right] \begin{bmatrix} \\ \boldsymbol{d}^g \\ \\ \end{bmatrix} \tag{3.5}$$

In this equation $\boldsymbol{A}^e$ is a 12×12 matrix, formed by the matrices $\boldsymbol{\Lambda}$ in the diagonal blocks and zeros in the remaining blocks. The stiffness matrix $\boldsymbol{K}^e$ is presented below:

$$\boldsymbol{K}^e = \left[\begin{array}{cccccc:cccccc}
\frac{EA}{L} & 0 & 0 & 0 & 0 & 0 & \frac{-EA}{L} & 0 & 0 & 0 & 0 & 0 \\
 & \frac{12EI_3}{L^3} & 0 & 0 & 0 & \frac{6EI_3}{L^2} & 0 & \frac{-12EI_3}{L^3} & 0 & 0 & 0 & \frac{6EI_3}{L^2} \\
 & & \frac{12EI_2}{L^3} & 0 & \frac{-6EI_2}{L^2} & 0 & 0 & 0 & \frac{-12EI_2}{L^3} & 0 & \frac{-6EI_2}{L^2} & 0 \\
\hdashline
 & & & \frac{GJ}{L} & 0 & 0 & 0 & 0 & 0 & \frac{-GJ}{L} & 0 & 0 \\
 & & & & \frac{4EI_2}{L} & 0 & 0 & 0 & \frac{6EI_2}{L^2} & 0 & \frac{2EI_2}{L} & 0 \\
 & & & & & \frac{4EI_3}{L} & 0 & \frac{-6EI_3}{L^2} & 0 & 0 & 0 & \frac{2EI_3}{L} \\
\hdashline
 & & & & & & \frac{EA}{L} & 0 & 0 & 0 & 0 & 0 \\
 & & & & & & & \frac{12EI_3}{L^3} & 0 & 0 & 0 & \frac{-6EI_3}{L^2} \\
 & & & & & & & & \frac{12EI_2}{L^3} & 0 & \frac{6EI_2}{L^2} & 0 \\
\hdashline
 & & & & & & & & & \frac{GJ}{L} & 0 & 0 \\
 & \text{Sym.} & & & & & & & & & \frac{4EI_2}{L} & 0 \\
 & & & & & & & & & & & \frac{4EI_3}{L}
\end{array}\right] \tag{3.6}$$

Where L is the element length, E and G are the material Young's modulus and the shear modulus, respectively. The remaining quantities: A, I_2, I_3, and J are the area, moments of inertia and torsional constant of the element cross-section. For the torsional constant the approximate formula, valid for rectangular sections, $J = [\frac{1}{3} - 0.21(\frac{b}{a}) + 0.0176(\frac{b}{a})^5]ab^3$ was used, where a is the maximum side of the rectangular column and b is the minimum.

The equivalent nodal force vector, ${\boldsymbol{f_{fix}}}^e$, is required to balance the loads acting on the element. For simplicity we only considered uniform loads distributed along the element length, both forces (p) acting according to $\boldsymbol{e_3}$ or moments (m) about $\boldsymbol{e_1}$. The ${\boldsymbol{f_{fix}}}^e$ vector of this 3D element is:

$${\boldsymbol{f_{fix}}}^e = \left[0, 0, -\frac{pL}{2}, -\frac{mL}{2}, \frac{pL^2}{12}, 0, 0, 0, -\frac{pL}{2}, -\frac{mL}{2}, -\frac{pL^2}{12}, 0\right]^T \tag{3.7}$$

Combining equation (3.5): $\boldsymbol{d}^e = \boldsymbol{A}^e \boldsymbol{d}^g$ with the relation between applied forces and displacements given by: $\boldsymbol{K}^e \boldsymbol{d}^e = \boldsymbol{f}^e$, we conclude that $\boldsymbol{K}^e \boldsymbol{A}^e \boldsymbol{d}^g = \boldsymbol{f}^e$. Also having the transformation of coordinates written for the force vector $\boldsymbol{f}^g = \boldsymbol{A}^{eT} \boldsymbol{f}^e$ it is possible to conclude that:

$$\boldsymbol{f}^g = \left(\boldsymbol{A}^{eT} \boldsymbol{K}^e \boldsymbol{A}^e\right) \boldsymbol{d}^g \quad \Leftrightarrow \quad \boldsymbol{K}^g = \boldsymbol{A}^{eT} \boldsymbol{K}^e \boldsymbol{A}^e \tag{3.8}$$

A different stiffness matrix must be defined for the structure as a whole, $\boldsymbol{K}$. The structure has a maximum of six freedom degrees for each node, three translations and three rotations. It should be noted that some nodes have boundary conditions, and for that reason less than six freedom-degrees, and also that one node may have several confluent elements whose individual responses should be added. Setting a counter for the effective degrees of freedom of the structure we reach the dimension of the $\boldsymbol{K}$ matrix: $N \times N$. Each entry is the sum of the several confluent terms of $\boldsymbol{K}^g$ which are already defined in a global referential. The same procedure is applied to the equivalent nodal force vector and to

the exterior force vector, $\boldsymbol{f_{ext}}$, that includes the concentrated forces directly applied to the nodes. This can be translated by the assembly operator in the equations below:

$$\boldsymbol{K} = \bigwedge_{e=1}^{n} \boldsymbol{A^{eT} K^e A^e} \quad ; \quad \boldsymbol{f} = \bigwedge_{e=1}^{n} \boldsymbol{A^{eT} f^e} \tag{3.9}$$

With these quantities, the method equation that guarantees the equilibrium of each node in the structure degrees of freedom is given by:

$$\boldsymbol{d} = \boldsymbol{K}^{-1}(\boldsymbol{f_{ext}} - \boldsymbol{f_{fix}}) \tag{3.10}$$

Taking the vector $\boldsymbol{d}$ and reversing the transformation in order to get the displacements of each bar in its 1×12 dimension we obtain the vector $\boldsymbol{d}^g$, which can be converted into the bar referential, $\boldsymbol{d}^e$, and then used to compute the nodal forces.

$$\boldsymbol{f}^e = \boldsymbol{K}^e \boldsymbol{d}^e + \boldsymbol{f_{fix}}^e \tag{3.11}$$

Having the forces and displacements in the elements degrees of freedom we can calculate the stress-resultants using equation (3.12) in any section of a bar, varying x from 0 to L:

$$\begin{aligned} &N(x) = -{f_1}^e \quad ; \quad V_3(x) = -{f_3}^e - p\,x \quad ; \quad M_2(x) = -{f_5}^e - x{f_3}^e - \frac{px^2}{2} + m\,x \\ &T(x) = -{f_4}^e \quad ; \quad V_2(x) = -{f_2}^e \quad ; \quad M_3(x) = -{f_6}^e + x{f_2}^e \end{aligned} \tag{3.12}$$

The deformed shape can also be written as a three component vector, $\boldsymbol{u}$, using the interpolation functions ψ_i that correspond to the exact solution without regarding the applied loads.

$$\begin{bmatrix} u_1 \\ u_2 \\ u_3 \end{bmatrix} = \left[\begin{array}{cccccc:cccccc} \psi_1 & 0 & 0 & 0 & 0 & 0 & \psi_7 & 0 & 0 & 0 & 0 & 0 \\ 0 & \psi_2 & 0 & 0 & 0 & \psi_6 & 0 & \psi_8 & 0 & 0 & 0 & \psi_{12} \\ 0 & 0 & \psi_3 & 0 & \psi_5 & 0 & 0 & 0 & \psi_9 & 0 & \psi_{11} & 0 \end{array}\right] \begin{bmatrix} {d_1}^e \\ {d_2}^e \\ \vdots \\ {d_{12}}^e \end{bmatrix} \tag{3.13}$$

where the interpolation functions ψ_i are the following (the absence of ψ_4 and ψ_{10} in $\boldsymbol{u}$ will be explained later):

$$\begin{cases} \psi_1(x) = \psi_4(x) = 1 - \frac{x}{L} \\ \psi_2(x) = \psi_3(x) = -1 + 3\frac{x^2}{L^2} - 2\frac{x^3}{L^3} \\ \psi_5(x) = \psi_6(x) = -x + 2\frac{x^2}{L} - \frac{x^3}{L^2} \\ \psi_7(x) = \psi_{10}(x) = \frac{x}{L} \\ \psi_8(x) = \psi_9(x) = -3\frac{x^2}{L^2} + 2\frac{x^3}{L^3} \\ \psi_{11}(x) = \psi_{12}(x) = \frac{x^2}{L} - \frac{x^3}{L^2} \end{cases} \tag{3.14}$$

To include the loads effect we add to u_3 the term $\frac{p}{EI_2}(\frac{x^4}{24} - \frac{x^3 L}{12} + \frac{x^2 L^2}{24})$.

3.2 Structural Dynamics

With a structural dynamic analysis, we intend to evaluate the displacements and stress-resultants of a structure when it is submitted to a dynamic load, such as an earthquake, an explosion or other softer vibrations.

The dynamic equation of equilibrium for a seismic action can be written as a forced regime equation, where the applied force is in fact a part of the inertial force generated by the earthquake related to $\ddot{\boldsymbol{q}}_{\boldsymbol{s}}$, the soil acceleration defined below. In a 3D structure with multiple degrees of freedom this equation is given in a matrix form by:

$$\boldsymbol{M}\ddot{\boldsymbol{q}} + \boldsymbol{C}\dot{\boldsymbol{q}} + \boldsymbol{K}\boldsymbol{q} = -\boldsymbol{M}\ddot{\boldsymbol{q}}_{\boldsymbol{s}} \tag{3.15}$$

where $\boldsymbol{q}$ is the vector of the relative displacements between the soil and the structure, $\boldsymbol{q_s}$ is directly the soil displacement and the sum of the two $\boldsymbol{q_t} = \boldsymbol{q} + \boldsymbol{q_s}$ is the vector with the total displacements of the structure. In order to apply this equation, we need to define the mass, damping and stiffness matrices.

The $\boldsymbol{K}$ is equal to the one previously defined for the static analysis and the damping matrix will only be detailed further ahead. We present here the 3D element consistent-mass matrix:

$$\boldsymbol{M}^e = \frac{pL}{420g} \times \left[\begin{array}{ccc:ccc:ccc:ccc} 140 & 0 & 0 & 0 & 0 & 0 & 70 & 0 & 0 & 0 & 0 & 0 \\ & 156 & 0 & 0 & 0 & 22L & 0 & 54 & 0 & 0 & 0 & 13L \\ & & 156 & 0 & -22L & 0 & 0 & 0 & 54 & 0 & -13L & 0 \\ \hdashline & & & 0 & 0 & 0 & 0 & 0 & 0 & 0 & 0 & 0 \\ & & & & 4L^2 & 0 & 0 & 0 & 13L & 0 & -3L^2 & 0 \\ & & & & & 4L^2 & 0 & -13L & 0 & 0 & 0 & -3L^2 \\ \hdashline & & & & & & 140 & 0 & 0 & 0 & 0 & 0 \\ & & & & & & & 156 & 0 & 0 & 0 & -22L \\ & & & & & & & & 156 & 0 & 22L & 0 \\ \hdashline & & & & & & & & & 0 & 0 & 0 \\ & \text{Sym.} & & & & & & & & & 4L^2 & 0 \\ & & & & & & & & & & & 4L^2 \end{array}\right] \tag{3.16}$$

where p is the uniform load distributed linearly on the element and g is the acceleration of gravity.

The consistent-mass matrix is a different concept from the lumped-mass matrix, which only places mass in the freedom degrees associated with displacements. To construct the consistent-mass matrix we use interpolation functions and the Finite Element Method.

As the element can bend in two orthogonal directions, we have two identical sets of four interpolations functions, ψ, associated with bending, plus two related to the axial force. We will not consider the torsion functions, resulting in the null lines and columns (numbers 4 and 10). $\boldsymbol{M}^e$ being a singular matrix will not be a computational problem because we will actually only need to invert the structure combined matrix, $\boldsymbol{M}$, which is nonsingular. To calculate each entry of the combined matrix, associated with each nodes freedom degrees, we add the individual matrices of all the convergent elements in that node. In

the examples used all the nodes have at least one bar with loads applied. Thus, the matrix $\boldsymbol{M}$ will not be singular.

Each interpolation function ψ is assigned to the plane that contains its deformed shape (x, y or, z) forming a vector. For example, if $\boldsymbol{\psi_i}$ produces a deformed shape in the y plane, then $\boldsymbol{\psi_i} = [0\ ,\ \psi_i\ ,\ 0]$. Mixing functions of different directions produces a null entry in the mass matrix, for instance the term M_{25}. This is explicit in equation (3.17).

The integration is only made in the x coordinate, assuming the dimensions in the other directions are smaller and constant. This approximation takes into account that the uniformly distributed mass is not in fact just the mass of the element as it includes the slab weight and the live loads. These loads should not be mixed in the evaluation of the elements torsional effects. With this approximation, we assume that all the mass is concentrated on the bar axis and no integration in the other directions is needed.

$$M_{ij}{}^{e} = \int_0^L m(x)\boldsymbol{\psi_i} \cdot \boldsymbol{\psi_j} \mathrm{d}x \tag{3.17}$$

As an example, we detail the calculation of a non-null entry:

$$\begin{aligned} M_{26}{}^{e} &= \int_0^L m(x)\psi_2(x)\psi_6(x)\mathrm{d}x \\ M_{26}{}^{e} &= \int_0^L m(x)(-1+\frac{3x^2}{L^2}-\frac{2x^3}{L^3})(-x+\frac{x^2}{L}-\frac{x^3}{L^2})\mathrm{d}x \\ M_{26}{}^{e} &= m\frac{11L^2}{210} = \frac{pL}{420g}22L \end{aligned} \tag{3.18}$$

Finally, we calculate the structure global matrix $\boldsymbol{M}$ in the same way we did for $\boldsymbol{K}$, assembling all the elements contributions.

3.2.1 Modal Analysis

The $\boldsymbol{K}$ and $\boldsymbol{M}$ matrices are necessary to calculate some properties of the structure: frequencies and vibration mode shapes. This calculation is done with the dynamic equilibrium equation in the free regime and without damping, which is obtained from simplifying equation (3.15):

$$\boldsymbol{M\ddot{q}} + \boldsymbol{Kq} = \boldsymbol{0} \tag{3.19}$$

Assuming that the structure will have a harmonic behavior, it is described by $\boldsymbol{q(t)} = \boldsymbol{v}\ \cos(pt-\theta)$, where the vector $\boldsymbol{v}$ describes the configuration of each vibration mode, p is its frequency and θ adjusts the phase of the response. Differentiating two times we get: $\boldsymbol{\ddot{q}(t)} = -p^2\ \boldsymbol{v}\ \cos(pt-\theta)$ and can then rearrange the previous equation into:

$$(\boldsymbol{K} - p^2\boldsymbol{M})\boldsymbol{v} = \boldsymbol{0} \ \Leftrightarrow\ \boldsymbol{M}^{-1}\boldsymbol{Kv} = p^2\boldsymbol{v} \tag{3.20}$$

Therefore the eigenvalues of $(\boldsymbol{M}^{-1}\boldsymbol{K})$ are the square angular frequency values, p^2 $[\mathrm{rad/s}]$, and the eigenvectors are column vectors with the vibration mode shapes, $\boldsymbol{v}$.

For a given mode, i, the vibration mode shape, $\boldsymbol{v_i}$, gives a relation between all the displacements of the structure enabling the representation of its deformed shape. The absolute values do not have actual meaning, only the relative values. This explains why this vector can be normalized and used to rewrite equation (3.15) in modal coordinates to get a system of independent equations, as will be explained below. The mode shape vectors are normalized with respect to the mass matrix:

$$\boldsymbol{\phi_i} = \frac{\boldsymbol{v_i}}{\sqrt{\boldsymbol{{v_i}^T M v_i}}} \tag{3.21}$$

Joining all the mode shape vectors, we get a matrix : $\boldsymbol{\Phi} = [\boldsymbol{\phi_1}, \boldsymbol{\phi_2}, \cdots, \boldsymbol{\phi_N}]$ with which we normalize the other variables:

$$\boldsymbol{M_G} = \boldsymbol{\Phi}^T \boldsymbol{M} \boldsymbol{\Phi} = \boldsymbol{I} \tag{3.22}$$

$$\boldsymbol{K_G} = \boldsymbol{\Phi}^T \boldsymbol{K} \boldsymbol{\Phi} = \begin{bmatrix} {p_1}^2 & & \\ & \ddots & \\ & & {p_n}^2 \end{bmatrix} \tag{3.23}$$

As written above, the modal mass matrix, $\boldsymbol{M_G}$, is equal to the identity matrix. This is explained by the orthogonality property of the modes, $\boldsymbol{\phi_m^T M \phi_n} = 0 \text{ with } m \neq n$, and due to the chosen normalization, $\boldsymbol{\phi_n^T M \phi_n} = 1$. Also the $\boldsymbol{K_G} = \text{diag}[{p_i}^2]$ matrix is a diagonal matrix where each term is the square of the mode angular frequency, p. To show this, let us write equation (3.20) as $\boldsymbol{Kv} = p^2 \boldsymbol{Mv}$, substituting $\boldsymbol{v} = \boldsymbol{\phi_n}$ and pre-multiplying it by ${\boldsymbol{\phi_n}}^T$:

$${\boldsymbol{\phi_n}}^T \boldsymbol{K} \boldsymbol{\phi_n} = {p_n}^2 \times {\boldsymbol{\phi_n}}^T \boldsymbol{M} \boldsymbol{\phi_n} \;\Leftrightarrow\; K_{Gn} = {p_n}^2 \times 1 \tag{3.24}$$

The transformation of coordinates from modal to the coordinates of the structure is made by:

$$\boldsymbol{q_G} = \boldsymbol{\Phi}^{-1} \boldsymbol{q} \;\Leftrightarrow\; \boldsymbol{q} = \boldsymbol{\Phi} \boldsymbol{q_G} \tag{3.25}$$

The purpose of rewriting the complete seismic equation, equation (3.15), with the quantities defined above is that the matrices are diagonal resulting in N independent equations with just one degree of freedom each. Pre-multiplying every term by $\boldsymbol{\Phi}^T$ and introducing the identity matrix in the form of $(\boldsymbol{\Phi}\boldsymbol{\Phi}^{-1})$ we get:

$$\begin{aligned} \boldsymbol{\Phi}^T \boldsymbol{M} \boldsymbol{\Phi} \boldsymbol{\Phi}^{-1} \ddot{\boldsymbol{q}} + \boldsymbol{\Phi}^T \boldsymbol{C} \boldsymbol{\Phi} \boldsymbol{\Phi}^{-1} \dot{\boldsymbol{q}} + \boldsymbol{\Phi}^T \boldsymbol{K} \boldsymbol{\Phi} \boldsymbol{\Phi}^{-1} \boldsymbol{q} &= -\boldsymbol{\Phi}^T \boldsymbol{M} \ddot{\boldsymbol{q}}_{\boldsymbol{s}} \\ \boldsymbol{M_G} \ddot{\boldsymbol{q}}_{\boldsymbol{G}} + \boldsymbol{C_G} \dot{\boldsymbol{q}}_{\boldsymbol{G}} + \boldsymbol{K_G} \boldsymbol{q_G} &= -\boldsymbol{\Phi}^T \boldsymbol{M} \ddot{\boldsymbol{q}}_{\boldsymbol{s}} \end{aligned} \tag{3.26}$$

In equation (3.26), $\boldsymbol{C_G} = \boldsymbol{\Phi}^T \boldsymbol{C} \boldsymbol{\Phi}$ is the damping matrix in modal coordinates, which is assumed to be diagonal with each term equal to $2\xi_i p_i$, when $M_{Gi} = 1$. The variable ξ_i is the viscous damping ratio defined as $\xi_i = \frac{c}{c_{ci}}$, where the critic modal damping is $c_{ci} = 2 p_i M_{Gi}$.

If we decompose the soil motion in the three principal directions (x, y and z), we have three different accelerations: $\ddot{\boldsymbol{q}}_{\boldsymbol{s}} = \boldsymbol{1_x} \ddot{q}_{sx} + \boldsymbol{1_y} \ddot{q}_{sy} + \boldsymbol{1_z} \ddot{q}_{sz}$. These $\boldsymbol{1_x}$, $\boldsymbol{1_y}$ and $\boldsymbol{1_z}$ vectors are formed by unitary elements in the positions correspondent to the freedom degrees aligned with the direction of the acceleration.

Using this we can define the modal participation factor, P, for each earthquake direction and for each mode. For example, for mode i we have:

$$P_{xi} = \boldsymbol{\phi_i}^T \boldsymbol{M} \mathbf{1_x} \quad ; \quad P_{yi} = \boldsymbol{\phi_i}^T \boldsymbol{M} \mathbf{1_y} \quad ; \quad P_{zi} = \boldsymbol{\phi_i}^T \boldsymbol{M} \mathbf{1_z} \tag{3.27}$$

With this definitions each individual equation from (3.26) can be written in a simpler form:

$$\ddot{q}_{Gi} + (2\xi_i p_i)\dot{q}_{Gi} + ({p_i}^2) q_{Gi} = -P_{xi}\ddot{q}_{xs} - P_{yi}\ddot{q}_{ys} - P_{zi}\ddot{q}_{zs} \quad \text{with } i = 1, \ldots, N \tag{3.28}$$

All of these N equations can be solved individually and then regrouped to get the total response of the structure using equation (3.25).

Finally, we can introduce the concept of the effective modal mass, m_{eff}, that is shown to be the square of the modal participation factor. To chose the relevant number of modes, $n < N$, we consider every mode until the sum of m_{eff} equals 90% of the total mass.

In order to explain why the sum of m_{eff} must equal the total mass of the structure, we will follow the demonstration of Clough and Penzien [24]. Let us define a_i as the amplitude of each mode and $\boldsymbol{a}$ as the correspondent vector with all the modes amplitudes. The response of the structure is described by the vector $\boldsymbol{q}$ with all the displacements of the structure. We can write the vector $\boldsymbol{q}$ in the form of: $\boldsymbol{q} = \boldsymbol{\Phi a}$. Comparing this with equation (3.25), we see that $\boldsymbol{a}$ is equal to $\boldsymbol{q_G}$ but let us maintain the notation.

The vector $\mathbf{1_x}$ can be written in the same form as $\boldsymbol{q}$. By adapting the definition of the $\boldsymbol{a}$ vector we can write the following: $\mathbf{1_x} = \boldsymbol{\Phi a_{1_x}}$. Pre-multiplying by $(\boldsymbol{\Phi}^T \boldsymbol{M})$ on both sides:

$$\begin{aligned} \boldsymbol{\Phi}^T \boldsymbol{M} \mathbf{1_x} &= \boldsymbol{\Phi}^T \boldsymbol{M} \boldsymbol{\Phi a_{1_x}} \\ \boldsymbol{P_x} &= \boldsymbol{M_G a_{1_x}} \end{aligned} \tag{3.29}$$

where $\boldsymbol{P_x} = \{P_{xi}\}$. As $\boldsymbol{M_G}$ is a diagonal matrix (actually the identity matrix), $P_{xi} = M_{Gi} \times a_{1xi}$.

Therefore, $a_{1xi} = \frac{P_{xi}}{M_{Gi}}$ and $\boldsymbol{a_{1_x}} = \left\{ \frac{P_{xi}}{M_{Gi}} \right\}$. That is why $\mathbf{1_x}$ can be written as:

$$\mathbf{1_x} = \boldsymbol{\Phi} \left\{ \frac{P_{xi}}{M_{Gi}} \right\} \tag{3.30}$$

At the same time, the structure mass $M_t = \mathbf{1_x}^T \boldsymbol{M} \mathbf{1_x}$, because in each earthquake direction the total mass vibrates. Combining all the equations, we get that:

$$M_t = \mathbf{1_x}^T \boldsymbol{M} \mathbf{1_x} = \left\{ \frac{P_{xi}}{M_{Gi}} \right\}^T \boldsymbol{\Phi}^T \boldsymbol{M} \boldsymbol{\Phi} \left\{ \frac{P_{xi}}{M_{Gi}} \right\} = \left\{ \frac{P_{xi}}{M_{Gi}} \right\}^T \boldsymbol{M_G} \left\{ \frac{P_{xi}}{M_{Gi}} \right\} = \sum_{i=1}^{n\ modes} \frac{P_{xi}^2}{M_{Gi}} \tag{3.31}$$

and since we have constructed the modal shape vector to have $M_{Gi} = 1$:

$$M_t = \sum_{i=1}^{n\ modes} P_{xi}^2 \quad \Leftrightarrow \quad m_{eff\ i} = {P_{xi}}^2 \tag{3.32}$$

3.2.2 Response Spectra Analysis

It remains to be determined the individual response of each equation with one degree of freedom (3.28). For design purposes, we can use a response spectrum to get the maximum acceleration on the structure when it is submitted to a ground motion.

As we already have the angular frequencies of each mode, p, obtained from equation (3.20), it is simple to calculate the cyclic frequencies: $f = p/2\pi$ [Hz] and the periods: $T = 1/f$ [s]. Using the response spectrum described in the EC8, see Figure 3.3 and equation (3.33), we get the design spectral acceleration $S_d(T, \xi)$ [m/s^2] for each mode. The spectrum is defined by the ground characteristics (ground type), the location (defined by zones according to the seismic action type 1 or 2), the importance factor of the structure, γ_I, and the behavior factor, q.

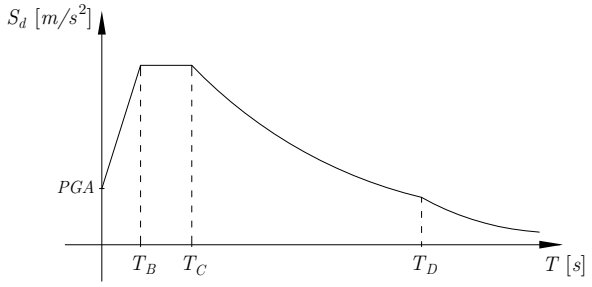

Figure 3.3: Design response spectrum in accelerations as defined in EC8.

The damping value suited for reinforced concrete structures is 5% which corresponds to a unit damping correction factor: $\eta = \sqrt{10/(5+\xi)}$. This parameter is not explicit in the following equation as it is included in the value of the behavior factor.

$$S_d(T) = \begin{cases} a_g S \times \left[\frac{2}{3} + \frac{T}{T_B} \times \left(\frac{2.5}{q} - \frac{2}{3}\right)\right] & \text{if} \quad 0 < T < T_B \\ a_g S \times \frac{2.5}{q} & \text{if} \quad T_B < T < T_C \\ a_g S \times \frac{2.5}{q} \times \frac{T_C}{T} & \text{if} \quad T_C < T < T_D \\ a_g S \times \frac{2.5}{q} \times \frac{T_C T_D}{T} & \text{if} \quad T_D < T < 4\ s \end{cases} \tag{3.33}$$

The dynamic equation for a one freedom degree oscillator submitted to a ground acceleration is given by:

$$\ddot{q}_G + 2\xi p \dot{q}_G + p^2 q_G = -\ddot{q}_s \tag{3.34}$$

The solution of this equation, given by the response spectrum, leads to: $\ddot{q}_{Gmax} = S_d(T)$.

Comparing equations (3.34) and (3.28), we see there is only one acceleration in the later (correspondent to one earthquake direction). This difference is explained because equation (3.34) uses a maximum value of the acceleration, obtained from the response spectrum. Additionally we conclude that in a multiple degree of freedom oscillator the acceleration for each mode, i, and earthquake direction is corrected by the modal participation factor. For example, for the x direction we have:

$$\ddot{q}_{Gi_{max}} = P_{xi} S_d(p_i, \xi) \ \Leftrightarrow \ q_{Gi_{max}} = \frac{P_{xi} S_d(p_i, \xi)}{{p_i}^2} \tag{3.35}$$

For each relevant mode and earthquake direction (x, y and z) we calculate the maximum node displacements by:

$$\boldsymbol{q_i} = \boldsymbol{\phi_i} \frac{P_{xi} S_d(p_i, \xi)}{p_i^2} \tag{3.36}$$

Having the displacement vector in the structure coordinates we can calculate the stress-resultants of each mode, with the Displacement Method described before ($\boldsymbol{f_i}^e = \boldsymbol{K}^e \boldsymbol{q_i}^e$). We remark that these forces have a defined sign and are not sensitive to the normalization chosen for Φ, in particular to its sign (note that $\boldsymbol{q_i}$ has a quadratic dependence on Φ_i: Φ_i and P_{xi}). It should be underlined that for a serviceability limit state verification, the displacements in each mode must be obtained from the $\boldsymbol{q_i}$ vector multiplied by the behavior factor, q.

3.2.3 Earthquake Characteristics

This section intends to detail the seismic action used in the examples, which was always identical for a matter of simplicity.

Based on what would be the design in the city of Lisbon an earthquake of Type 1 is chosen, in particular in the zone 1.3, with a type B ground (described in EC8 as "deposits of very dense sand, gravel, or very stiff clay, at least several tens of meters in thickness, characterized by a gradual increase of mechanical properties with depth").

The structure will have an importance factor of $\gamma_I = 1$, suited for an ordinary building, and a behavior factor of $q = 2.5$ adequate for a frame system with many joints where the energy dissipation is possible.

Table 3.1: Earthquake Characteristics.

a_{gR}	$1.5\ \mathrm{m/s^2}$
a_g	$1.5\ \mathrm{m/s^2}$
T_B	$0.1\ \mathrm{s}$
T_C	$0.6\ \mathrm{s}$
T_D	$2.0\ \mathrm{s}$
S_{max}	1.35
S	1.2917
$a_g S$	$1.9375\ \mathrm{m/s^2}$

Table 3.1 displays the values for the reference peak ground acceleration on type A ground, a_{gR} and its correspondent design ground acceleration, a_g. The expressions needed to calculate a_g and the soil factor, S are in equation (3.37).

$$\begin{aligned} a_g &= a_{gR} \times \gamma_I \\ S &= S_{max} - (S_{max} - 1) \times (a_g - 1)/3 \end{aligned} \tag{3.37}$$

We reiterate that this will be used in every example to calculate stress-resultants in dynamic analysis.

3.2.4 Combination Methods

Having the stress-resultant values (N, M_2, M_3, V_2, V_3 and T) in every node of the structure for each mode and for each direction of the earthquake, there is a need to combine the values and calculate the design stress-resultants.

To combine all the n relevant modes there are three alternatives:

- The absolute combination (ABS) is used when the maximum values occur simultaneously.

$$F_{comb} = \sum_{i=1}^{n\ modes} |F_i| \tag{3.38}$$

- The Square Root of Sum of Squares (SRSS) assumes the maximum values are independent and is a good approximation for well separated mode frequencies.

$$F_{comb} = \sqrt{\sum_{i=1}^{n\ modes} F_i^2} \tag{3.39}$$

- The Complete Quadratic Combination (CQC) is used for unknown frequency relations.

$$\begin{aligned} F_{comb} &= \sqrt{\sum_{i=1}^{n\ modes} \sum_{j=1}^{n\ modes} F_i F_j \mu_{ij}} \\ \mu_{ij} &= \frac{8\xi^2(1+r)r^{(3/2)}}{(1-r^2)^2 + 4\xi^2 r(1+r)^2} \text{ and } r = \frac{p_j}{p_i} \end{aligned} \tag{3.40}$$

It is important to note that the CQC combination includes the limit cases of the other two. Considering two modes, i and j: when $p_i \gg p_j, \quad \mu_{ij} \to 0, \quad F_{comb} = \sqrt{F_1^2 + F_2^2}$ which corresponds to the SRSS combination. On the other hand, if $p_i \approx p_j, \quad \mu_{ij} \to 1, \quad F_{comb} = \sqrt{F_1^2 + F_2^2 + 2F_1F_2} = \sqrt{(F_1 + F_2)^2} = |F_1 + F_2|$. If F_1 and F_2 have the same sign this equals the ABS combination.

To combine the three directions of the earthquake it is usual to use the SRSS combination, once again assuming the independence of the motion in the three directions.

After this step we have a complete dynamic analysis of the structure, with the design displacements and stress-resultants.

Chapter 4

Response Interaction Envelopes

At the end of Chapter 3 are calculated the design maximum values for each separate stress-resultant. However, it may be too conservative to admit that all stress-resultant maximums occur at the exact same time and for that reason, it may be helpful to develop a method to correlate the stress-resultants. A combination of particular interest for the design phase is the axial force and bending moments acting on a column section.

4.1 Classical Approach

The common approach to the design of elements with more than one variable estimated by the response spectra analysis is to combine the individual maximum results.

Without loss of generality let us consider just two variables (x_1 and x_2), whose maximum responses are calculated in each mode from the displacement vector given in equation (3.36) and then combined by the most suitable method. The two final values can be written as a vector $\boldsymbol{x_f} = [X_{f1}, X_{f2}]^T$ and represented in a coordinate space. The classical envelope we would get is a rectangle constructed from the intersections of the straight lines defined by: $x_i = X_{fi}$ and $x_i = -X_{fi}$. Its representation is in Figure 4.1.

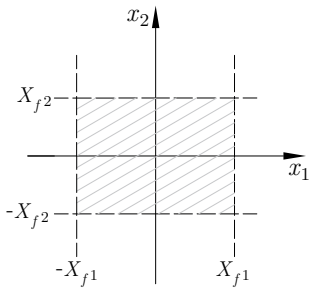

Figure 4.1: Standard envelope in $(x_1 - x_2)$.

Clearly, not all the points inside this rectangle reproduce a feasible response of the structure. The response in terms of each variable is co-related to the other as they are the result of several modal responses combined, each with a well-defined correspondence between stress-resultants.

4.2 Interaction of stress-resultants

The starting point for this study has to be the analysis of each mode where there is an unequivocal relation between the stress-resultants or other quantities we may want to consider.

The information of each mode may be written in a vector form as $\boldsymbol{x_i} = [x_{i1}, x_{i2}]^T$, which graphic representation is a straight line connecting the point defined by $\boldsymbol{x}$ and its symmetric, due to the cyclic response of the structure.

We will demonstrate that the interaction surface has an elliptical shape, when multiple modes are considered. To do so, we begin by defining the counterclockwise angle θ in the same coordinate space $(x_1 - x_2)$ and its vectorial representation $\boldsymbol{t} = [\cos\theta, \sin\theta]^T$, see Figure 4.2.

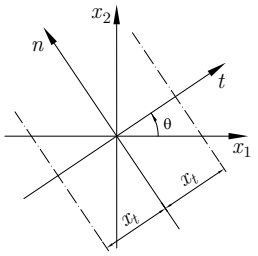

Figure 4.2: Coordinate space $(x_1 - x_2)$.

Considering the projection of $\boldsymbol{x}$ on any vector $\boldsymbol{t}$ we introduce a distance x_t. For one mode x_{ti} and its square value are simply defined as:

$$x_{ti} = \boldsymbol{t}^T \boldsymbol{x_i} \tag{4.1}$$

$$x_{ti}{}^2 = \boldsymbol{t}^T \boldsymbol{x_i}\ \boldsymbol{t}^T \boldsymbol{x_i} = \boldsymbol{t}^T \boldsymbol{x_i}\ \boldsymbol{x_i}{}^T \boldsymbol{t} \tag{4.2}$$

Extending this to all the n relevant modes results that:

$$x_t{}^2 = \sum_{i=1}^{n} x_{ti}{}^2 = \sum_{i=1}^{n} \boldsymbol{t}^T \boldsymbol{x_i}\ \boldsymbol{x_i}{}^T \boldsymbol{t} = \boldsymbol{t}^T \sum_{i=1}^{n} \left(\boldsymbol{x_i}\ \boldsymbol{x_i}{}^T\right) \boldsymbol{t} = \boldsymbol{t}^T \boldsymbol{X} \boldsymbol{t} \tag{4.3}$$

Here was introduced the positive semi-definite matrix $\boldsymbol{X} = \sum \boldsymbol{x_i} \boldsymbol{x_i}{}^T$ where all the modes information is synthesized. As was discussed in section 3.2.4 the modes can be associated using different combination methods. That justifies the need to further detail this matrix.

For the SRSS combination, the definitions above directs us to:

$$\boldsymbol{X} = \sum_{i=1}^{n} \boldsymbol{x_i}\ \boldsymbol{x_i}{}^T = \begin{bmatrix} \sum\limits_{i=1}^{n} x_{i1}{}^2 & \sum\limits_{i=1}^{n} x_{i1} x_{i2} \\ \sum\limits_{i=1}^{n} x_{i1} x_{i2} & \sum\limits_{i=1}^{n} x_{i2}{}^2 \end{bmatrix} \tag{4.4}$$

On the other hand, for the CQC combination the definition of $x_t{}^2$ should be adapted to:

$$x_t{}^2 = \sum_{i=1}^{n} \sum_{j=1}^{n} \mu_{ij} x_{ti} x_{tj} = \sum_{i=1}^{n} \sum_{j=1}^{n} \mu_{ij} \boldsymbol{t}^T \boldsymbol{x_i}\ \boldsymbol{x_j}{}^T \boldsymbol{t} = \boldsymbol{t}^T \boldsymbol{X} \boldsymbol{t} \tag{4.5}$$

In this equation the matrix $\boldsymbol{X}$ is now written as:

$$\boldsymbol{X} = \sum_{i=1}^{n} \sum_{j=1}^{n} \mu_{ij} \, \boldsymbol{x_i} \, \boldsymbol{x_j}^T \tag{4.6}$$

where μ_{ij} is defined as in equation (3.40).

The value x_t is the maximum distance any point of the envelope can take along the direction $\boldsymbol{t}$. This is why we can add two new straight lines to the set of lines that define the boundary of the envelope, see Figure 4.2. These new lines are perpendicular to $\boldsymbol{t}$ at a distance of x_t from the origin and will reduce the size of the original rectangular envelope, see Figure 4.3.

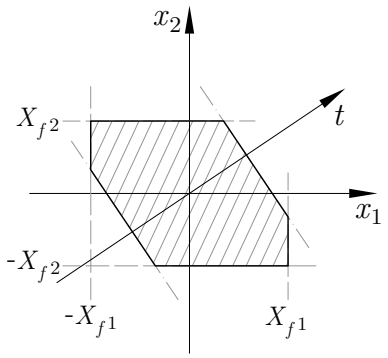

Figure 4.3: Reduced envelope.

This is the starting point for the three methods to construct interaction envelopes explained below.

4.3 Construction of the Elliptical Envelopes

4.3.1 Intersection Method

Continuing the previous derivation, it should be noted that the point defined by $\boldsymbol{p} = x_t \times \boldsymbol{t}$ is not a point of the interaction envelope. In fact, the point of the envelope can be any one belonging to the line perpendicular to $\boldsymbol{t}$ that contains $\boldsymbol{p}$, see Figure 4.4 (a). Taking two values of θ sufficiently close and their x_t, the envelope point is the intersection of the two perpendicular lines.

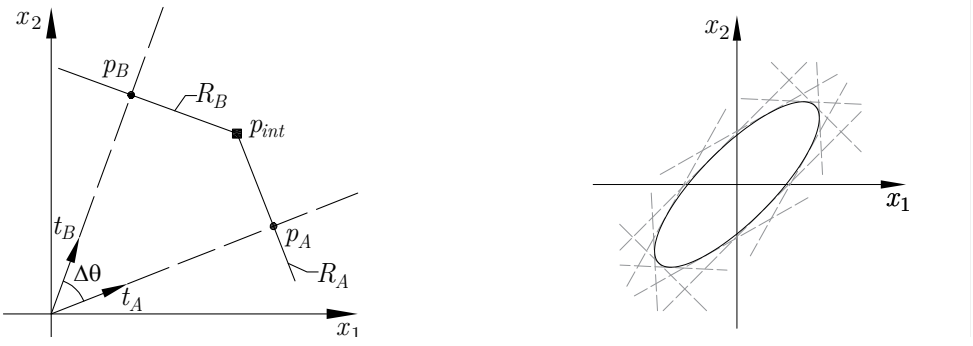

(a) Interpretation of the intersection point, p_{int}

(b) Envelope construction

Figure 4.4: Intersection Method.

We define point A as: $\boldsymbol{p_A} = x_{tA}\boldsymbol{t_A}$, with $\boldsymbol{t_A}$ associated with a given θ_A and x_{tA} given by equation (4.5). The perpendicular line is: $R_A = x_{tA}\boldsymbol{t_A} + k_A\boldsymbol{n_A}$, where k_A is any real number and $\boldsymbol{n_A}$ as a realization of $\boldsymbol{n} = [-\sin\theta, \cos\theta]^T$. Doing the same for point B and matching the two perpendicular lines, the intersection point results in the following:

$$\begin{aligned} & x_{t_A}\boldsymbol{t_A} + k_A\boldsymbol{n_A} = x_{t_B}\boldsymbol{t_B} + k_B\boldsymbol{n_B} \\ & x_{t_A}\boldsymbol{t_A}^T\boldsymbol{t_B} + k_A\boldsymbol{n_A}^T\boldsymbol{t_B} = x_{t_B} + 0 \\ & k_A = \frac{x_{t_B} - x_{t_A}(\boldsymbol{t_A}^T\boldsymbol{t_B})}{\boldsymbol{n_A}^T\boldsymbol{t_B}} \\ & \boldsymbol{p_{int}} = x_{tA}\boldsymbol{t_A} + k_A\boldsymbol{n_A} \end{aligned} \tag{4.7}$$

By applying the same procedure to a range of θ values contained in $[0-2\pi]$, the shape of the envelope becomes apparent, as shown in Figure 4.4 (b).

This method is directly applicable to the CQC and SRSS combinations by altering the matrix $\boldsymbol{X}$. Nonetheless, it is possible to adapt it for the ABS combination by changing the x_t definition:

$$x_t = \sum_{i=1}^{n} \left|\boldsymbol{t}^T\boldsymbol{x_i}\right| \tag{4.8}$$

All the envelopes attained with this method are illustrated in Figure 4.5. We resorted to a generic example of a structure with three relevant modes (that will be detailed in section 4.3.4). The stress-resultants (N and M) were evaluated in the base section of a column. In each graphic is displayed the resultant envelope for the chosen combination and also the previous envelopes drawn in gray to ease the comparison. Were used 315 points which corresponds to $\Delta\theta = 0.02$ rad.

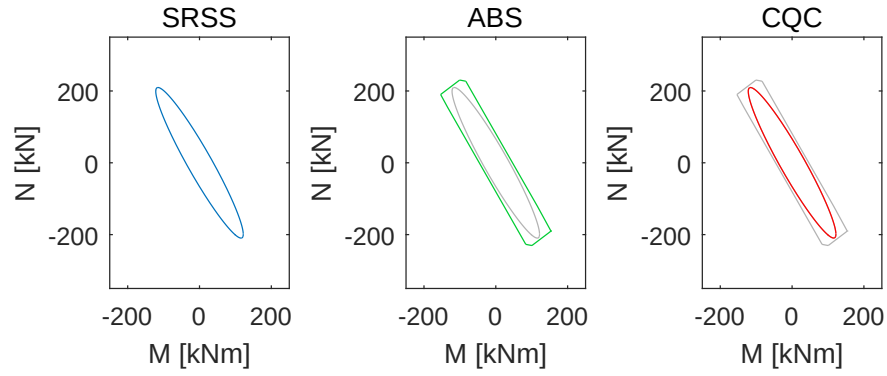

Figure 4.5: Perpendicular Method: SRSS, ABS, CQC.

It is apparent that the resultant shape for the SRSS combination is elliptical with a significant correlation between the two variables, meaning one of the semi-axis is significantly larger than the other. The ABS envelope is a convex polygon exhibiting the same correlation which encloses the SRSS envelope, showing it behaves as an upper bound to the other envelopes. It can be depicted as a group of pairs of parallel lines, each one introduced by one mode and whose length translates the mode relevance to the behavior of the structure, observe Figure 4.6. Even thought the envelope could be constructed this way, it is more systematic to span the θ angles, calculate its x_t and use the intersection method.

Lastly, the CQC envelope is so close to the SRSS solution that they overlap, meaning the modes have well-separated frequencies in this example.

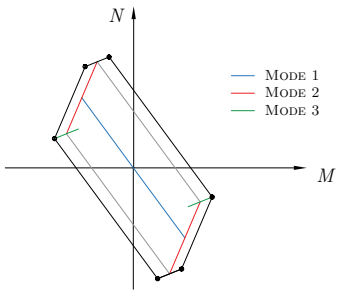

Figure 4.6: Construction of the ABS envelope.

What is more, changing the angular frequencies, p, making them all equal produces the following CQC envelope, in Figure 4.7.

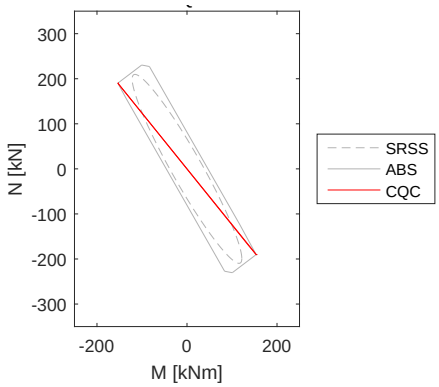

Figure 4.7: CQC envelope for $p_i = p_j$.

As can be seen, the CQC envelope is a particular case of an ellipse, a straight line. If the frequencies of every mode are equal, then $r = 1$, and because of this, the method is actually adding the contribution of each mode, as is done for the ABS combination.

In the ABS method, each vertex of the envelope is the sum of the vectors of each mode, $\boldsymbol{x_i}$, which can be assigned to both positive or negative signs. Of course, some of the vector sums produce points in the interior of the envelope, so the number of vertices is not $2 \times 2 \times 2 = 8$, but actually 6. With the CQC method there is no need to consider all the possible sign combinations as we know exactly how the modes are correlated, and so it provides the actual response of the structure. To clarify, choosing a sign for the first mode response means that all the others are thereafter established and do not remain arbitrary. Choosing the inverse sign produces the other extremity point of the envelope.

As the ABS and SRSS methods do not take the frequency relation in consideration, the gray lines in the Figure would also be their envelopes for this $p_i = p_j$ situation. It can be seen that the CQC response clearly exceeds the SRSS envelope in one direction but not in the perpendicular one. This illustrates the advantages of the CQC combination in providing the correct behavior of the structure.

It should be said that only the perpendicular method, from the ones explored, can reproduce the ABS envelope as it cannot be expressed by the means of a $\boldsymbol{X}$ matrix.

4.3.2 Divider Method

Following the idea of assigning maximum distances to given directions, Menun and Der Kiureghian [1] developed an alternative procedure for constructing the elliptical envelopes for the SRSS and CQC combination.

Hereafter will be reproduced the authors' derivation, starting by introducing the variables in Figure 4.8.

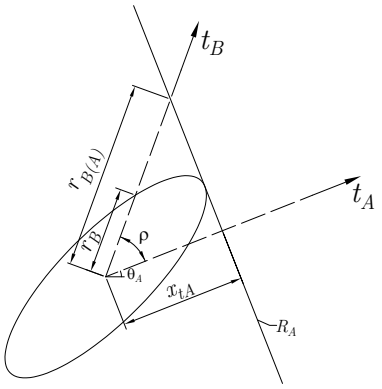

Figure 4.8: Identification of variables for the Divider Method.

Considering the vector $\boldsymbol{t_B} = [\cos\theta_B, \sin\theta_B]^T$, the new distance $r_{B(A)}$ is defined as the length along the direction $\boldsymbol{t_B}$ from the origin until the perpendicular line, R_A, defined for θ_A in the previous method. The angle between the two directions $\boldsymbol{t_A}$ and $\boldsymbol{t_B}$ is named as ρ.

$$r_{B(A)} = \frac{x_{t_A}}{\cos(\rho)} = \frac{(\boldsymbol{t_A}^T \boldsymbol{X} \boldsymbol{t_A})^{(1/2)}}{\boldsymbol{t_B}^T \boldsymbol{t_A}} \tag{4.9}$$

We will keep the direction $\boldsymbol{t_B}$ fixed and rotate $\boldsymbol{t_A}$. This causes the line R_A to follow the rotation and change the length of $r_{B(A)}$. The minimum value $r_{B(A)}$ can take is named r_B and corresponds to the real distance to the envelope. In other words, r_B is the minimum of $r_{B(A)}$ with respect to $\boldsymbol{t_A}$.

$$\frac{\mathrm{d}r_{B(A)}}{\mathrm{d}\boldsymbol{t_A}} = \frac{\frac{1}{2}(\boldsymbol{t_A}^T \boldsymbol{X} \boldsymbol{t_A})^{(-1/2)} 2\boldsymbol{t_A}^T \boldsymbol{X} (\boldsymbol{t_B}^T \boldsymbol{t_A}) - (\boldsymbol{t_A}^T \boldsymbol{X} \boldsymbol{t_A})^{(1/2)} \boldsymbol{t_B}^T}{(\boldsymbol{t_B}^T \boldsymbol{t_A})^2} = \boldsymbol{0}^T \tag{4.10}$$

In this step is used the following property of vector derivation when $\boldsymbol{X}$ is a symmetric matrix:

$$\frac{\mathrm{d}(\boldsymbol{t}^T \boldsymbol{X} \boldsymbol{t})}{\mathrm{d}\boldsymbol{t}} = \boldsymbol{t}^T \boldsymbol{X}^T + \boldsymbol{t}^T \boldsymbol{X} = \boldsymbol{t}^T (\boldsymbol{X}^T + \boldsymbol{X}) = 2\boldsymbol{t}^T \boldsymbol{X} \tag{4.11}$$

Solving (4.10) we find:

$$\boldsymbol{t_A}^T \boldsymbol{X} (\boldsymbol{t_B}^T \boldsymbol{t_A}) = (\boldsymbol{t_A}^T \boldsymbol{X} \boldsymbol{t_A}) \boldsymbol{t_B}^T \tag{4.12}$$

Then using equation (4.9):

$$\boldsymbol{t_A}^T \boldsymbol{X} (\boldsymbol{t_B}^T \boldsymbol{t_A}) = [(\boldsymbol{t_B}^T \boldsymbol{t_A}) r_{B(A)}]^2 \boldsymbol{t_B}^T \tag{4.13}$$

Dividing by $(\boldsymbol{t_B}^T \boldsymbol{t_A})$:

$$\boldsymbol{t_A}^T \boldsymbol{X} = (\boldsymbol{t_B}^T \boldsymbol{t_A}) r_{B(A)}^2 \boldsymbol{t_B}^T \tag{4.14}$$

And assuming for the moment $\boldsymbol{X}$ is not a singular matrix:

$$\boldsymbol{t_A}^T = (\boldsymbol{t_B}^T \boldsymbol{t_A}) r_{B(A)}^2 \boldsymbol{t_B}^T \boldsymbol{X}^{-1} \tag{4.15}$$

Using this and returning to equation (4.9):

$$r_{B(A)} = \frac{[(\boldsymbol{t_B}^T \boldsymbol{t_A}) r_{B(A)}^2 \boldsymbol{t_B}^T \boldsymbol{X}^{-1} \boldsymbol{X} \boldsymbol{X}^{-1} \boldsymbol{t_B} r_{B(A)}^2 (\boldsymbol{t_B}^T \boldsymbol{t_A})]^{(1/2)}}{\boldsymbol{t_B}^T \boldsymbol{t_A}} \tag{4.16}$$

Simplifying the expression we lose the dependence of $\boldsymbol{t_A}$:

$$\begin{aligned} r_{B(A)} &= r_{B(A)}^2 (\boldsymbol{t_B}^T \boldsymbol{X}^{-1} \boldsymbol{t_B})^{(1/2)} \\ r_B &= (\boldsymbol{t_B}^T \boldsymbol{X}^{-1} \boldsymbol{t_B})^{(-1/2)} \end{aligned} \tag{4.17}$$

Finally, the envelope point has coordinates given by $\boldsymbol{x} = r_B \boldsymbol{t_B}$. We emphasize that equation (4.17) describes an ellipse, where r_B is the distance to the envelope in the direction $\boldsymbol{t_B}$, thus proving the mathematical nature of the envelopes.

Furthermore, this equation can be expressed in an alternative simpler form. Let us use Figure 4.9 where $\boldsymbol{t_A}$ is the orientation that minimizes $r_{B(A)}$, causing $r_{B(A)} = r_B$.

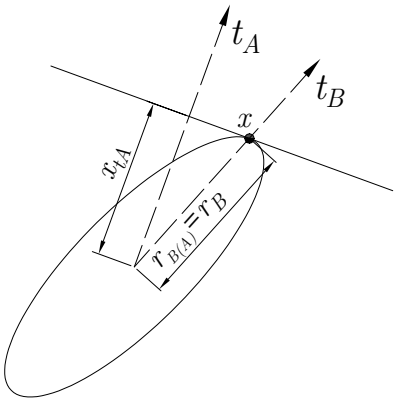

Figure 4.9: Alternative form for the Divider Method.

Point $\boldsymbol{x}$ is defined by: $\boldsymbol{x} = r_B \boldsymbol{t_B}$ and also satisfies the relation $\boldsymbol{t_A}^T \boldsymbol{x} = x_{tA}$. Using equation (4.3) where ${x_t}^2 = \boldsymbol{t}^T \boldsymbol{X} \boldsymbol{t}$ we can write that:

$$\boldsymbol{t_A}^T \boldsymbol{x} = (\boldsymbol{t_A}^T \boldsymbol{X} \boldsymbol{t_A})^{(1/2)} = \frac{(\boldsymbol{t_A}^T \boldsymbol{X} \boldsymbol{t_A})}{(\boldsymbol{t_A}^T \boldsymbol{X} \boldsymbol{t_A})^{(1/2)}} \tag{4.18}$$

Finally, because $\boldsymbol{t_A}$ is an arbitrary vector it yields that:

$$\boldsymbol{x} = \frac{\boldsymbol{X} \boldsymbol{t_A}}{\sqrt{\boldsymbol{t_A}^T \boldsymbol{X} \boldsymbol{t_A}}} \tag{4.19}$$

This equation provides the Cartesian coordinates of the envelope associated with the direction $\boldsymbol{t_A}$. This is the point where the perpendicular line to $\boldsymbol{t_A}$ intersects the ellipse. Comparing it to equation (4.17) there is no longer the need to invert the matrix $\boldsymbol{X}$, which is a computational advantage.

4.3.3 Equation Method

Having established the envelopes are ellipses it is justifiable to directly recur to the parametric equation of these identities. Such equations associate a semi-axis to a given direction θ, having as input the length of the two principal semi-axes of the ellipse.

Doing a transformation of coordinates, resorting to a specific transformation matrix $\boldsymbol{A}$, can be equivalent to an eigenvalue and eigenvector analysis of $\boldsymbol{X}$. With it we calculate the principal semi-axes as they are the square roots of the eigenvalues, as evidenced in Figure 4.10.

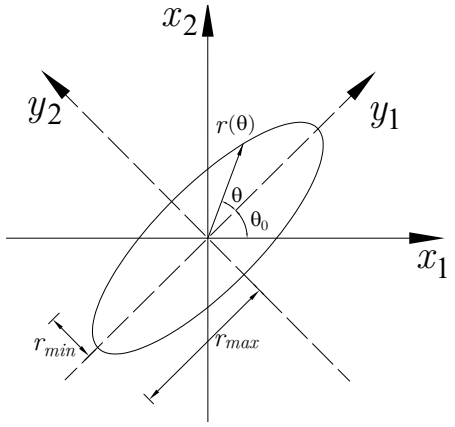

Figure 4.10: Coordinate space $(y_1 - y_2)$.

$$\boldsymbol{Y} = \boldsymbol{A}^T \boldsymbol{X} \boldsymbol{A} = \begin{bmatrix} {y_1}^2 & 0 \\ 0 & {y_2}^2 \end{bmatrix} = \begin{bmatrix} {r_{max}}^2 & 0 \\ 0 & {r_{min}}^2 \end{bmatrix} \tag{4.20}$$

Starting with the definition of an ellipse presented in equation (4.17), $r_B = ({\boldsymbol{t_B}}^T \boldsymbol{X}^{-1} \boldsymbol{t_B})^{(-1/2)}$:

$$\boldsymbol{t_B^T} \boldsymbol{X}^{-1} \boldsymbol{t_B} = \frac{1}{{r_B}^2} \tag{4.21}$$

$$(r_B \boldsymbol{t_B^T}) \boldsymbol{X}^{-1} (r_B \boldsymbol{t_B}) = 1 \tag{4.22}$$

$$\boldsymbol{x}^T \boldsymbol{X}^{-1} \boldsymbol{x} = 1 \tag{4.23}$$

Including the transformation of coordinates of equation (4.20), we can write:

$$\boldsymbol{y}^T \boldsymbol{Y}^{-1} \boldsymbol{y} = 1 \tag{4.24}$$

Because these are principal directions, it yields that:

$$\frac{{y_1}^2}{{r_{max}}^2} + \frac{{y_2}^2}{{r_{min}}^2} = 1 \tag{4.25}$$

Defining $y_1 = r\cos\theta$ and $y_2 = r\sin\theta$ we conclude that:

$$r(\theta) = \frac{r_{min} \times r_{max}}{\sqrt{r_{max}^2 \times \sin^2\theta + r_{min}^2 \times \cos^2\theta}} \tag{4.26}$$

In the other hand, if we use a different set of coordinates, that are not principal directions, we would get:

$$\begin{bmatrix} r\cos\theta & r\sin\theta \end{bmatrix} \begin{bmatrix} A & B \\ B & C \end{bmatrix} \begin{bmatrix} r\cos\theta \\ r\sin\theta \end{bmatrix} = 1 \tag{4.27}$$

$$Ar^2\cos\theta + 2Br^2\cos\theta\sin\theta + Cr^2\sin\theta = 1 \tag{4.28}$$

$$r(\theta) = \frac{1}{A\cos^2\theta + 2B\sin\theta\cos\theta + C\sin^2\theta} \tag{4.29}$$

Equation (4.26) parameterizes an ellipse with the maximum semi-axis aligned with the horizontal axis.

As such, it is still necessary to rotate the ellipse to align the maximum semi-axis with the correspondent principal direction. To do so, we will use the first column of the principal directions matrix, $\boldsymbol{A}$.

$$\theta_0 = \arctan\left(\frac{A_{11}}{A_{21}}\right) \tag{4.30}$$

By plotting in a polar mode all the realizations of $(r(\theta), \theta + \theta_0)$ the elliptical figure is correctly reproduced.

In the Matlab program, the maximum semi-axis corresponds to the second eigenvalue as they are sorted by increasing order. For this reason, this is implemented with the second column of the matrix $\boldsymbol{A}$.

4.3.4 Computational Implementation

In this subsection, the 2D framed structure used previously as an example in section 4.3.1 will be specified and analyzed in detail to illustrate the construction of an elliptical envelope.

The geometric information, the materials and the loads are summarized in Table 4.1.

Table 4.1: 2D Structure Description.

story height	$3\ \mathrm{m}$
span	$6\ \mathrm{m}$
columns	$0.3 \times 0.3\ \mathrm{m}^2$
beams	$0.3 \times 0.6\ \mathrm{m}^2$
concrete	C30/37
steel	A500
load	$34.5\ \mathrm{kN/m}$ (in all beams)

The first three vibration modes are displayed in Figure 4.11. We will use more than the two relevant modes to better explain the solution.

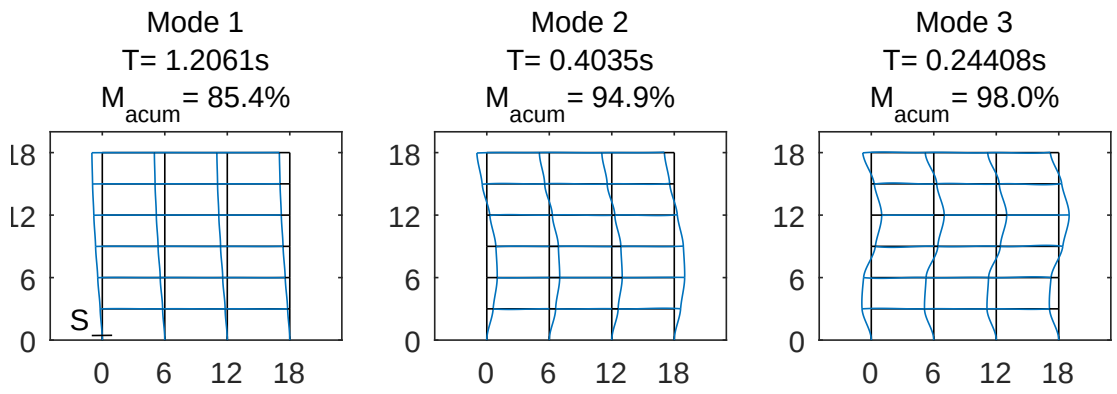

Figure 4.11: Vibration modes in a 2D structure.

For each mode, we calculate the N and M values for the base section of the left column and construct the matrix that quantifies the ellipse:

$$\boldsymbol{X} = \begin{bmatrix} M^2 & MN \\ MN & N^2 \end{bmatrix} \tag{4.31}$$

Since the two values obtained in each mode are completed correlated the ellipse constructed for each individual mode degenerates in a line segment.

As was already introduced in the beginning of this chapter, for each mode there is a point in the coordinate space $(x_1 - x_2)$ whose coordinates are the two maximum values of these quantities obtained from the dynamic analysis. Given the cyclic response of the structure, the symmetric point, and every other one over the line that connects the two can also occur. Thus, forming a line segment in this space for each mode, see Figure 4.12.

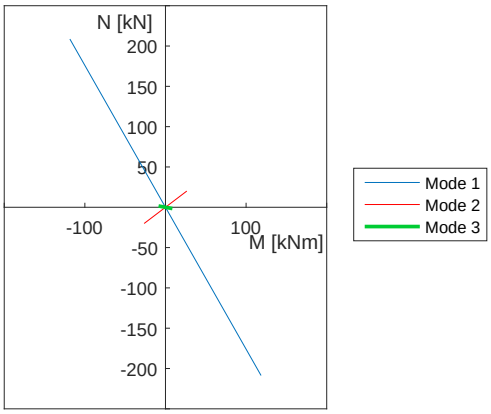

Mode	Pairs $(M - N)$
1	$[-118.57\ \text{kNm},\ +208.66\ \text{kN}]$
2	$[-\ 26.46\ \text{kNm},\ -\ 20.11\ \text{kN}]$
3	$[-\ 8.59\ \text{kNm},\ +\ 1.61\ \text{kN}]$

Figure 4.12: Pairs $(M\ -\ N)$ for each mode.

Joining the three modes, the stress-resultants stop being completely correlated and the actual form of an ellipse becomes apparent. In Figure 4.13 is showed the evolution of the ellipse with the addition of each mode. The interior lines are the same pairs $M - N$ displayed above and the exterior dotted lines represent the envelope we would get using only the maximum values. In the first mode the total envelope is equal to the mode contribution and the two overlap. The following modes adjust the ellipse principal

semi-axes: being the second mode almost perpendicular to the first increases the minor principal semi-axis, and the third mode has a small contribution for both. We remark that the elliptical envelope is included in its totality in the rectangular one.

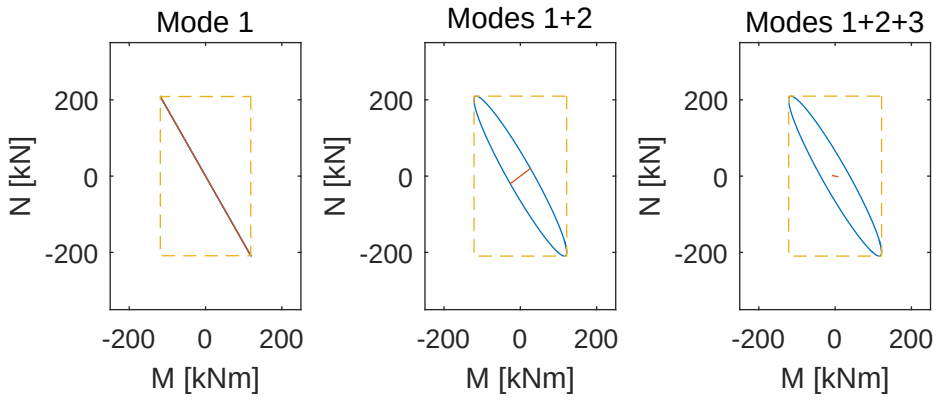

Figure 4.13: Cumulative ellipse.

These ellipses were constructed with the divider method, specified in section 4.3.2, by continually adapting the $\boldsymbol{X}$ matrix (for these were used SRSS combinations).

Alternatively, any of the methods previously explained would originate the same envelopes, which is evidenced by Figure 4.14.

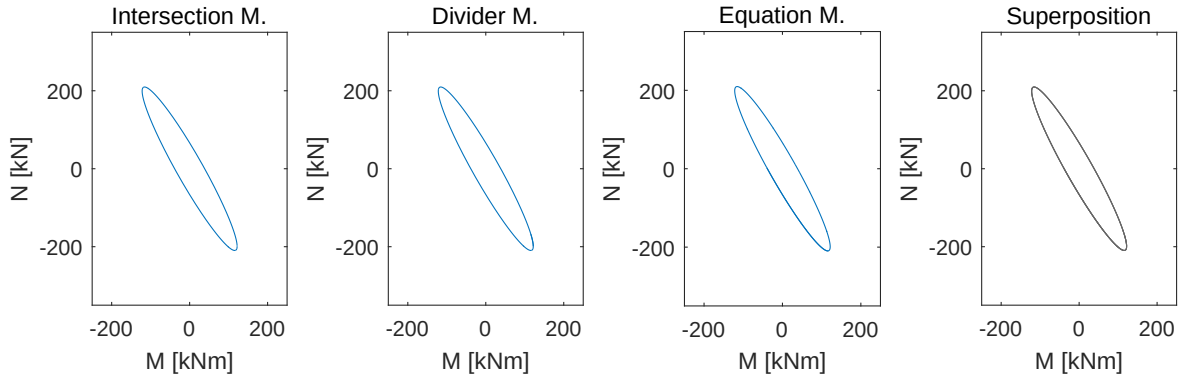

Figure 4.14: Ellipses by the three methods.

We remark that the Intersection method requires a high number of points and perpendicular lines to reproduce the correct elliptical shape. With fewer points, the results might not be identical to the Divider and Equation methods, whose shape and size does not depend upon the number of points.

4.4 Ellipsoidal Envelopes - Extension to 3D

Returning to the beginning of this section, the dimension of $\boldsymbol{x}_i$ can be increased to three components. This has a practical application in sections with bi-axial bending and axial forces, such as columns in 3D structures. As the three methods described above produce equal results we will continue with the simpler one to implement, the equation method.

The matrix $\boldsymbol{X}$ is still defined by equations (4.4) or (4.6) for the SRSS, or CQC combinations, respectively. The eigenvalues, as defined above, are the square values of the semi-axes of the resultant geometrical form called an ellipsoid. When ordered, they are labeled: a, b, and c. Using two angles α and β and making them vary in the respective ranges: $-\pi/2 < \alpha < \pi/2$ and $0 < \beta < 2\pi$, any point of the ellipsoid is defined in its principal axes by a vector $\boldsymbol{y}$:

$$\begin{cases} y_1 = a\cos(\alpha)\cos(\beta) \\ y_2 = b\cos(\alpha)\sin(\beta) \\ y_3 = c\sin(\alpha) \end{cases} \tag{4.32}$$

To write this vector $\boldsymbol{y}$ in the global coordinates, we need to define the ellipsoid principal directions with the vectors: $\boldsymbol{v_i} = \sum_{k=1}^{3} V_{ki}\boldsymbol{e_k}$, which correspond to the individual columns of the matrix $\boldsymbol{V}$.

With them $\boldsymbol{y}$ is simply given by:

$$\boldsymbol{y} = y_1\boldsymbol{v_1} + y_2\boldsymbol{v_2} + y_3\boldsymbol{v_3} = \sum_{i=1}^{3} y_i\boldsymbol{v_i} \tag{4.33}$$

To write this in the form of a vector $\boldsymbol{x}$ associated with the global unit vectors, $\boldsymbol{e_k}$, it results that:

$$\sum_{k=1}^{3} x_k\boldsymbol{e_k} = \sum_{i=1}^{3} y_i\boldsymbol{v_i} = \sum_{i=1}^{3}\sum_{k=1}^{3} y_i V_{ki}\boldsymbol{e_k} \tag{4.34}$$

Finally, the k-th element of $\boldsymbol{x}$ is:

$$x_k = \sum_{i=1}^{3} y_i V_{ki} \tag{4.35}$$

Doing this to an extensive number of combinations of the angles α and β materializes the 3D shape of the ellipsoid.

4.4.1 Computational Implementation

Once again this section is intended to clarify the construction of the elliptical envelope based on a simple example. Since this is a complex 3D form two ways will be presented to ease its visualization: one by projecting it in the coordinate planes and the other by intersecting it with a set of horizontal planes.

We will resort to the four-story structure with different spans in each direction described in Figure 4.15. The materials are also specified in the Figure and the loads are the following: $28.58\ \mathrm{kN/m}$ for beams aligned with x and $30.30\ \mathrm{kN/m}$ for beams aligned with y. The calculation of these values is based on re-partition coefficients and will be further explained in Chapter 6 for a more complex structure.

This structure has five relevant modes, the ones necessary to sum 90% of the total mass of the structure in both directions. Their periods and configurations are in Figure 4.16.

In order of increasing frequency appear the translation modes in y and x, the torsional mode (that does not increase the accumulated effective modal mass in neither direction) and finally the translation second order modes with one inflection point.

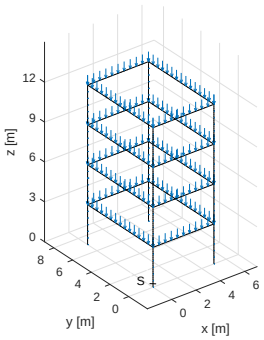

concrete	C30/37
steel	A500
columns	0.3×0.3 m^2
beams	0.3×0.6 m^2
story height	3 m
span x	5 m
span y	7 m
p_x	28.58 kN/m
p_y	30.30 kN/m

Figure 4.15: 3D Structure Description.

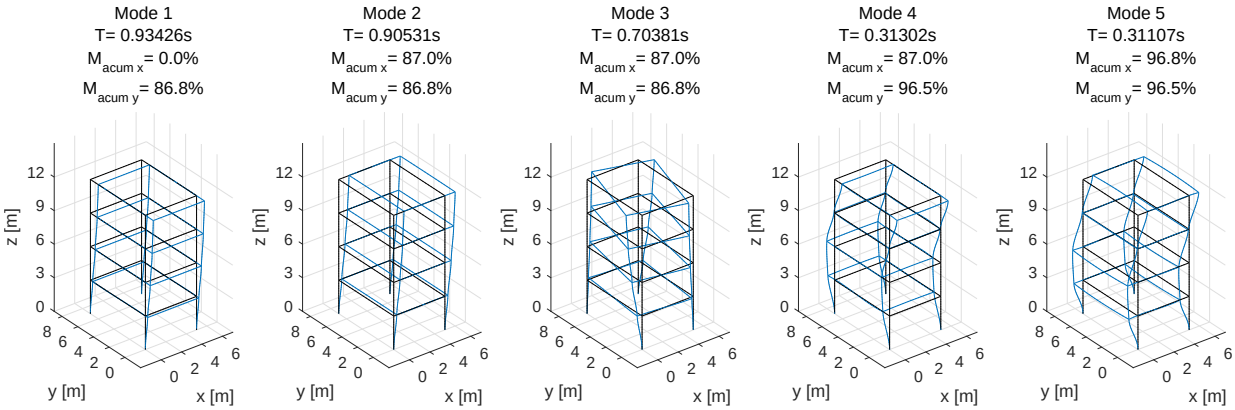

Figure 4.16: 3D Structure Modes.

For the base section of the column in the $(0,0,0)$ position each mode, i, and earthquake direction, k, is separately analyzed gathering all the stress-resultants in the matrix:

$$\boldsymbol{X_{ik}} = \begin{bmatrix} {M_{2ik}}^2 & M_{2ik}M_{3ik} & M_{2ik}N_{ik} \\ M_{2ik}M_{3ik} & {M_{3ik}}^2 & M_{3ik}N_{ik} \\ M_{2ik}N_{ik} & M_{3ik}N_{ik} & {N_{ik}}^2 \end{bmatrix} \tag{4.36}$$

With the values M_{2ik}, M_{3ik} and N_{ik} it is simple to plot the straight lines in a coordinate space representing the viable stress-resultant combinations. Figure 4.17 plots the mode lines for the two earthquakes acting according to the directions x and y. The first and second translation modes are represented for each direction and the rotation mode (the third) that has no representation.

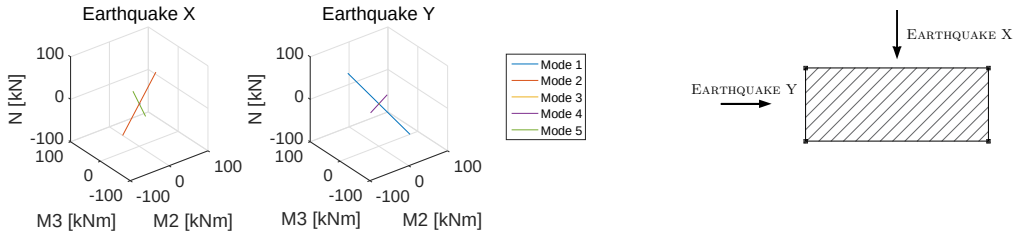

Figure 4.17: Representation of each mode.

We begin the ellipsoid construction by combining the modes using the CQC combination, for each direction k of the earthquake. This combination is described in equation (4.6), that is here reproduced:

$$\boldsymbol{X_k} = \sum_{i=1}^{n}\sum_{j=1}^{n} \mu_{ij}\ \boldsymbol{x_{ik}}\ \boldsymbol{x_{jk}^T}$$

As explained in the beginning of section 4.4 we will calculate the envelopes coordinates in its principal directions, defining a matrix $\boldsymbol{Y}$, and then realign it with the ellipsoid principal directions. To combine the two earthquake directions we sum the two response matrices:

$$\boldsymbol{X} = \sum_{k=1}^{2} \boldsymbol{X_k} \tag{4.37}$$

This simulates the SRSS combination because the summed identities are square values that will be subjected to a square root operation when calculating the ellipsoid semi-axes.

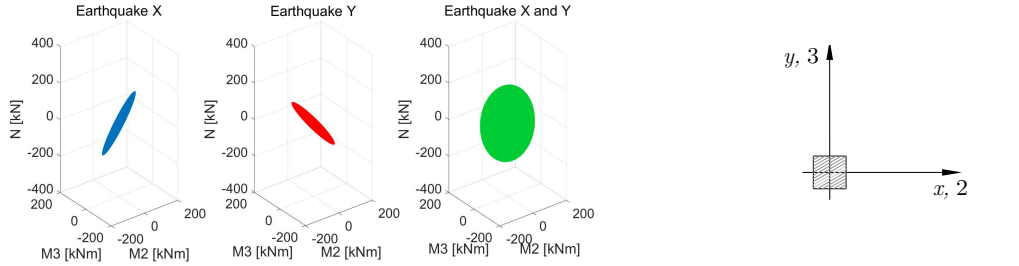

(a) 3D Views

(b) Correspondence (x,y) - $(2,3)$

Figure 4.18: Ellipsoid for X and Y direction and the Total.

Figure 4.18 displays the ellipsoids for each separate seismic direction and the total envelope. We remark that the z direction is not included but could be addressed in a similar manner. Given how difficult it is to interpret these figures in 3D, they will be complemented to ease their visualization.

Firstly, they will be projected in the three coordinate planes. We begin by subdividing the matrix $\boldsymbol{X}$ (or $\boldsymbol{X_k}$), which is achieved by isolating a pair of stress-resultants. For example, taking the bottom right corner of the $\boldsymbol{X}$ matrix we have:

$$\boldsymbol{P_{M_3N}} = \begin{bmatrix} {M_3}^2 & M_3N \\ M_3N & N^2 \end{bmatrix} \tag{4.38}$$

This returns to the formulation of an ellipse, which can be defined in a similar way to what was done in subsection 4.3.3:

$$\boldsymbol{x}^T \boldsymbol{P}^{-1} \boldsymbol{x} = 1 \tag{4.39}$$

Where $\boldsymbol{x} = [x_1, x_2]^T$, and can also be written as $\boldsymbol{x} = [r\cos(\theta), r\sin(\theta)]^T$. Furthermore, naming three new constants $A = \boldsymbol{P}^{-1}_{[1,1]}$, $B = \boldsymbol{P}^{-1}_{[1,2]}$ and $C = \boldsymbol{P}^{-1}_{[2,2]}$ and introducing them in the equation above, we get:

$$r(\theta) = \pm\sqrt{\frac{1}{A\cos^2\theta + 2B\sin\theta\cos\theta + C\sin^2\theta}} \tag{4.40}$$

Plotting all the realizations of $r(\theta)$ we generate the graphs in Figure 4.19. The matrix $\boldsymbol{P_{M_3N}}$ originates the green exterior line representing the total envelope in the first graph, which portrays the (M_3-N) coordinate space.

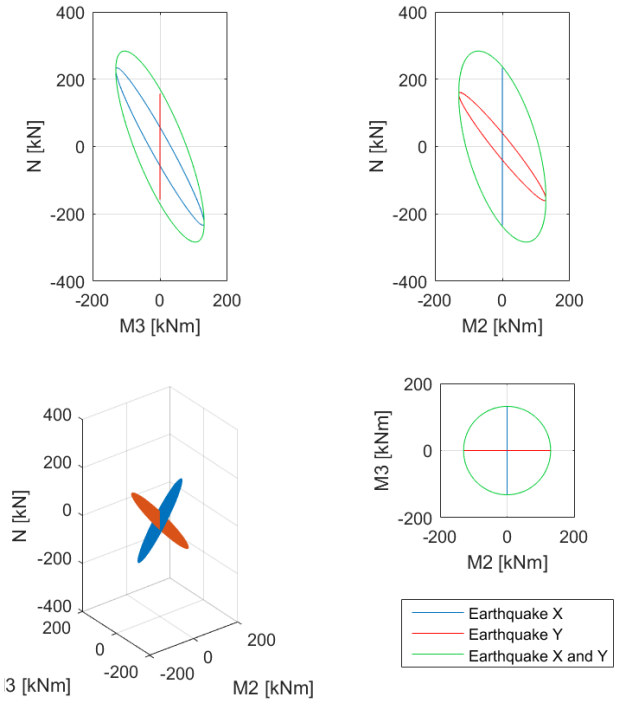

Figure 4.19: Ellipsoid projections.

Given the symmetry of the structure, each earthquake direction only produces one bending moment in the column. This results in the straight lines with a null coordinate in each $(M_i - N)$ graphic and the two ones in the $(M_2 - M_3)$ space. On the other hand, there is a strong correlation between the axial force and the bending moment produced by each direction, which is expressed by the narrow ellipses in the $(M_i - N)$ representations. The ellipsoid for the y direction reaches smaller values of N because its span is larger than the one oriented along x.

An alternative way to simplify the visualization of the ellipsoids is to intersect them with horizontal planes ($N = \text{Const.}$) and plot the resulting contour.

The matrix $\boldsymbol{X}$ formerly introduced has the stress-resultants complete characterization after the modes and directions are combined. Using this matrix in the ellipse definition already used in equation (4.39), and subdividing $\boldsymbol{X}^{-1}$:

$$\begin{bmatrix} M_2 & M_3 & N \end{bmatrix} \left[\begin{array}{cc|c} \multicolumn{2}{c|}{\boldsymbol{C_{MM}}} & \boldsymbol{c_{MN}} \\ \hline \multicolumn{2}{c|}{\boldsymbol{c_{MN}}^T} & C_{NN} \end{array}\right] \begin{bmatrix} M_2 \\ M_3 \\ N \end{bmatrix} = 1 \tag{4.41}$$

Defining $\boldsymbol{m} = [M_2, M_3]^T$ we can expand the previous equation to:

$$\boldsymbol{m}^T \boldsymbol{C_{MM}} \boldsymbol{m} + N \boldsymbol{c_{MN}}^T \boldsymbol{m} + \boldsymbol{m}^T \boldsymbol{c_{MN}} N + N C_{NN} N = 1 \tag{4.42}$$

At the same time, for a given value of N, the intersection ellipse can be described as follows, where $\boldsymbol{m_0}$ is a vector with the center coordinates and ${R_0}^2$ is an equivalent semi-axis:

$$\begin{aligned}&(\boldsymbol{m}^T - \boldsymbol{m_0}^T)\boldsymbol{C_{MM}}(\boldsymbol{m} - \boldsymbol{m_0}) = {R_0}^2\\&\boldsymbol{m}^T\boldsymbol{C_{MM}}\boldsymbol{m} - \boldsymbol{m_0}^T\boldsymbol{C_{MM}}\boldsymbol{m} - \boldsymbol{m}^T\boldsymbol{C_{MM}}\boldsymbol{m_0} + \boldsymbol{m_0}^T\boldsymbol{C_{MM}}\boldsymbol{m_0} = {R_0}^2\end{aligned} \tag{4.43}$$

In order for equations (4.42) and (4.43) to be identical we find two conditions that $\boldsymbol{m_0}$ and R_0 must fulfill. From the equality of the second and third terms of the left side of each equation (note that the third term is the transpose of the second one), we write:

$$N{\boldsymbol{c_{MN}}}^T = -\boldsymbol{m_0}^T\boldsymbol{C_{MM}} \tag{4.44}$$

which after transposing and taking into account the symmetry of $\boldsymbol{C_{MM}}$ provides:

$$\boldsymbol{m_0} = -\boldsymbol{C_{MM}}^{-1}\boldsymbol{c_{MN}}N \tag{4.45}$$

On the other hand, from the identity of the terms independent of $\boldsymbol{m}$, in equations (4.42) and (4.43), we get:

$$\begin{aligned}&{R_0}^2 - \boldsymbol{m_0}^T\boldsymbol{C_{MM}}\boldsymbol{m_0} = 1 - NC_{NN}N\\&{R_0}^2 = 1 - NC_{NN}N + \boldsymbol{m_0}^T\boldsymbol{C_{MM}}\boldsymbol{m_0}\end{aligned} \tag{4.46}$$

Having $\boldsymbol{m_0}$ and ${R_0}^2$ properly defined the intersection ellipse can be formalized as:

$$(\boldsymbol{m}^T - \boldsymbol{m_0}^T)\frac{\boldsymbol{C_{MM}}}{{R_0}^2}(\boldsymbol{m} - \boldsymbol{m_0}) = 1 \tag{4.47}$$

Given the similarity between this and equation (4.39), the same relations can be used to define the two ellipse coordinates for each value of θ.

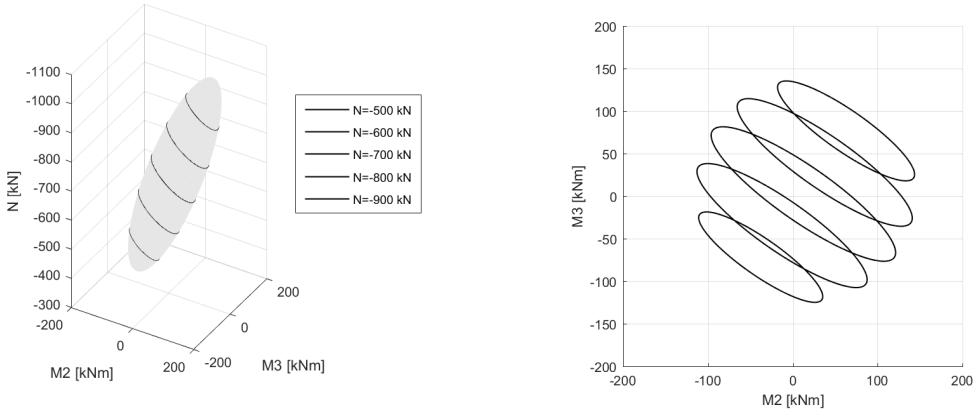

(a) 3D View

(b) Top View

Figure 4.20: Ellipsoid sections.

In Figure 4.20 (a) is displayed the final ellipsoid with the elliptical intersections in black. The N axis is reversed and the ellipsoid is centered in the static stress-resultants coordinates ($N = -710$ kN; $M_2 = 15.02$ kNm; $M_3 = 6.18$ kNm) rather than the origin. The Figure 4.20 (b) clearly portrays the orientation and inclination of this 3D geometrical form in space.

To continue with the design of a reinforced concrete section subjected to a dynamic excitation is necessary to overlay a capacity surface to the interaction envelope developed so far. Consequently, the assembly of capacity surfaces is the topic addressed in the next Chapter.

4.5 Equivalent Static Forces

In this section we develop a different methodology for calculating the effects of the seismic action, based on equivalent static forces.

The main goal of this approach is to avoid constructing an interaction matrix of stress-resultants and an ellipsoid for every section being designed. This method does so by calculating a set of static forces equivalent to a given seismic action. When applied to the structure, these forces will generate stress-resultants in the multiple sections under consideration, calculated by one simple static analysis. Hopefully, these stress-resultants will lead to a simpler (and more conservative) design of the sections, than the one based on the section interaction matrices.

Besides being a simpler analysis, what this method loses in accurately describing the seismic action it gains in providing a better physical understanding of the structural behavior.

4.5.1 The 2D Case

When studying the equivalent static forces in a 2D structure it is appropriate to base the calculations on the column shear forces. In a simple and regular structure, it is possible to define the shear forces of a floor as the sum of all the individual contributions of the columns in that given floor.

To calculate the equivalent forces one first performs a standard dynamic analysis based on response spectra. This provides the shear forces of all the columns in each vibration mode.

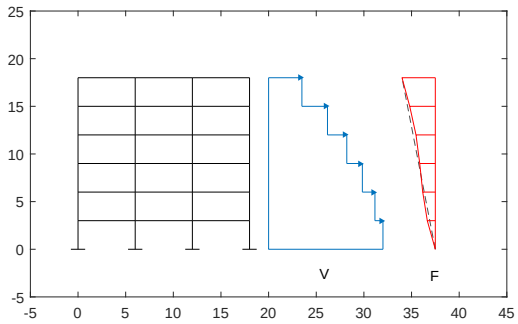

Figure 4.21: Shear Forces - Combined V.

One common procedure in the design of 2D frames is to sum the shear forces of all the columns in

a given floor for each vibration mode, and after combine them with a CQC combination. This results in a single shear value for each floor.

Between floors, the shear forces have a constant value, which are plotted in blue in Figure 4.21 for a generic structure. The differences between the shear forces of consecutive floors can be understood as the equivalent static forces that simulate the effect of the seismic action. As it can be seen in Figure 4.21, these forces, plotted in red, follow the typical inverted triangle, in gray.

To this approach is given the name of "Combined V" because the CQC combination is applied to shear forces.

A different method to estimate the equivalent forces is to start by calculating forces (differences of sequential shear values) in every mode and only after combining them with the CQC combination. This will be called the "Combined F version". The two sequences of calculations are summarized in Table 4.2.

Table 4.2: Comparison of sequences to calculate Equivalent Forces.

Calculate total shear forces in each floor for each mode	
↙	↘
CQC combination of shear forces in each mode	Diferences between floors
Diferences between floors	CQC combination of equivalent forces in each mode
Obtain Equivalent Forces	Obtain Equivalent Forces
↓	↓
Combined V	Combined F

These two methods to calculate equivalent static forces in 2D will be applied to an example and compared in Chapter 6.

4.5.2 The 3D Case

The extrapolation of these methods to calculate equivalent forces in a 3D structure is not immediate.

In 3D dynamic analysis are commonly applied two separate earthquakes: one aligned with the direction x and the other with y. To recreate each of these earthquakes, the 3D structure has to be loaded with forces in the two directions x and y plus a torsional moment, at each floor. This is schematically shown in Figure 4.22, for the earthquake aligned with x.

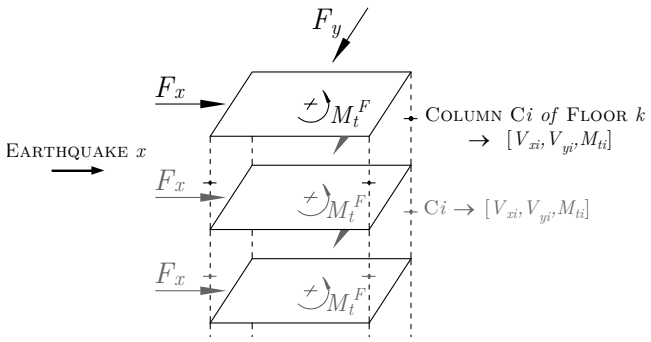

Figure 4.22: 3D Equivalent Static Forces and Stress-resultants of the Columns.

Doing a dynamic analysis based on response spectra, we calculate the stress-resultants for each column of the structure and for each vibration mode.

At the level of each floor k and for each vibration mode j, the total shear forces and torsional moments are calculated by adding the contributions of each column, i, of that floor:

$$\begin{aligned} V_x &= \sum_{i=1}^{n\ columns} V_{xi} \quad ; \quad V_y = \sum_{i=1}^{n\ columns} V_{yi} \\ {M_t}^V &= \sum_{i=1}^{n\ columns} (M_{ti} - V_{xi} y_i + V_{yi} x_i) \end{aligned} \tag{4.48}$$

Where x_i and y_i are the columns coordinates in any given referential. For convenience we put the referential origin in the stiffness center, to be introduced later. In these equations V_{xi}, V_{yi} and M_{ti} are the columns stress-resultants.

Afterward, the values calculated for each floor are combined with the CQC combination. Finally, for each floor, k, is created a correlation matrix $\boldsymbol{X}$, with the variables V_x, V_y and ${M_t}^V$. Note that these matrices have the same formal structure than the ones previously used to define the interaction envelopes in terms of M_2, M_3 and N.

$$\boldsymbol{X_k} = \begin{bmatrix} {V_x}^2 & V_x V_y & V_x {M_t}^V \\ V_x V_y & {V_y}^2 & V_y {M_t}^V \\ V_x {M_t}^V & V_y {M_t}^V & {M_t}^{V\,2} \end{bmatrix} \tag{4.49}$$

These matrices have a graphic representation determined by the same procedure detailed above. These geometric figures are also ellipsoids and each point over that surface is a trio $[V_x, V_y, {M_t}^V]$, developed at the floor k and caused by a seismic action along one direction.

The principle of the equivalent static forces is to choose one of these trios to represent the entire seismic action. For the orientation of the earthquake applied, in this case is the direction x, we plot the ellipsoid and determine the point with the maximum value of V_x, see Figure 4.23. For an earthquake acting along the direction y is searched the point with the maximum V_y.

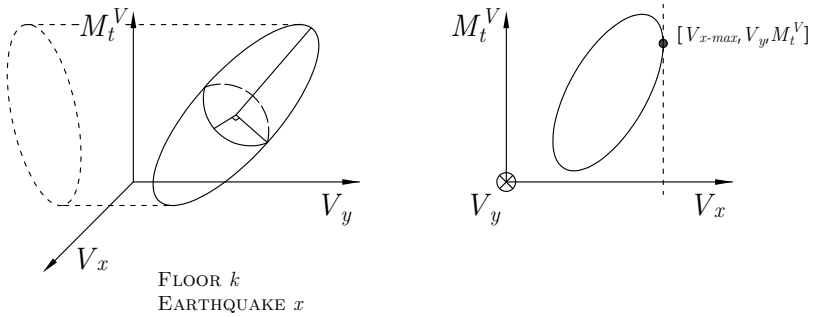

Figure 4.23: Trio of Equivalent Forces.

Obtaining the trios for each floor, and calculating the differences between them generates a set of equivalent forces $[F_x, F_y, {M_t}^F]$ that simulate the effect of each earthquake direction. Note this follows

the principle of the Combined V method used in 2D because it is the least conservative one (which will be shown in Chapter 6).

The two sets of equivalent forces are then applied to the structure in two separate static analysis (one for each seismic direction).

Once the forces are calculated for each floor arises the question of how to apply them to the model described in Chapter 3, which does not enforce the rigid floor explicitly. A possible solution is to decompose them into pairs of forces applied to each node of the structure. These forces are calculated with the following equations, see Mendes and Pedro [27]:

$$\begin{aligned} F_{xi} &= \frac{K_{xi}}{\sum(K_{xj})}F_x - \frac{K_{xi}y_i}{\sum(K_{yj}{x_j}^2 + K_{xj}{y_j}^2)}{M_t}^V \\ F_{yi} &= \frac{K_{yi}}{\sum(K_{yj})}F_y + \frac{K_{yi}x_i}{\sum(K_{yj}{x_j}^2 + K_{xj}{y_j}^2)}{M_t}^V \end{aligned} \tag{4.50}$$

where i identifies a column, K_{xi} and K_{yi} are values proportional to the columns lateral bending stiffness and x_i and y_i are its coordinates relative to their stiffness center. For consistency this was the referential used in equation (4.48).

In a simple structure were all the columns are identical and have equal stiffness, $K_x = K_y$, the expressions above can be condensed to:

$$\begin{aligned} F_{xi} &= \frac{1}{n_c}F_x - \frac{y_i}{\sum({x_j}^2 + {y_j}^2)}{M_t}^V \\ F_{yi} &= \frac{1}{n_c}F_y + \frac{x_i}{\sum({x_j}^2 + {y_j}^2)}{M_t}^V \end{aligned} \tag{4.51}$$

where n_c is the number of columns in each floor.

These sets of nodal forces calculated for each seismic direction are applied separately to the structure and generate stress-resultants. We remark that until this phase it is not relevant which sections of the structure we want to detail. We will now address how to use these results in the design of the cross-sections.

The values M_2, M_3 and N calculated for the desired section are gathered in the vectors $\boldsymbol{p_x}$ and $\boldsymbol{p_y}$. For each seismic direction, the possible combinations of stress-resultants are the ones over the lines that join the point defined by p to its symmetric. These are the colored lines in Figure 4.24.

However, these two lines are not sufficient to assess the safety of the cross-section. To do so is necessary to recreate an ellipse that combines the information of both seismic directions applying the principle of an SRSS combination. Note that it is only possible to recreate an ellipse and not the entire ellipsoid.

This ellipse in contained in an inclined plane in the 3D coordinate space and is defined by its normal vector:

$$\boldsymbol{n} = \frac{\boldsymbol{p_x} \times \boldsymbol{p_y}}{|\boldsymbol{p_x} \times \boldsymbol{p_y}|} \tag{4.52}$$

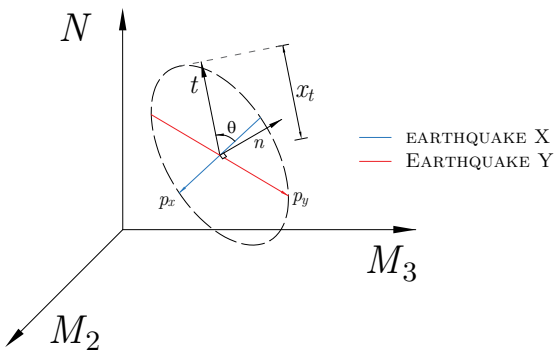

Figure 4.24: Result of the Static Analysis.

Applying a rotation θ about this normal vector, $\boldsymbol{n}$, defines multiple directions $\boldsymbol{t}$, each associated with a distance x_t. This distance is defines as:

$$x_t = \sqrt{(\boldsymbol{p_x}^T \boldsymbol{t})^2 + (\boldsymbol{p_y}^T \boldsymbol{t})^2} \tag{4.53}$$

The distances x_t have the same geometrical interpretation as previously: it is the maximum distance any point of the ellipse can have when is projected in the direction $\boldsymbol{t}$, and not necessarily a point of the envelope. To recreate the ellipse we resort to the intersection method described in subsection 4.3.1. It uses two rotations θ_A and θ_B to calculate one point of the envelope, p_{int}:

$$\begin{aligned} \boldsymbol{p_{int}} &= x_{tA}\boldsymbol{t_A} + k_A \boldsymbol{n_A} \\ k_A &= \frac{x_{t_B} - x_{t_A}(\boldsymbol{t_A}^T \boldsymbol{t_B})}{\boldsymbol{n_A}^T \boldsymbol{t_B}} \end{aligned} \tag{4.54}$$

These are the same expressions, although in this case the definition of $\boldsymbol{n_A}$ is not immediate. See the construction in Figure 4.25, with $\boldsymbol{x_1} = \frac{\boldsymbol{p_x}}{|\boldsymbol{p_x}|}$ and $\boldsymbol{x_2} = \boldsymbol{n} \times \boldsymbol{x_1}$.

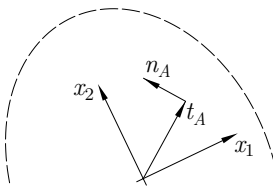

Figure 4.25: Definition of $\boldsymbol{n_A}$.

With $\boldsymbol{x_1}$ and $\boldsymbol{x_2}$ being a set of coordinate axis over the ellipse plane, it is possible to define two conditions for $\boldsymbol{n_A}$: one being $\boldsymbol{n_A} \cdot \boldsymbol{t_A} = 0$ and the other $\boldsymbol{n_A} = \alpha \boldsymbol{x_1} + \beta \boldsymbol{x_2}$.

From this it yields that:

$$\begin{aligned} &\alpha(\boldsymbol{x_1}^T \boldsymbol{t_A}) + \beta(\boldsymbol{x_2}^T \boldsymbol{t_A}) = 0 \\ &\alpha = -\frac{\beta(\boldsymbol{x_2}^T \boldsymbol{t_A})}{\boldsymbol{x_1}^T \boldsymbol{t_A}} \end{aligned} \tag{4.55}$$

Finally, as $\boldsymbol{n_A}$ is a unit vector, one first takes $\beta = 1$ to calculate α and then the resulting vector $\boldsymbol{n_A} = \alpha \boldsymbol{x_1} + \boldsymbol{x_2}$ is normalized.

Given that the correlation of directions is done with the SRSS combination, it can also be done by the other methods described, which resort to an interaction matrix.

With $\boldsymbol{t}$ representing any direction in a 3D coordinate space, we can write that:

$$x_t{}^2 = \boldsymbol{t}^T \boldsymbol{p_x} \boldsymbol{p_x}^T \boldsymbol{t} + \boldsymbol{t}^T \boldsymbol{p_y} \boldsymbol{p_y}^T \boldsymbol{t} \tag{4.56}$$

Which corresponds to having the following correlation matrix $\boldsymbol{X}$:

$$\boldsymbol{X} = \begin{bmatrix} p_{x1}^2 + p_{y1}^2 & p_{x1}p_{x2} + p_{y1}p_{y2} & p_{x1}p_{x3} + p_{y1}p_{y3} \\ p_{x1}p_{x2} + p_{y1}p_{y2} & p_{x2}^2 + p_{y2}^2 & p_{x2}p_{x3} + p_{y2}p_{y3} \\ p_{x1}p_{x3} + p_{y1}p_{y3} & p_{x2}p_{x3} + p_{y2}p_{y3} & p_{x3}^2 + p_{y3}^2 \end{bmatrix} \tag{4.57}$$

Following the principle of the equation method, an eigenvalue and vector analysis easily presents the semi-axes of the ellipse and its principal directions. Clearly, one of these semi-axes is equal to zero and the others are the square roots of the eigenvalues. Naming these two semi-axes as r_{max} and r_{min} and recalling equation (4.25):

$$\frac{{t_1}^2}{{r_{max}}^2} + \frac{{t_2}^2}{{r_{min}}^2} = 1$$

it is simple to calculate the coordinates of the ellipse in a 2D plane $(t_1 - t_2)$. Afterward, it has to be aligned with its principal directions in the 3D space, see Figure 4.26.

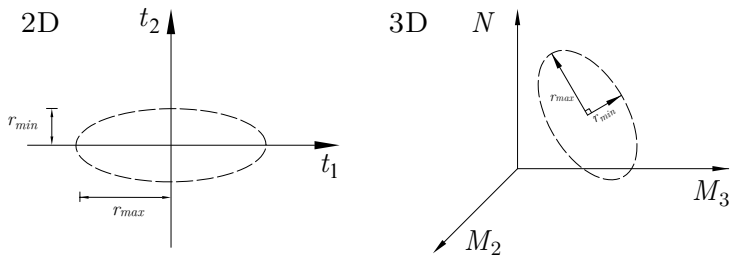

Figure 4.26: Equation method: Ellipse semi-axes.

In Chapter 6 the resultant ellipse will be exemplified and compared to the complete interaction ellipsoid, in particular, its semi-axes calculated by this method.

Chapter 5

Resistant Interaction Surfaces

This Chapter will proceed with the detailing of the implemented computational solution, now with the focus on the construction of resistant curves for a cross-section.

Such curves are conceived for the 2D and 3D cases allowing the overlapping of action and resistant representations, which assists the design of a reinforced concrete section. This has a particular benefit once it is not clear from the beginning which point of the envelope will compromise the design.

Lastly, will be particularized a method to analyze combined foundations from both perspectives: action and resistance, again for the purpose of verifying its safety.

5.1 Resistant Curves

5.1.1 Materials

The reinforced concrete resistant curves will be reproduced in a $(M_i - N)$ coordinated space. All the 2D and the 3D examples explored in this dissertation consider the same materials.

The materials chosen and its properties (notable values of stresses, strains and the Elasticity modulus) are summarized in Table 5.1.

Table 5.1: Material properties.

A500	C30/37
$\varepsilon_{ud} = 0.01$	$\varepsilon_{cu2} = -0.0035$
$\varepsilon_{yd} = 2.1753 \times 10^{-3}$	$\varepsilon_{c2} = -0.002$
$f_{yd} = 435 \times 10^{+3}\ \mathrm{kN/m^2}$	$f_{cd} = 20 \times 10^{+3}\ \mathrm{kN/m^2}$
$E_s = 200 \times 10^{+6}\ \mathrm{kN/m^2}$	$E_c = 33 \times 10^{+6}\ \mathrm{kN/m^2}$

For steel it is assumed an elastic perfectly plastic diagram, see Figure 5.1. To calculate stresses and forces in a steel bar of area A_s are used the expressions:

$$\sigma_s = \min\left(|\varepsilon_s \times E_s|, f_{yd}\right) \times \mathrm{sgn}(\varepsilon_s) \quad \Rightarrow \quad F_s = \sigma_s A_s \tag{5.1}$$

where sgn(ε_s) is a function equal to 1 or -1 depending on the signal of ε_s.

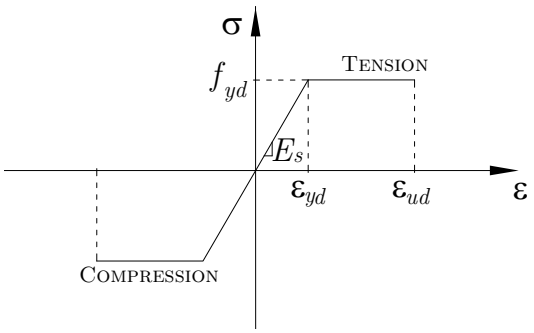

Figure 5.1: Stress-strain diagram of steel.

For concrete it is possible to use a parabolic-rectangular diagram, described in equation (5.2), or a simplified rectangular stress block diagram, see Figure 5.2 (a) and (b). We use the first for the 3D curves and the second for the 2D ones to illustrate both material models.

$$\sigma_c = \begin{cases} f_{cd} & \text{if} \quad \varepsilon_c < \varepsilon_{c2} \\ f_{cd}\left[1-\left(1-\frac{\varepsilon_c}{\varepsilon_{c2}}\right)^2\right] & \text{if} \quad 0 > \varepsilon_c \geqslant \varepsilon_{c2} \\ 0 & \text{if} \quad \varepsilon_c \geqslant 0 \end{cases} \quad \Rightarrow \quad F_c = \sigma_c A_c \tag{5.2}$$

In this equation A_c is the area of a steel element of concrete or of a uniformly stressed area.

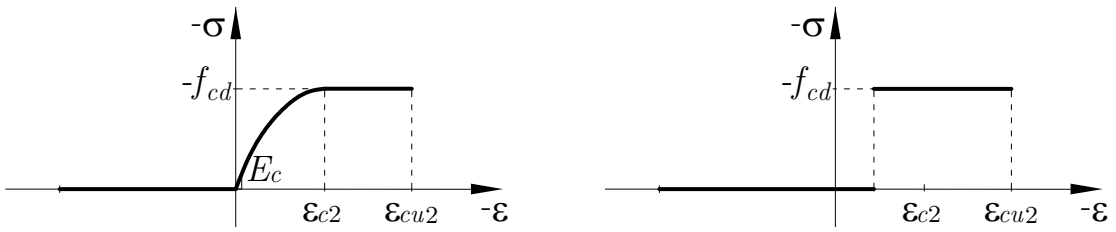

(a) Parabolic-rectangular (b) Rectangular stress block

Figure 5.2: Stress-strain diagram of concrete.

5.1.2 2D Interaction curves

The geometry of a rectangular reinforced concrete section is defined in Figure 5.3. The geometric variables are the dimensions b, h and a cover, c, the distance from the center of the steel bars to the exterior, all measured in [m]. To each total percentage of reinforcement, w_{tot}, corresponds a curve in Figure 5.4 varying the neutral axis position, x_{NA}, from the bottom to the top of the cross-section, even beyond its h dimension to cover the pure tension and pure compression cases.

The area of steel in each extremity, in [m^2], is half of the total: $As = w_{tot} h b \frac{fcd}{fyd} \times \frac{1}{2}$.

Given the symmetry of the cross-section, it is always assumed the bending moment is positive, $M > 0$, and therefore the curvature is $\chi > 0$.

For a given position of the neutral axis, we can calculate the maximum curvature that ensures that each point strain is below the limit, ε_{ud} or ε_{cu2} . There are three situations to consider: the tension in the

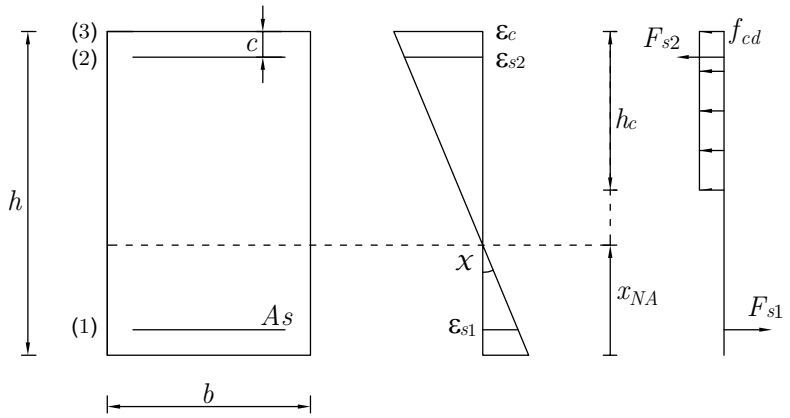

Figure 5.3: Geometry of the 2D cross-section.

steel (1), the compression in the steel (2) and the compression in the concrete (3), that are indicated in the Figure. For each situation the maximum curvature is:

$$\begin{aligned} \chi_{s1} &= \frac{\varepsilon_{ud}}{x_{NA} - c} \\ \chi_{s2} &= \frac{\varepsilon_{ud}}{h - x_{NA} - c} \\ \chi_{c} &= \frac{-\varepsilon_{cu2}}{h - x_{NA}} \end{aligned} \tag{5.3}$$

The second one is added for completion, although it is probably not relevant. The real curvature, χ, applied to the structure can only reach the minimum of the positive values described above. With it we can calculate the strains:

$$\begin{aligned} \varepsilon_{s1} &= \chi(x_{NA} - c) \\ \varepsilon_{s2} &= -\chi(h - x_{NA} - c) \\ \varepsilon_{c} &= -\chi(h - x_{NA}) \end{aligned} \tag{5.4}$$

To calculate the resultant force in the concrete a simplified rectangular stress block was used. To do so an auxiliary height was defined $h_c = \min(0.8 \times (h - x_{NA}), h)$, see Figure 5.3, and the corresponding concrete force $F_c = -f_{cd} \times h_c b$. Each steel force, F_{s_1} and F_{s_2}, is obtained by equation (5.1) as explained in the materials subsection. Finally the stress-resultants are calculated by equation (5.5).

$$\begin{aligned} N &= F_c + F_{s_1} + F_{s_2} \\ M &= -F_c \times y_c + F_{s_1} \times y_{s1} - F_{s_2} \times y_{s2} \end{aligned} \tag{5.5}$$

where,

$$\begin{cases} y_c = (h/2) - (h_c/2) \\ y_{s1} = (h/2) - c \\ y_{s2} = (h/2) - c \end{cases} \tag{5.6}$$

Using the reduced axial force $\nu = \frac{N}{bhf_{cd}}$ and the reduced bending moment $\mu = \frac{M}{bh^2 f_{cd}}$ definitions, the dimensionless resistant interaction curves can be plotted, see Figure 5.4.

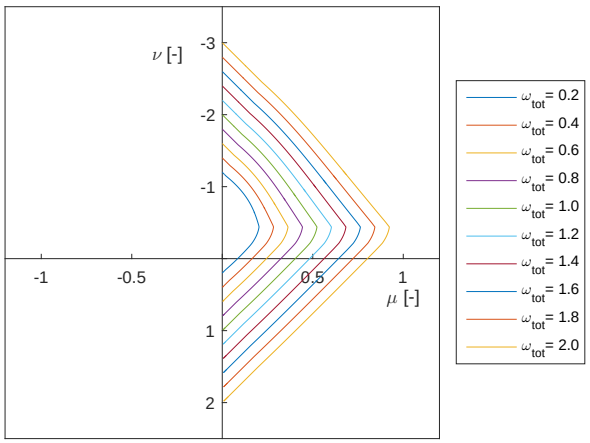

Section	
concrete	C30/37
steel	A500
b	0.3 m
h	0.3 m
c	0.03 m

Figure 5.4: Interaction curves in 2D.

5.1.3 3D Interaction curves

This solution will be obtained numerically and so the cross-section is subdivided in $n_c = 100$ rectangular divisions with concrete properties and $n_s = 16$ circular ones in the contour, simulating the steel bars. The area of each steel division is: $A_{si} = w_{tot} hb \frac{fcd}{fyd} \times \frac{1}{n_s}$. On the other hand, the area of each concrete division is: $A_{ci} = \frac{b}{10}\frac{h}{10}$, both are expressed in [m^2]. The numbering of the divisions and the sign convention is illustrated in Figure 5.5.

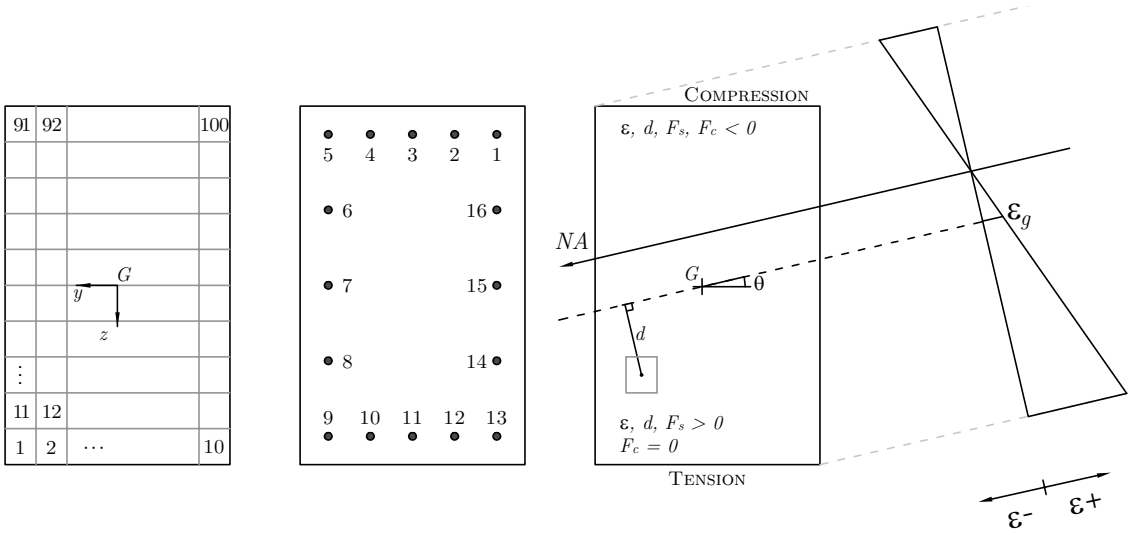

Figure 5.5: Discretization and sign convention.

The neutral axis will be defined by two variables: the counterclockwise angle θ and ε_g, the strain at the origin, G, the geometric center of the cross-section.

Since the representation of the interaction curves of N, M_2 and M_3 is a 3D surface, the intersection

of this surface with horizontal planes will be drawn. These horizontal planes correspond to given values of the axial force, $N = N_p$.

The angle θ will vary in 360° and for each value, will be determined the ε_g that produces the desired axial force of the horizontal plane, N_p.

Initializing the variable $\varepsilon_g = 0$, the process starts by determining the maximum curvature for each element of the discretization. Defining d as the perpendicular distance of each point to a parallel to the neutral axis that passes at G: $d_i = z_i \times \cos\theta - y_i \times \sin\theta$.

The curvatures, χ, are calculated for each material type by:

$$\begin{aligned} \chi_{ci} &= \frac{\varepsilon_{cu2} - \varepsilon_g}{d_i} \\ \chi_{si} &= \frac{\varepsilon_{ud} - \varepsilon_g}{d_i} \end{aligned} \tag{5.7}$$

The maximum curvature possible to apply to the section is the minimum positive value of all the curvatures calculated by (5.7). With the value χ is evaluated the strain of each division:

$$\varepsilon_i = \varepsilon_g + \chi d_i \tag{5.8}$$

To calculate the stress-resultants one uses the expressions in the materials subsection for the forces, F_{ci} and F_{si}, and the following sums:

$$N_{calc} = \sum_{i=1}^{n_c+n_s} f_i \quad ; \quad My_{calc} = \sum_{i=1}^{n_c+n_s} f_i \times z_i \quad ; \quad Mz_{calc} = \sum_{i=1}^{n_c+n_s} f_i \times (-y_i) \tag{5.9}$$

where f_i is defined below, and y_i and z_i follow the same rule.

$$\boldsymbol{f} = \{f_i\} = \left\{ \begin{array}{c} F_{s,i} \\ \vdots \\ F_{s,ns} \\ \hline F_{c,i} \\ \vdots \\ F_{c,nc} \end{array} \right\} \tag{5.10}$$

However, the value of N we calculate, N_{calc}, probably is not the one we where searching for, N_p. Therefore we have to adjust the ε_g, using a Newton method.

$$\varepsilon_{g_{i+1}} = \varepsilon_{g_i} - \frac{N_{calc} - N_p}{EA} \tag{5.11}$$

where EA is the axial stiffness of the cross-section evaluated by:

$$EA = \sum_{ic=1}^{n_c} E_{ci} \times A_{ci} + \sum_{is=1}^{n_s} E_{si} \times A_{si} \tag{5.12}$$

And each value of the Young's modulus E_{ci} and E_{si} has the following definition:

$$E_{si} = \begin{cases} 0.1E_s & \text{if} \quad \sigma_{si} = f_{yd} \\ E_s & \text{if} \quad \sigma_{si} \neq f_{yd} \end{cases} \tag{5.13}$$

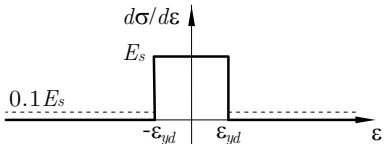

Figure 5.6: Young's modulus of steel.

$$E_{ci} = \begin{cases} 0 & \text{if} \quad \varepsilon_{ci} < \varepsilon_{c2} \\ 2f_{cd}\dfrac{-\varepsilon_{c2} + \varepsilon_{ci}}{\varepsilon_{c2}^2} & \text{if} \quad \varepsilon_{c2} \leqslant \varepsilon_{ci} < 0 \\ 2f_{cd}\dfrac{-\varepsilon_{c2}}{\varepsilon_{c2}^2} & \text{if} \quad 0 \leqslant \varepsilon_{ci} < \varepsilon^\star \\ 0 & \text{if} \quad \varepsilon_{ci} \geqslant \varepsilon^\star \end{cases} \tag{5.14}$$

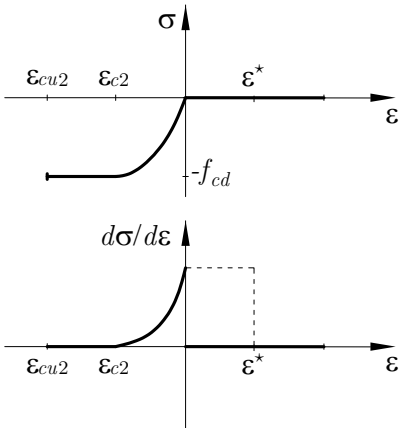

Figure 5.7: Young's modulus of concrete.

It is important to underline that the two moduli of elasticity, $E = \frac{d\sigma}{d\varepsilon}$, are not exactly coherent with the stress-strain diagrams presented in the Materials subsection and presented in bold in Figures 5.6 and 5.7. Given that equation 5.11 calculates the next value of ε_g with the axial stiffness, EA, in the denominator, is used this computational artifice to avoid null numbers of E and thus making convergence easier. In the concrete case we added an auxiliary point $\varepsilon^\star = -\varepsilon_{c2} > 0$. In the interval between 0 and $\varepsilon^\star$, E takes the value of the derivative $\frac{d\sigma}{d\varepsilon}$ in the origin point. The assumed moduli of elasticity are plotted as dotted lines.

The resultant surface, for a particular choice of steel bars, is presented in Figure 5.8. This Figure was made using 37 iterations of θ, in each plane of $N = N_p$ to complete a quarter of the total capacity surface. The maximum number of iterations to approximate the value of ε_g was 32.

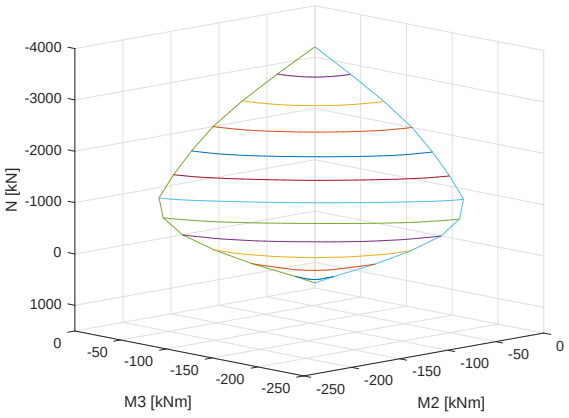

Section	
concrete	C30/37
steel	A500
b	0.3 m
h	0.3 m
c	0.05 m
ω_{tot}	0.78 $(16\phi16)$

Figure 5.8: Interaction curves in 3D.

5.1.4 Safety Assessment

Overlapping the action with the resistant interaction curves that are intersected with the same horizontal planes we have a visual understanding of the safety of a certain section. The same is done in a systematic way by creating two vectors of points that describe the resistant and action curves in polar coordinates (r, θ), for each given value of N_p. This is followed by dividing the plane into sectors centered in each point of the resistant vector, and analyzing if any of the action vector points are within that section. If so we compare all the action point radii in the sector with the radius of the resistant point. Given the case that in all sectors, all action point radii are smaller than the resistant point radius, we can ensure the safety of the cross-section.

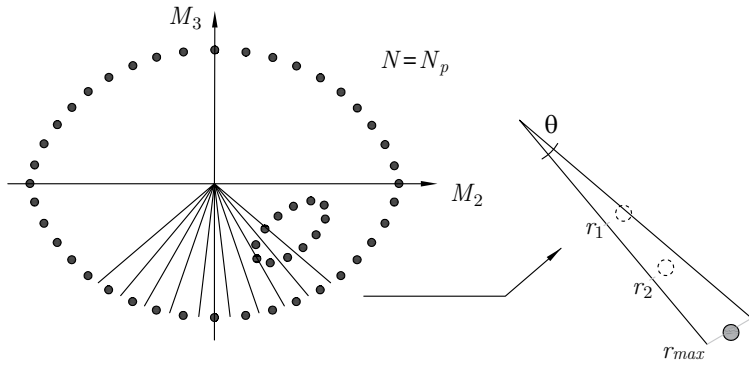

Figure 5.9: Safety verification mechanism.

Additionally, this verification can be done in a cycle that increments the value of w_{tot} allowing to find the optimized solution for the cross-section design. Note the increments do not need to be fixed and can be associated with a specific choice of commercials diameters for the steel bars.

To recap the algorithm presented in this subsection we summarize it in the following Table:

Table 5.2: Safety verification algorithm.

1. Calculate the response ellipsoid $\rightarrow$ Determine the increments of N_p

   2. Initialize $w_{tot} = 0.2$

      3. For each value of N_p $\rightarrow$ Calculate the resistant capacity surface

         4. For each value of θ $\rightarrow$ Is safety verified? $\begin{cases} \text{Yes} \rightarrow \text{ next } \theta \text{ (or } N_p\text{)} \\ \text{No} \rightarrow \text{ increase } \mathrm{w_{tot}} \end{cases}$

            5. When safety is verified for every θ of every N_p $\rightarrow$ w_{tot} is optimized

5.2 Columns with Combined Footing

This is a particular design situation that arises when two columns are located sufficiently close to build a combined footing instead of two individual ones. The main reason to do so is the difficulty in verifying the safety to overturning due to column tension or large bending moments. It also has economical advantages as the construction becomes easier, in particular, the formwork. This elements dimensions are defined in Figure 5.10.

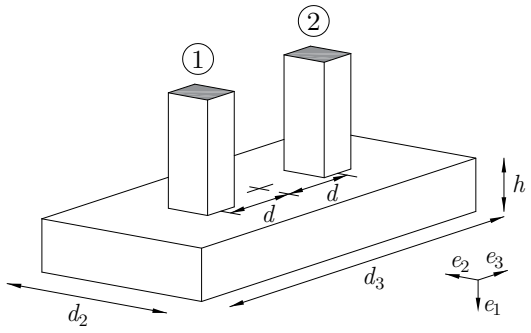

Figure 5.10: Combined footing.

We begin with the stress-resultants in the base of each column for each mode, i, and earthquake direction, k.

$$N_{ik} = N_{1ik} + N_{2ik} + S_W \tag{5.15}$$

$$M3_{ik} = M3_{1ik} + M3_{2ik} \tag{5.16}$$

$$M2_{ik} = M2_{1ik} + M2_{2ik} - N_{1ik} \times d + N_{2ik} \times d \tag{5.17}$$

To correctly evaluate the axial force N_{ik}, the footing self-weight, S_W, must be included.

The next stages are similar to what is done for a single section, assembling a matrix $\boldsymbol{X}$ with the stress-resultants correlated after the modes and directions are combined.

To evaluate the resistance of the footing, we adopt a plastic response of the soil, see Figure 5.11, according to which the stress in the soil can only be null or equal to the maximum value, $\sigma = 0$ or $\sigma = \sigma_{max}$, in [$\mathrm{kN/m^2}$].

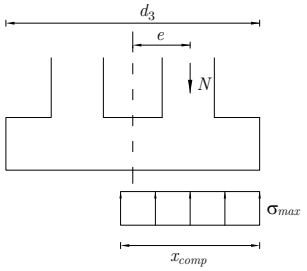

Figure 5.11: Soil model and eccentricity.

If a simple 2D analysis is done, each value of N is related to a compressed dimension x_{comp} and a

corresponding maximum bending moment M_{comp}:

$$x_{comp} = \frac{N}{\sigma_{max} d_2} \tag{5.18}$$

$$M_{comp} < N \times e = N \times \frac{(d_3 - x_{comp})}{2} \quad \Leftrightarrow \quad M_{comp} < \frac{N}{2}\left(d_3 - \frac{N}{\sigma_{max} d_2}\right) \tag{5.19}$$

In addition to this, we can define other criteria such as limiting the eccentricity so that the soil reaction is inside the footing, $e < d_3/2$.

Conversely, for a 3D analysis will be used a computational approach. We start by dividing the footing area in $n_f = 100$ subdivisions, each with the corresponding area, A_f, and defining the coordinates of the center of each subdivision as a vector $\boldsymbol{r_k} = [y_k, z_k]^T$.

To define the neutral axis we use the counterclockwise angle with the horizontal, α, and the distance to the origin, d. A new vector with a normal orientation to the neutral axis can be written as $\boldsymbol{n} = [\cos\alpha, \sin\alpha]^T$, see Figure 5.12.

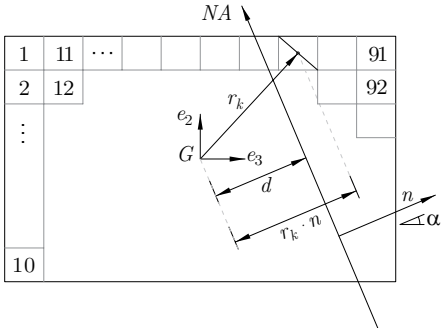

Figure 5.12: Discretization of the combined footing.

The area of each subdivision, A_f, is either considered totally compressed or without contact with the soil. The variable $A_{f,c}$, where the "c" stands for compressed, is equal to A_f when it is completely compressed and 0 in the other case. $A_{f,c}$ can be determined by the following:

$$A_{f,c} = \frac{< \boldsymbol{r_k} \cdot \boldsymbol{n} - d >}{|\boldsymbol{r_k} \cdot \boldsymbol{n} - d|} A_f \tag{5.20}$$

where the operator $< \cdot >$ is described as:

$$< x >= \begin{cases} x & \text{if} \quad x > 0 \\ 0 & \text{if} \quad x < 0 \end{cases} \quad \Leftrightarrow \quad \frac{< x >}{x} = \begin{cases} 1 & \text{if} \quad x > 0 \\ 0 & \text{if} \quad x < 0 \end{cases} \tag{5.21}$$

We will use the same procedure applied above for the cross-section resistant curves and intersect the resistant surface with horizontal planes of specific values of N.

Searching for a specific value of $N = N_p$ is the same as searching for the value of the total compressed area of the footing, $A_p = -N_p/\sigma_{max}$. Note this is not the area of the footing. This area A_p is estimated by the sum of all the $A_{f,c}$, which is a discontinuous function of d. This means that is not possible to approximate the value of $A_c = \sum A_{f,c}$ to A_p with the required precision, as illustrated in Figure 5.13.

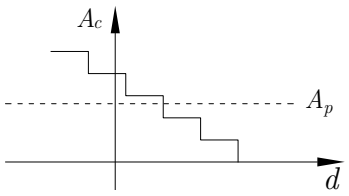

Figure 5.13: Discontinuity of the function $A_c(d)$.

Increasing the number of subdivisions, for example considering all the four corners of each subdivision, would still have the same discontinuity problem. This would correspond to the following equation:

$$A_{f,c} = \sum_{k=1}^{4} \frac{< \boldsymbol{r_k} \cdot \boldsymbol{n} - d >}{|\boldsymbol{r_k} \cdot \boldsymbol{n} - d|} \frac{A_f}{4} \tag{5.22}$$

However, we can take the idea of using the corners in an alternative way, so to get a continuous function:

$$A_{f,c} = \frac{\sum_{k=1}^{4} < \boldsymbol{r_k} \cdot \boldsymbol{n} - d >}{\sum_{k=1}^{4} |\boldsymbol{r_k} \cdot \boldsymbol{n} - d|} A_f \quad \Leftrightarrow \quad A_c = \sum_{f=1}^{n} A_{f,c} \tag{5.23}$$

This allows us to determine the distance d that produces the wanted N_p or $A_p = -N_p/\sigma_{max}$, for each horizontal section and each value of α . We begin with $d = 0$, calculate the compressed area $A_c = A_{calc}$ and then improve the approximation for d.

$$d_{i+1} = d_i - \frac{A_{calc} - A_p}{\frac{\mathrm{d}A}{\mathrm{d}d}} \tag{5.24}$$

where,

$$\frac{d\,A}{d\,d} = -\sqrt{{d_2}^2 + {d_3}^2} \tag{5.25}$$

We use a simplified derivation of $\frac{d\,A}{d\,d}$ that corresponds to the diagonal dimension of the footing in order to get overestimated values. This increases the convergence of the iterative process.

To illustrate the accuracy of the method that estimates the compressed area of each section, we will use a simple square of 1×1 [un.^{2}] and two different values of α, see Figure 5.14. Varying the value of d we plot the two curves in Figure 5.15.

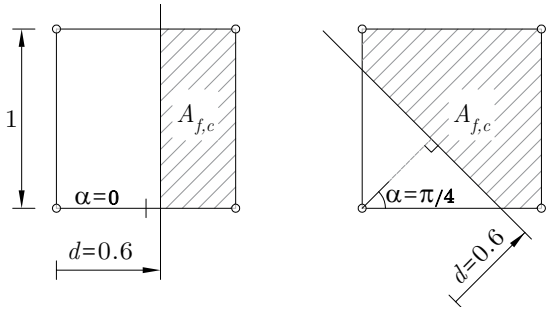

Figure 5.14: Examples used to test the method.

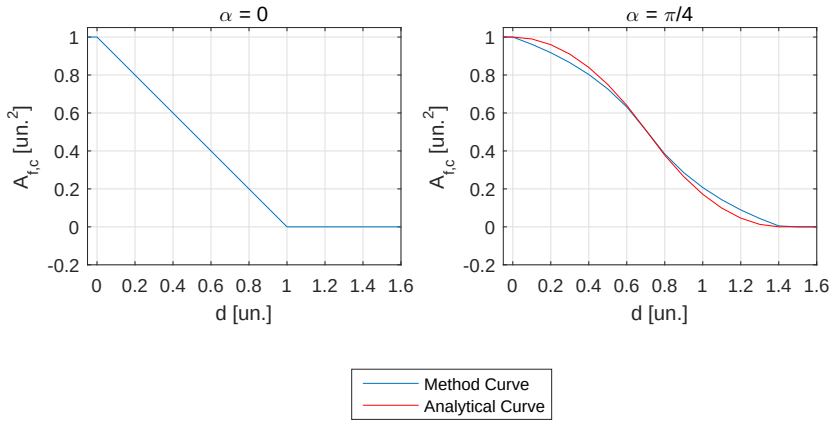

Figure 5.15: Percentage of compressed area.

There is an understandable linear behavior in the first graphic and a non-linear in the second. In the first, the two curves are completely coincident. In the second one, when $d = 0.6\ [\text{un.}]$, the area in tension is a triangle, with a side of $l = 0.6/\cos(\pi/4) = 0.8485\ [\text{un.}]$ and a tensioned area of $l^2/2 = 0.36\ [\text{un.}^2]$. That is why the compressed area is $1 - 0.36 = 0.64\ [\text{un.}^2]$ that is similar to the one in the graphic obtained by the method: $0.63\ [\text{un.}^2]$. For different values of d the errors might be up to 5%, see the red line in the second graphic. In spite of that, the final error in the estimation of N is mitigated by the high number of subdivisions as it properly identifies totally compressed or tensioned subdivisions and has a reasonable approximation for the combined ones.

The method has a practical advantage when different angles α are used to which is not simple to write an analytic expression for the tensioned area.

As an example, Figure 5.16 displays the resistant interaction curve, for four footings with different dimensions, all intersected at the level $N = -2000\ \text{kN}$ (measured at the base of the footing).

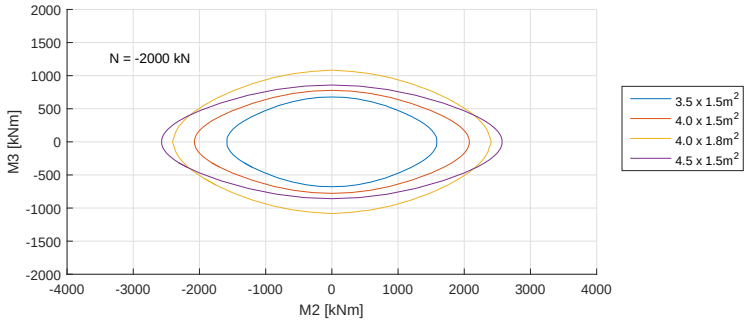

Figure 5.16: Resistant interaction of four footings.

Chapter 6

Results and Discussion

In this Chapter three different structures will be studied to assess the potential of the proposed analysis.

Example 1 resumes the study of the 2D structure considered in Chapter 4 to complete the design phase, with the capacity surface information. Additionally, we proceed to obtain an equivalent static analysis, based on the shear forces.

Example 2 deals with a very simple and symmetrical 3D structure to illustrate the advantages of using the CQC combination.

Finally, in Example 3 one considers a 3D structure featuring two close columns in a non-symmetrical disposition to study the torsional behavior in the interaction envelopes and also the design of a combined footing. The equivalent static analysis will be generalized to 3D.

6.1 Example 1

6.1.1 2D Application

Resorting to the same structure used in Chapter 4 it is now possible to overlap the response interaction envelopes on top of the 2D capacity surface (for combined bending and axial force). The first set of sections analyzed is the base of every column of the first floor ($\mathrm{C1}$, $\mathrm{C7}$, $\mathrm{C13}$ and $\mathrm{C19}$).

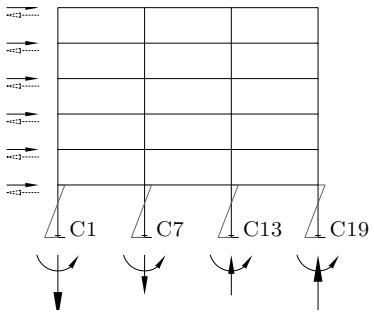

Figure 6.1: Ex1 - First set of columns.

To resist the overturning moment of the seismic action (schematically represented as horizontal forces acting along one direction or the other), the structure has two main mechanisms: bending mo-

ments in the fixed supports and a frame effect, materialized by axial forces with symmetrical signs in each pair of columns, see Figure 6.1.

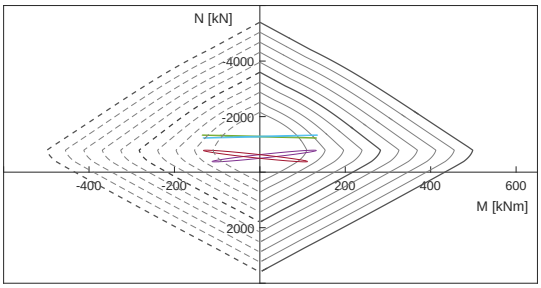

Column	Static M	Static N
1	10.14 kNm	-581.14 kN
7	-1.09 kNm	-1281.86 kN
13	1.09 kNm	-1281.86 kN
19	-10.14 kNm	-581.14 kN

Figure 6.2: Ex1 - General view and Static stress-resultants.

The static stress-resultants are presented because they are the centers of the ellipses. Figure 6.2 displays the classic image of the resistant capacity curves and Figure 6.3 presents a zoomed view of the ellipses.

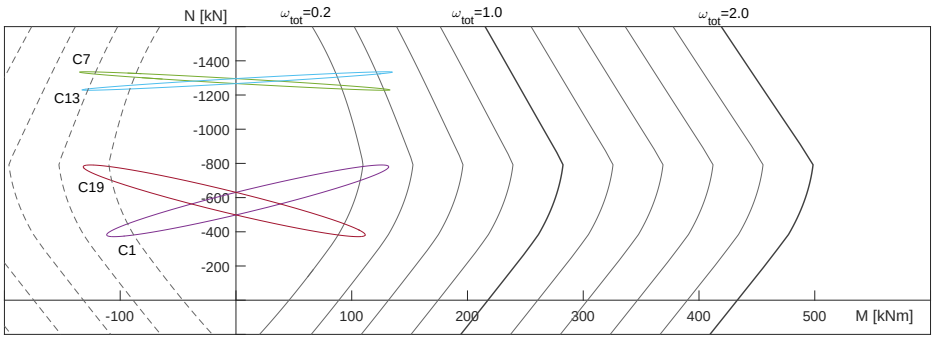

Figure 6.3: Ex1 - Action and resistant interaction curves for columns $\mathrm{C1}$, $\mathrm{C7}$, $\mathrm{C13}$ and $\mathrm{C19}$.

As it can be seen in both figures there is a substantial difference in the static values of N between interior and exterior columns. Additionally, the exterior ones have larger static M that slightly deviate the center of the envelopes, which will influence the design of section $C1$ presented below.

Due to the frame effect, the dynamic action produces a symmetric outcome between the left and right columns: the base sections have equal M combined with symmetric N that create a binary. This phenomenon is predominant in the outside columns which can draw larger values of N, the reason why these ellipses are more tilted.

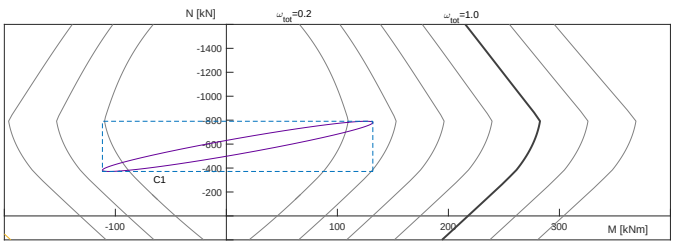

Figure 6.4: Ex1 - Comparison of envelopes for column $C1$.

Column $C1$ is isolated in Figure 6.4 and is added a dashed blue line indicating the rectangular envelope commonly used for design. With this criteria would be necessary to design the section for $\omega_{tot} = 0.4$ ($A_s = 17$ cm^2). Conversely, using the interaction envelope $\omega_{tot} = 0.3$ would suffice which corresponds to an $A_s = 12$ cm^2 that can be materialized with $12\phi12$, allowing a saving of 25%.

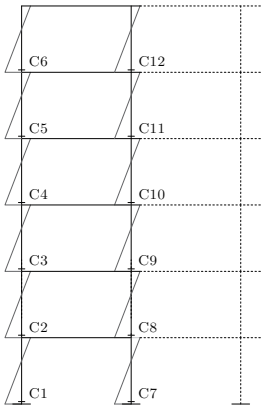

Figure 6.5: Ex1 - Second set of columns.

A different set of columns with an interesting representation is the one with all the columns of the same alignment in height. The two alignments are defined in Figure 6.5 and create the characteristic pattern plotted in Figure 6.6.

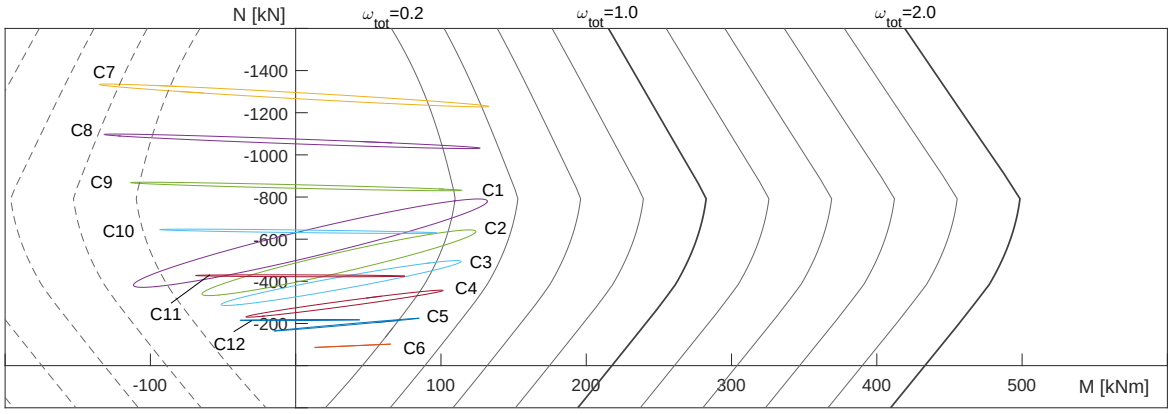

Figure 6.6: Ex1 - Action and resistant interaction curves for columns $\mathrm{C1} - \mathrm{C12}$.

In Figure 6.6 we see the clear variations in the static N in each alignment, with the lower columns appearing in the top of the graphic with larger compression forces. Also, the columns of the exterior alignment develop smaller static N.

Once again the dynamic action produces more inclined ellipses in the exterior columns which benefit from a larger frame effect. Finally, it is clear the ellipses of each alignment tend to become thinner as their height in the structure increases, meaning their behavior tends to be controlled (or dominated) by the first vibration mode. It is the relevance of sub-sequential modes and the different orientations in the $M - N$ space that promote the increase of the minor axis of an ellipse.

6.1.2 Equivalent Static Analysis

As discussed previously, the idea behind a static equivalent analysis is to reach results for stress-resultants or displacements that are not exact but can reproduce the structure general behavior, with the advantage of simplifying the calculations. This simplification comes from concentrating all the seismic information in a set of equivalent forces instead of constructing correlation matrices, $\boldsymbol{X}$, for each studied section of the structure.

The simplest way to accomplish a static analysis is to apply horizontal forces at the level of each floor, and those can be calculated by the two methods described in subsection 4.5.1: named the "Combined V" and the "Combined F" methods.

The second method calculates resulting forces for each vibration mode, which are plotted in Figure 6.7. The forces of each mode translate its vibration configuration: with zero, one and two inflection points, respectively. Additionally, the final forces have an evolution in height similar to the Combined V version and the typical inverted triangle.

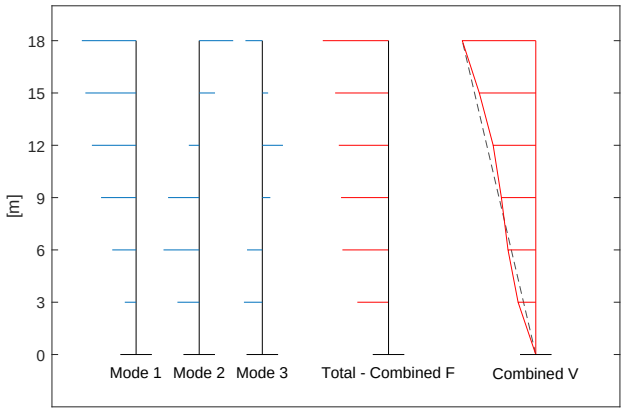

Figure 6.7: Ex1 - Equivalent forces in each mode and totals for the Combined F and Combined V.

To enable a more appropriate comparison of the two methods, the final values of the equivalent forces are grouped in Table 6.1.

Table 6.1: Ex1 - Equivalent Static Forces.

Floor	Combined V	Combined F
6	93.78 kN	93.78 kN
5	72.06 kN	76.16 kN
4	54.37 kN	70.92 kN
3	43.86 kN	67.73 kN
2	35.43 kN	65.79 kN
1	22.58 kN	44.50 kN
$\sum$	322.08 kN	418.58 kN

Note that the Combined F originates larger equivalent forces in every floor, except the last, were both methods correctly apply a force equal to the total shear force on that floor.

Furthermore, in the last line of Table 6.1 are presented the sums of the forces in the multiple floors to compare them to the Base Shear: the combination of the shear forces acting on the base level of the structure in each mode. This quantity does not depend on any sequence of calculations and takes the value of 322.09 kN. This shows the Combined V provides a more accurate description of the structure response.

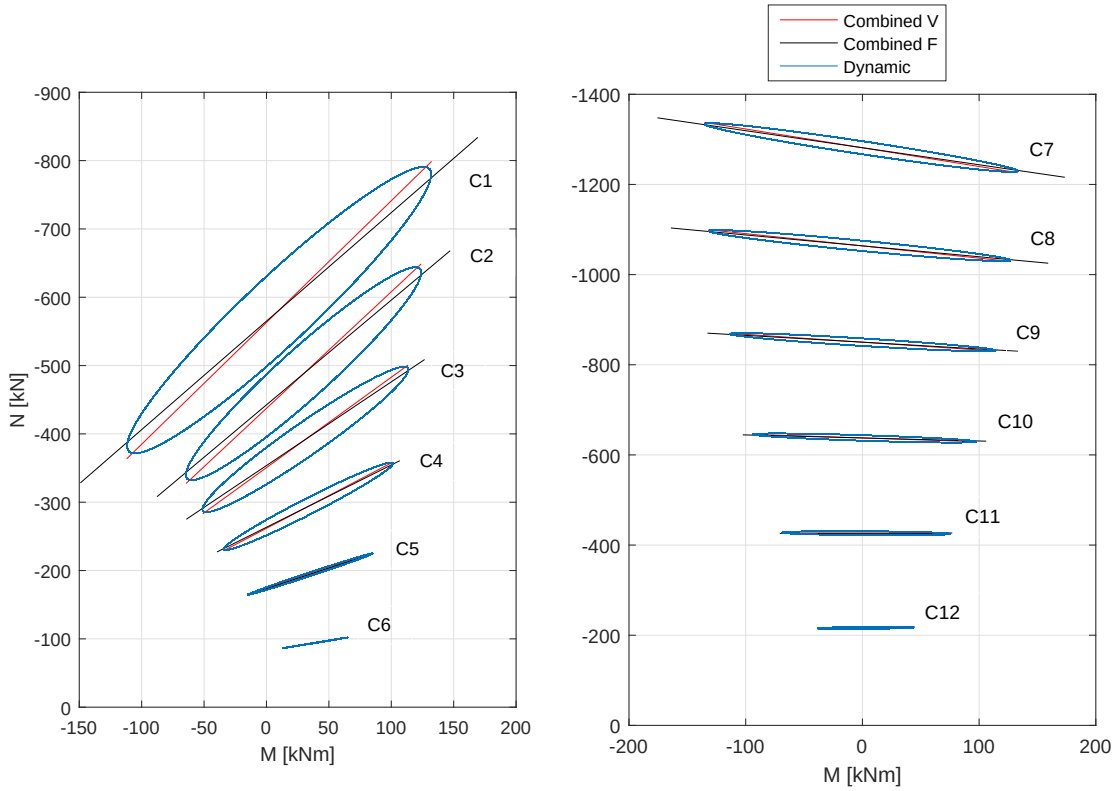

(a) Alignment 1 (b) Alignment 2

Figure 6.8: Ex1 - Comparison of stress-resultants from static and dynamic analysis.

Applying these equivalent forces to the structure originates stress-resultants in the studied sections, that are graphically represented by straight lines. Figure 6.8 shows the stress-resultants $M - N$ in the base section of the columns of the two alignments introduced in Figure 6.5 calculated for the two static analysis (Combined V and Combined F) and also the interaction envelopes previously constructed with a dynamic analysis.

Firstly, the three analysis reflect a similar correlation of stress-resultants, given by their inclination. It should be noted that both equivalent static results exceed the envelope along the principal axis but, of course, underestimate the response perpendicular to it (a line can not reproduce all the information contained in an interaction ellipse). This may aggravate the design of the section, depending on the positioning over the capacity surface.

It is also clear that the Combined F method produces more exaggerated results, as was expected.

Finally, the equivalent static analyses tend to be more similar to the ellipsoids in the sections of the upper floors.

6.2 Example 2

6.2.1 CQC Application

The second example concerns a symmetrical structure, with $7 \times 7\ \mathrm{m}^2$ of implanted area and four columns and four beams with the same characteristics.

For the construction of the mass matrix a generic distributed load, $p = 4.5\ \mathrm{kN/m}$, is considered. Placing this load uniformly in every beam would mean the structural system was completely symmetrical. As such, there would not be a defined direction for the translation modes: the first and second ones, and their vibration periods, T, would be equal.

To prevent this indeterminacy the load will be applied as portrayed in Figure 6.9, obligating the two modes to have a single and well-defined translation direction. These two directions are the symmetry axis: the two diagonals.

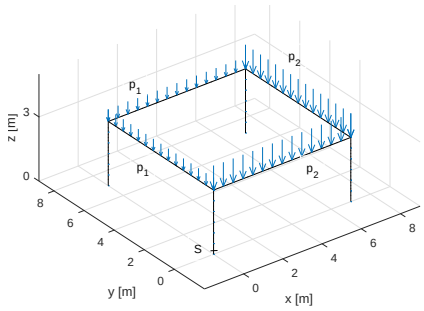

concrete	C30/37
steel	A500
columns	$0.3 \times 0.3\ \mathrm{m}^2$
beams	$0.3 \times 0.6\ \mathrm{m}^2$
height	$3\ \mathrm{m}$
span x	$7\ \mathrm{m}$
span y	$7\ \mathrm{m}$

Figure 6.9: Ex2 - 3D Structure Description.

It should be noted that the load difference is exaggerated in the image, as the larger load is actually $p_2 = p_1 \times 1.0001$ and $p_1 = 4.5\ \mathrm{kN/m}$, resulting from the beams geometry. With this artifice, the first and second modes only have a slight difference in their periods. As it can be seen in Figure 6.10 they do appear equal and have the desired configuration.

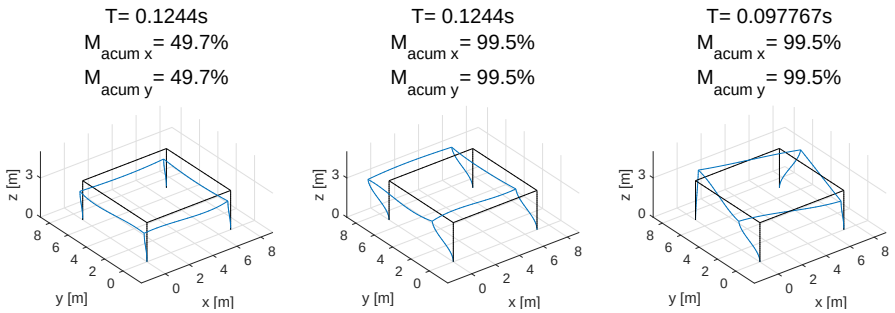

(a) 3D View

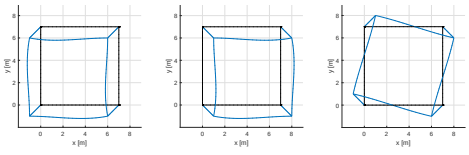

(b) Top View

Figure 6.10: Ex2 - Mode configuration.

The section in study is the base of the column in the origin, with coordinates $(0,0,0)$. The correspondence between the (x,y) referential and the one used for the bending moments (M_2,M_3) is displayed in Figure 6.11.

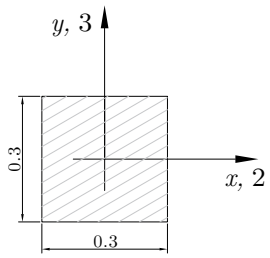

Figure 6.11: Ex2 - Correspondence (x,y) - $(2,3)$ dimensions in $[\mathrm{m}]$.

It is evident that for a seismic action along the x or y direction, the different modes produce both bending moments M_2 and M_3. In addition to this, attending to the structure symmetry all the pairs $M_2 - M_3$ have the same values. We present this result in Figure 6.12, in a top view of the 3D representation of the stress-resultants. The maximum value of each bending moment is $4.86\ \mathrm{kNm}$.

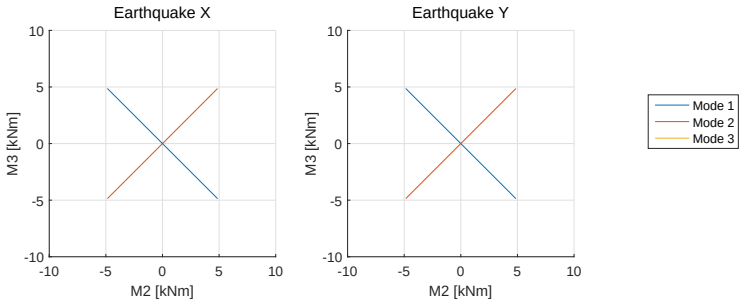

Figure 6.12: Ex2 - Stress-resultants for each mode and direction.

The CQC mode combination is introduced in the next step. Recalling the similarity between the mode frequencies, this combination rule provides an envelope that is just a straight line and not an ellipse enveloping the modes individual responses, see Figure 6.13. The envelope correctly reflects the behavior of a symmetrical structure being excited by an earthquake in the x direction, causing just the bending moments M_3 (or M_2 for the y direction).

The maximum value of each bending moment is the sum, or subtraction, of each mode contribution (this is the expected behavior of the CQC combination for equal mode frequencies):

$$\begin{aligned} M_{2x} &= {M_{2x}}^{mode\ 1} - {M_{2x}}^{mode\ 2} = 0\ \mathrm{kNm} \\ M_{3x} &= {M_{3x}}^{mode\ 1} + {M_{3x}}^{mode\ 2} = 2 \times 4.86 = 9.72\ \mathrm{kNm} \end{aligned} \tag{6.1}$$

The correlation matrices, $\boldsymbol{X_k}$, are presented below. Each line and column of these matrices is associated with one stress-resultant and each entry is the multiplication of those stress-resultant values. These values are calculated for each mode and after combined with the CQC combination, as explained before. There is one matrix $\boldsymbol{X_k}$ for each seismic direction:

$$\boldsymbol{X_x} = \begin{array}{c} \begin{matrix} M_2 & M_3 & N \end{matrix} \\ \begin{bmatrix} 0.00 & -0.07 & -0.02 \\ -0.07 & 94.61 & 24.19 \\ -0.02 & 24.19 & 6.18 \end{bmatrix} \end{array} \begin{matrix} M_2 \\ M_3 \\ N \end{matrix} \qquad \boldsymbol{X_y} = \begin{array}{c} \begin{matrix} M_2 & M_3 & N \end{matrix} \\ \begin{bmatrix} 94.59 & -0.07 & -24.19 \\ -0.07 & 0.00 & 0.02 \\ -24.19 & 0.02 & 6.18 \end{bmatrix} \end{array} \begin{matrix} M_2 \\ M_3 \\ N \end{matrix} \tag{6.2}$$

These matrices show the directions decoupling, with values close to zero in the terms associated with the bending moment that is not related to the seismic direction in question. They are used to plot the interaction ellipses of Figure 6.13 (we remark that the lines are particular cases of ellipses). The total response is calculated by adding the two matrices.

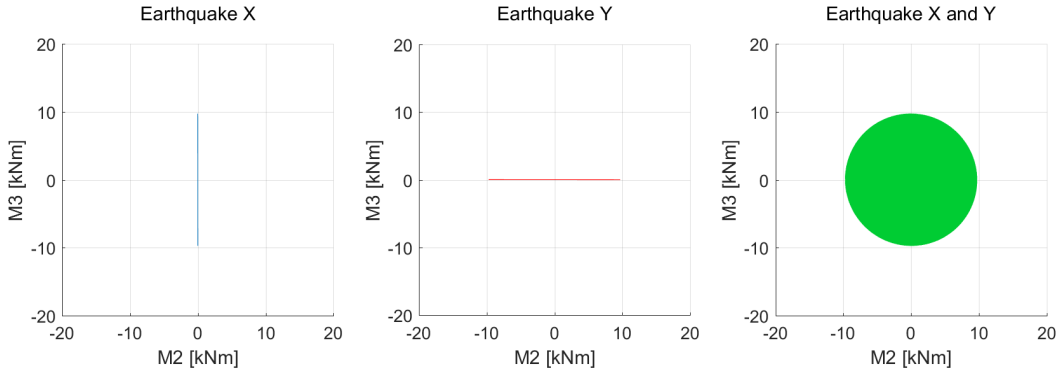

Figure 6.13: Ex2 - Result of the CQC combination.

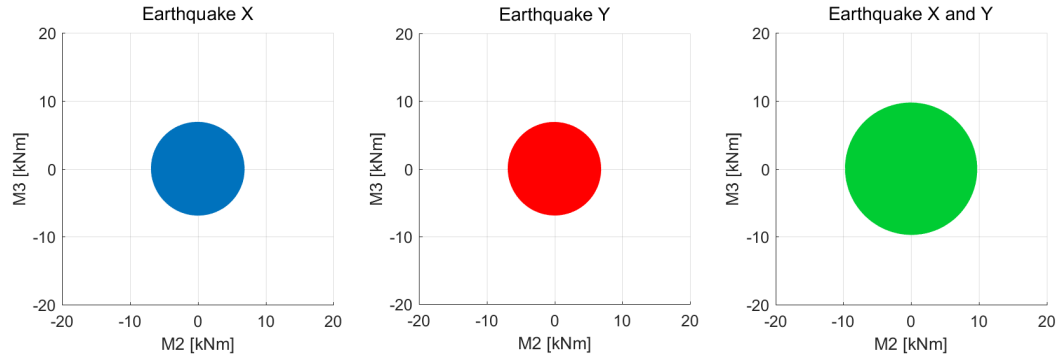

Figure 6.14: Ex2 - Result of the SRSS combination.

Figure 6.14 illustrates what would be the SRSS combination envelope. Contrary to the CQC case, each seismic direction x or y produce both M_2 and M_3 bending moments in the column in question, which is not reasonable.

The maximum value obtained by this method for each bending moment is:

$$M_{2x} = \sqrt{({M_{2x}}^{mode\ 1})^2 + ({M_{2x}}^{mode\ 2})^2} = \sqrt{2 \times 4.86^2} = 6.87 \text{ kNm} \tag{6.3}$$

which is smaller than the CQC result.

In addition to this the correlation matrices, $\boldsymbol{X_k}$, are identical for each direction and denote the similarity $(M_i - N)$.

$$\boldsymbol{X_x} = \boldsymbol{X_y} = \begin{matrix} \\ M_2 \\ M_3 \\ N \end{matrix} \begin{matrix} \begin{matrix} M_2 & M_3 & N \end{matrix} \\ \begin{bmatrix} 47.30 & -0.07 & -12.10 \\ -0.07 & 47.30 & -12.10 \\ -12.10 & 12.10 & 6.18 \end{bmatrix} \end{matrix} \tag{6.4}$$

Oddly enough, the total responses considering the earthquake acting independently in the two horizontal directions are equal. This can be observed on the total correlation matrix $\boldsymbol{X} = \boldsymbol{X_x} + \boldsymbol{X_y}$ presented below for the two methods.

$$\boldsymbol{X}^{CQC} = \begin{bmatrix} 94.59 & -0.14 & -24.20 \\ -0.14 & 94.61 & 24.21 \\ -24.20 & 24.21 & 12.37 \end{bmatrix} \qquad \boldsymbol{X}^{SRSS} = \begin{bmatrix} 94.59 & -0.14 & -24.20 \\ -0.14 & 94.61 & 24.21 \\ -24.20 & 24.21 & 12.37 \end{bmatrix} \tag{6.5}$$

Once again we will project the total response of Figure 6.13 in the three coordinate planes, with the intention of introducing the dependence of the N coordinate, that has been previously omitted.

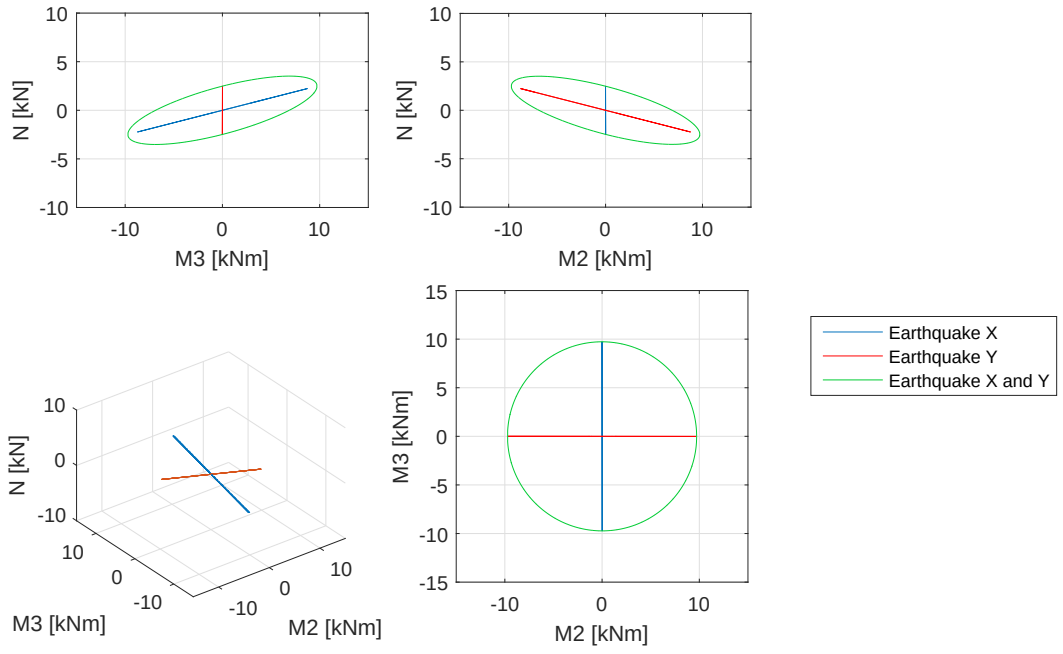

Figure 6.15: Ex2 - Interpretation of the Total Ellipsoid - CQC.

This 3D representation is in Figure 6.15. The structures response to an earthquake acting along the directions x or y are straight lines in the coordinate space $M_2 - M_3 - N$. They are represented in the 3D view and in the three projections. It is evident that both directions have a similar behavior: causing N and just one bending moment.

The total response of the structure, when the two earthquakes are acting simultaneously, is plotted in green. It is not represented in the 3D view because it would hide the two lines. Nevertheless, it is possible to visualize the shape and orientation of the resultant ellipsoid from its projections. It has two equal principal semi-axis and a third one significantly smaller, resembling a disk. The point with maximum N is located in the quadrant with positive M_3 and negative M_2.

Comparing this envelope to the one in Chapter 2 (Figure 4.19 on page 33) plotted for the simple four story structure, we note a difference in the $(M_i - N)$ graphics. In Figure 6.15 the representation of each direction is a line, whereas in Figure 4.19 ellipses appear. The reason for this is the number of relevant modes: in this example there is one relevant mode in each direction and in the other example there were two. Given how the different modes have different $(M_i - N)$ relations, they promote the enlargement of the ellipse semi-axes. Thus, the differences in the $(M_i - N)$ representations are explained.

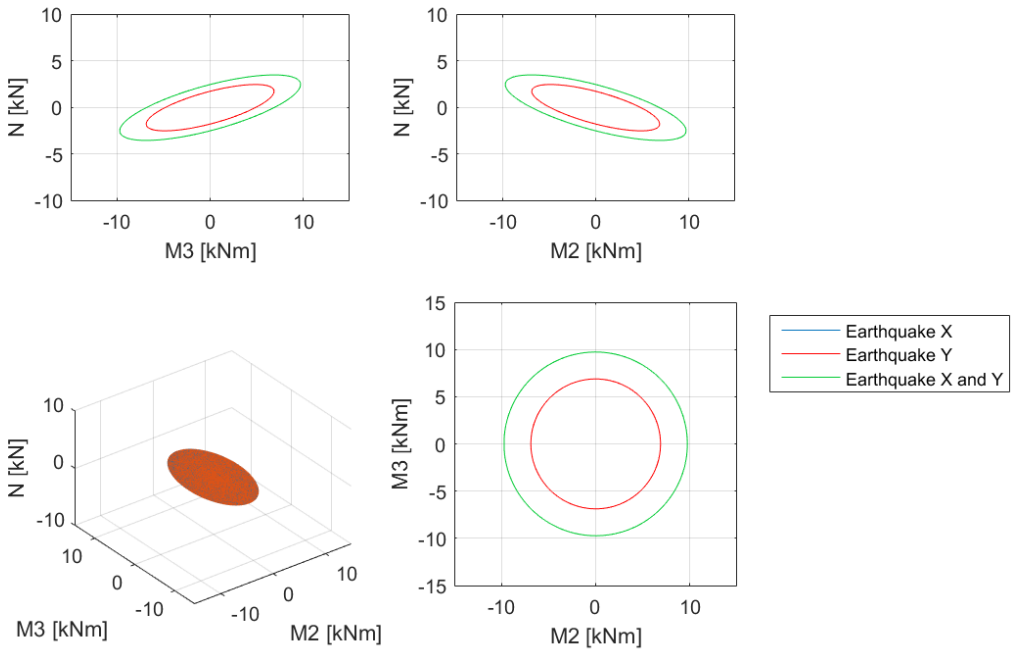

Figure 6.16: Ex2 - Interpretation of the Total Ellipsoid - SRSS.

We also present the projection of the SRSS envelope in Figure 6.16. Once again it is evident that the response to both earthquake directions is identical as they overlap in every graphic. Furthermore, the individual directional responses are ellipses, contrary to the lines obtained with the CQC combination. This is suggested by the correlation matrices in equation (6.4) that don't have entries close to zero.

Finally, it is evident that adding the directional matrices $\boldsymbol{X_x}$ and $\boldsymbol{X_y}$ to calculate the total response matrix $\boldsymbol{X}$ correctly translates an SRSS combination of directions (not modes). This means that the total envelope, in green, is not a result of summing the coordinates of the directional envelopes, but rather the square root of the sum of the squared coordinates. This also applies to the CQC modal combination.

6.3 Example 3

6.3.1 3D Application

The subject of the next study is a more complex structure that has an asymmetrical disposition of the columns, intended to correlate one earthquake direction to both bending moments, M_2 and M_3. In addition to this there is a set of two close columns in each x alignment, see Figure 6.17. They will be used to design the combined footings.

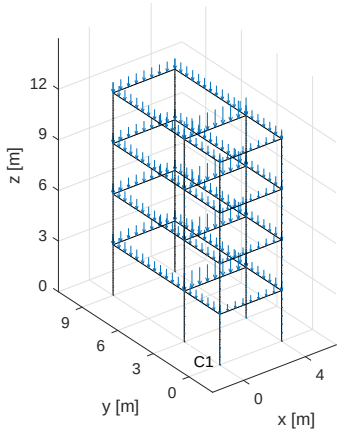

concrete	C30/37
steel	A500
columns	0.3×0.3 m^2
beams	0.3×0.6 m^2
story height	3 m
span x	4 m
1st span y	3 m
2nd span y	6 m

Figure 6.17: Ex3 - 3D Structure Description.

As we only discretize the structure in linear elements, the slabs are not included and its mass effect is introduced in the value of the loads applied to the different beams. To do so we used a re-partition of loads based on the length relations of the sides of the panels, (Costa [28]), that is presented in Figure 6.18.

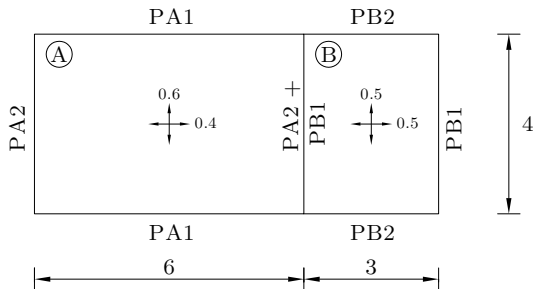

Panel A	
Area, A_{PA}	$6 \times 4 = 42$ m^2
Re-partition Coef., α_{PA}	0.6
Panel B	
Area, A_{PB}	$4 \times 3 = 12$ m^2
Re-partition Coef., α_{PB}	0.5

Figure 6.18: Ex3 - Slab panels and load re-partition.

From the set of ultimate limit state verifications, we will focus on the seismic combination of actions. Therefore, the distributed load on a beam includes its self-weight plus the correspondent re-partition of the slabs self-weight added to the remaining dead load, rdl, and to the combination value of the live load, q. For the self-weight, the volumic weight of concrete was taken as $\gamma = 25$ kN/m^3. The values chosen are larger than the ones typically used in residential buildings and are summarized in Table 6.2.

Table 6.2: Ex3 - Load Description.

Dead Loads		Live Loads	
slab height, h_s	0.4 m	combination factor, ψ_2	0.3
remaining dead load, rdl	6 kN/m^2	live load, q	4 kN/m^2

For every beam the distributed load is one of the following, or a combination of them.

$$\begin{aligned} PA1 &= \gamma bh + (\gamma h_s + rpl + \psi_2 q) \times \alpha_{PA} \times 2 = 25.14 \text{ kN/m} \\ PA2 &= \gamma bh + (\gamma h_s + rpl + \psi_2 q) \times (1 - \alpha_{PA}) \times 3 = 25.14 \text{ kN/m} \\ PB1 &= \gamma bh + (\gamma h_s + rpl + \psi_2 q) \times \alpha_{PB} \times 1.5 = 17.40 \text{ kN/m} \\ PB2 &= \gamma bh + (\gamma h_s + rpl + \psi_2 q) \times (1 - \alpha_{PB}) \times 2 = 21.70 \text{ kN/m} \end{aligned} \tag{6.6}$$

To account for the torsional effects, EC8 recommends moving the mass center 5% of the length of the structure. This was not implemented but could be easily done by adjusting the previous load values.

The first eight modes are presented in Figure 6.19:

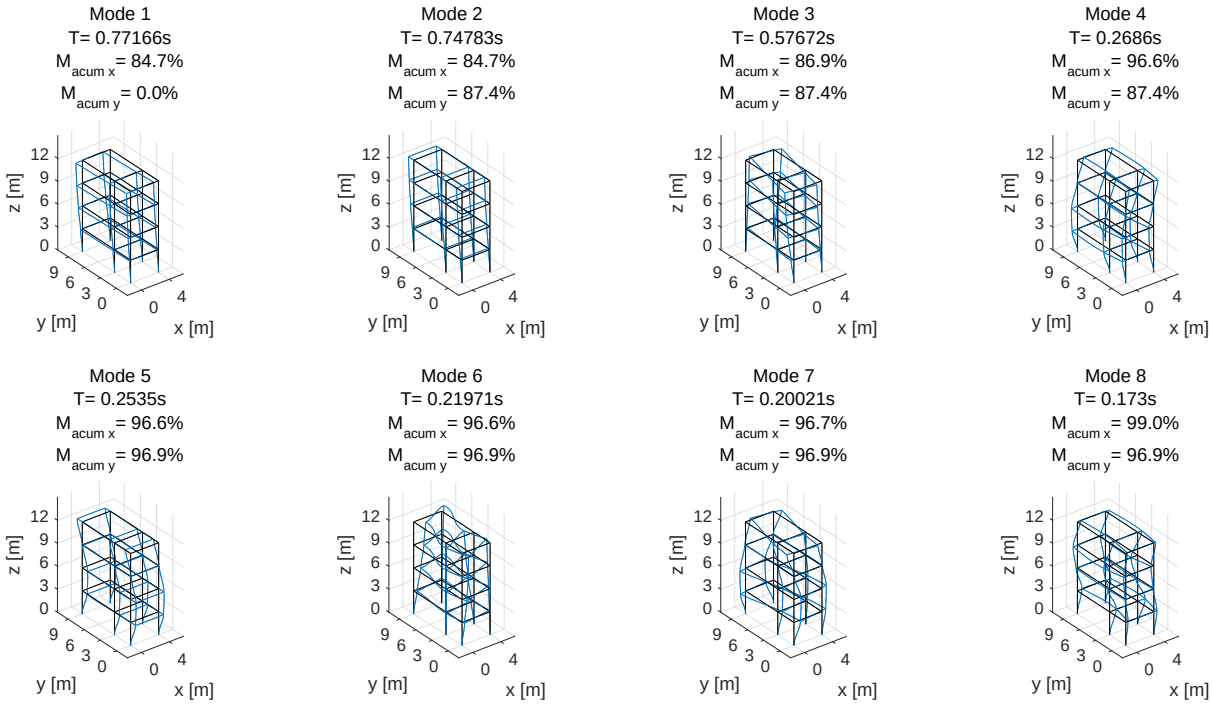

Figure 6.19: Ex3 - Modes Configuration.

Due to the non-symmetrical footprint of the structure, the first mode is in x, where the global structure is more flexible. Another important aspect is that the columns disposition is not symmetrical along x. This is why the 3$^{\text{th}}$ mode increases the accumulated mass in direction x, $M_{acum\ x}$, meaning this is a torsional mode with some contribution in x. Additionally, the 6$^{\text{th}}$ mode only appears because the condition of a rigid slab was not included. It could be materialized with two cross bars pinned at the ends and with a high axial rigidity. With it, the 6$^{\text{th}}$ mode would be replaced by the 2$^{\text{nd}}$ torsion mode.

For the base section of the column $C1$ of coordinates $(0,0,0)$, we calculate the stress-resultants for each mode and seismic direction. After the adequate combinations are applied, the ellipsoid is projected in the coordinate planes for a better interpretation, in Figure 6.20.

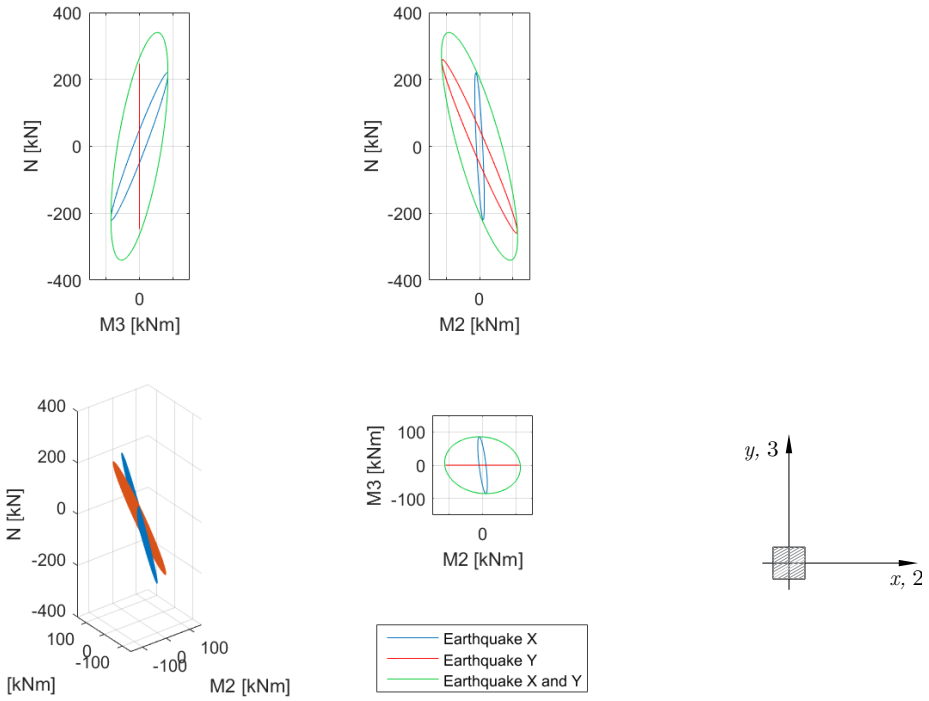

Figure 6.20: Ex3 - Ellipsoid projection (Column $C1$).

As it can be seen, the direction x produces N and both moments, and the direction y only produces N and M_2. Again this can be explained by the symmetry in the disposition of columns in one direction but not in the other. This also justifies why the direction x is represented by an ellipse in the $M_2 - M_3$ graphic.

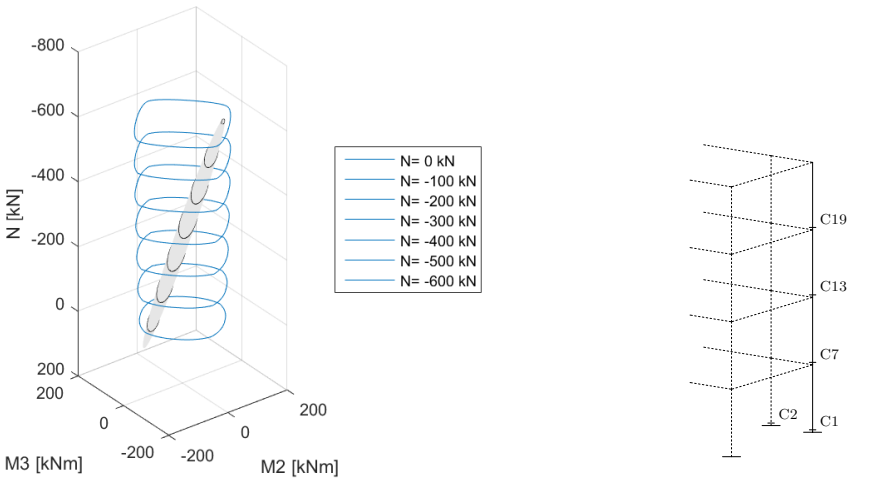

(a) Column $C1$ response

(b) Column identification

Figure 6.21: Ex3 - Action and Resistance for given values of N (Column $C1$).

For design purposes, we need to add the static stress-resultants, which will change the position of the ellipsoid center. With the correct placement, we can compare the action interaction ellipsoid with the resistant curves, using the safety verification method described in subsection 5.1.4. From it, we can conclude that the optimal total percentage of reinforcement is $\omega_{tot} = 0.7$. This correspond to $A_s = 29\,\mathrm{cm}^2$ that may be materialized with $16\ \phi 16$. Visually, it is clear in Figure 6.23 that this section verifies the safety criteria as the action curves are within the resistance curves for each value of the axial force, N, chosen to plot the curves.

However, it is not enough to only verify one section of the column. That is why we repeat this process to the top and base sections of all the four segments in the same vertical alignment. This is relevant to study the detailing of the steel bars, in particular, the sections to place laps and anchorages.

Figure 6.22 presents the representations of the ellipsoid and the resistant curves for each optimal value of ω_{tot}. There, it is clear the different orientation of the envelopes between base and top sections. The column identification is in Figure 6.23 (b).

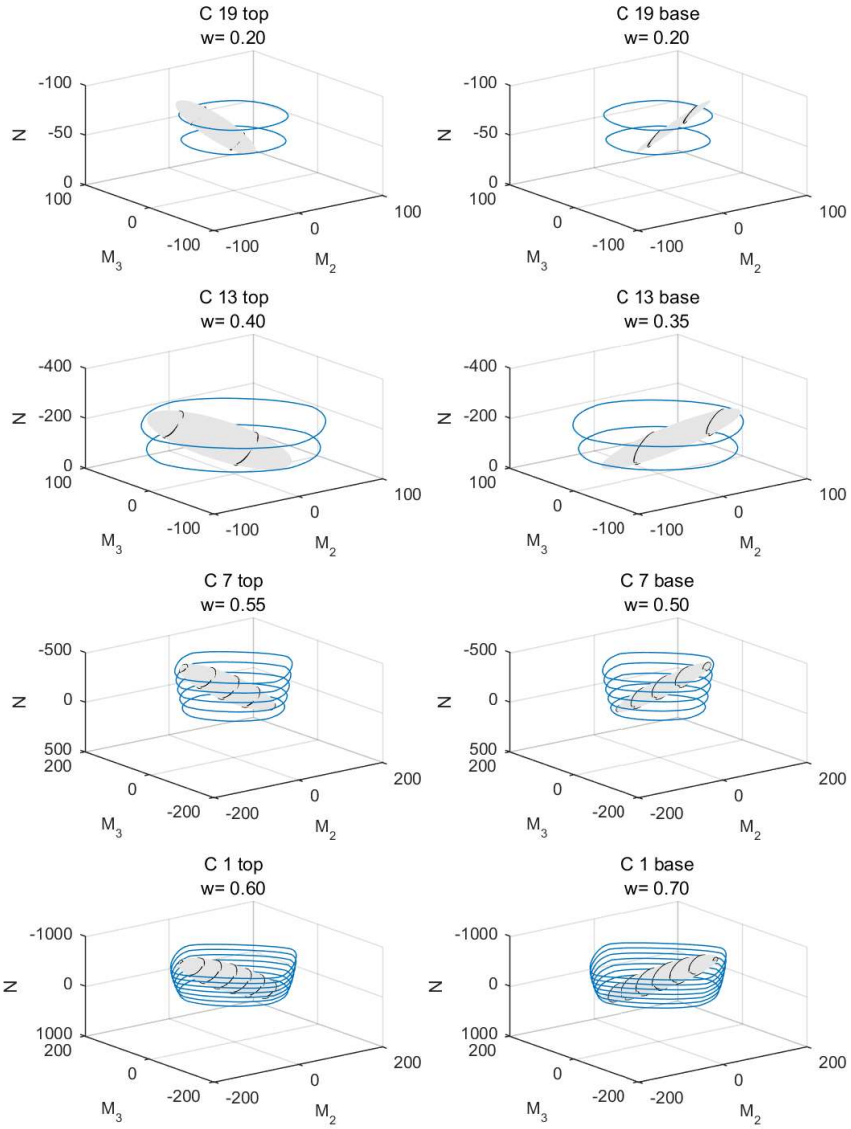

Figure 6.22: Ex3 - Design of multiple sections.

Lastly, we present what would be the classical envelope for column $C1$. In the 3D case, this envelope is a parallelepiped that encloses the ellipsoid already detailed. Designing the section for this envelope is necessary an optimal total percentage of reinforcement of $\omega_{tot} = 1.0$. Comparing this value with the $\omega_{tot} = 0.7$ obtained with the ellipsoidal, it is clear there is an economy of 30% in steel.

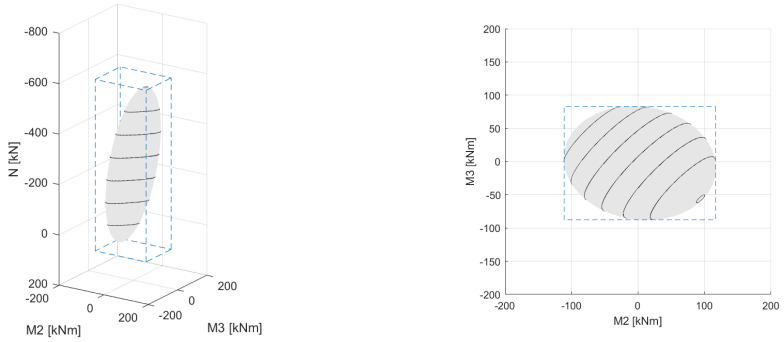

(a) 3D View (b) Top View

Figure 6.23: Ex3 - Parallelepipedic envelope.

6.3.2 Equivalent Static Analysis

This section will apply the methodology described in the section 4.5.2 to perform an equivalent static analysis to the 3D structure of this example. The values of the equivalent forces calculated for each floor and presented in Table 6.3.

Table 6.3: Ex3 - Equivalent Static Forces.

Floor	Earthquake x				Earthquake y		
	F_x	F_y	${M_t}^F$	${M_t}^F/F_x$	F_x	F_y	${M_t}^F$
4	156.35 kN	~ 0 kN	171.81 kNm	1.10 m	~ 0 kN	162.65 kN	~ 0 kNm
3	119.27 kN	~ 0 kN	137.14 kNm	1.15 m	~ 0 kN	127.66 kN	~ 0 kNm
2	85.22 kN	~ 0 kN	98.51 kNm	1.16 m	~ 0 kN	91.21 kN	~ 0 kNm
1	48.03 kN	~ 0 kN	52.32 kNm	1.09 m	~ 0 kN	51.00 kN	~ 0 kNm

Figure 6.24 displays the axis orientation and the location of the "column stiffness center". Note how the earthquake x, causes the structure to have a translation and rotation behavior, induced by the ${M_t}^F$. This is not verified for earthquake y. Also, note that the ratios ${M_t}^F/F_x$ are different for each floor. This evidences that the behavior of each floor cannot be calculated separately as it depends on the entire structure.

Each group of static forces—equivalent to earthquake x or y—is applied separately to the structure. As previously explained the three equivalent forces of each floor are transformed into nodal forces, and those are the ones actually introduced in the calculation model.

The stress-resultants of the desired sections are obtained with simple static analysis. We will detail the following process of construction of the interaction curve for the base section of column $C1$.

The two static analysis originate M_2, M_3 and N in this section. These stress-resultants are graphi-

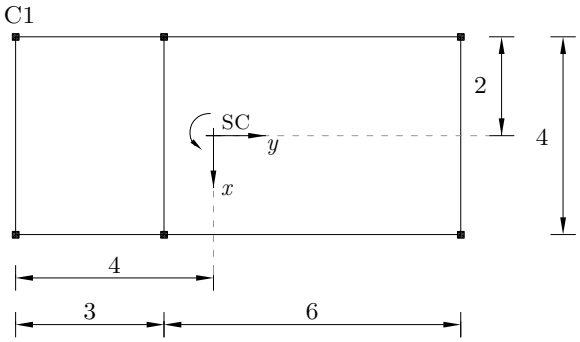

Figure 6.24: Ex3 - Axis orientation and stiffness center.

cally represented in the coordinate space by two straight lines. These lines are presented in Figure 6.25, not in 3D but projected in the coordinate planes. This is done to make clear how these lines compare to the ellipsoids developed in the first part of this example.

In this Figure, the results of the equivalent static analysis (dotted lines) are overlaid to the same graphics of Figure 6.20, the projections of the total ellipsoid and the ones for each direction. The same colors were used to distinguish the earthquake directions.

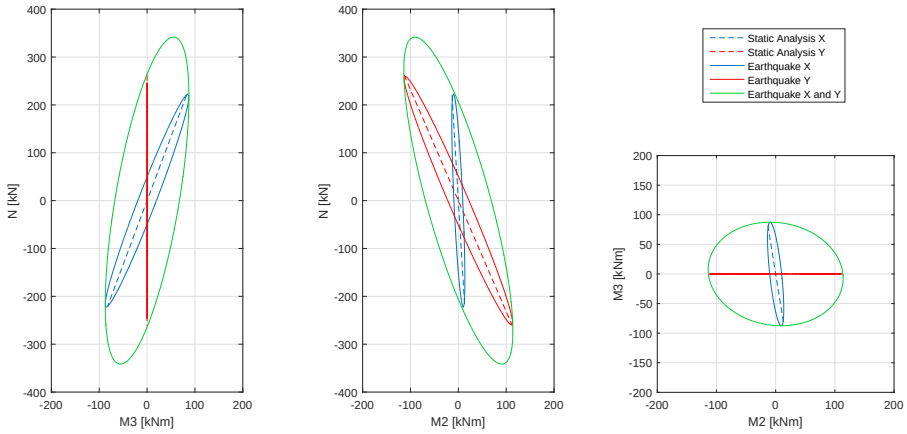

Figure 6.25: Ex3 - Projection of the dynamic and static analysis for column $C1$.

As it can be seen both static equivalent analyses reproduce the general inclination of the envelopes and very slightly exceed them along their major axis. Like in the 2D case this situation may aggravate the section design, depending on the resistant capacity.

We remark that is still necessary to combine the two earthquake directions to obtain an equivalent for the total interaction ellipsoid, plotted in green above and in gray in Figure 6.26 (b). The resultant equivalent surface is an ellipse, constructed with the intersection method and applying the principles of the SRSS combination of directions, see details in subsection 4.5.2. Note that the ellipse is contained in the inclined plane defined by the response of the two earthquake directions, see Figure 6.26 (a).

The maximum value N of the ellipse is 368.2 kN larger than the ellipsoid correspondent, which is 341.2 kN. This shows that along the major axis of the ellipse it does behave as an upper bound to the ellipsoid.

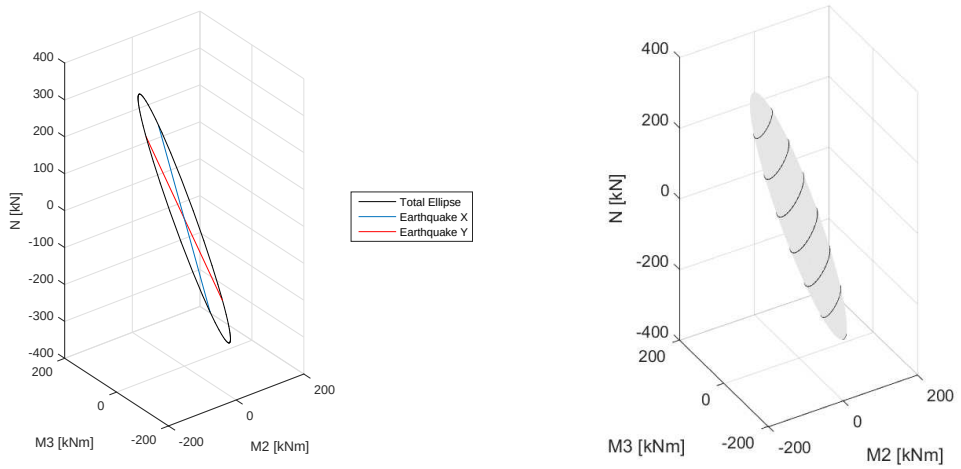

(a) Equivalent Ellipse (b) Total Ellipsoid

Figure 6.26: Ex3 - Comparison of the equivalent static ellipse and the interaction ellipsoid.

In the same manner of the 2D static analysis, where the equivalent lines underestimate the ellipses behavior along their minor axis, so does this ellipse when compared to the ellipsoid. The reason it can be used to approximate the real behavior of the structure is that the ellipsoid does have one principal axis significantly smaller than the other two: the one perpendicular to the ellipse plane. See these values in Table 6.4.

Table 6.4: Ex3 - Ellipsoid and Ellipse semi-axes.

Semi-axis	Ellipsoid	Ellipse
1	357.94	359.46
2	93.96	86.61
3	19.76	0

Finally, Figure 6.27 displays the projections of the Ellipsoid and the static equivalent Ellipse, for a better comparison of both.

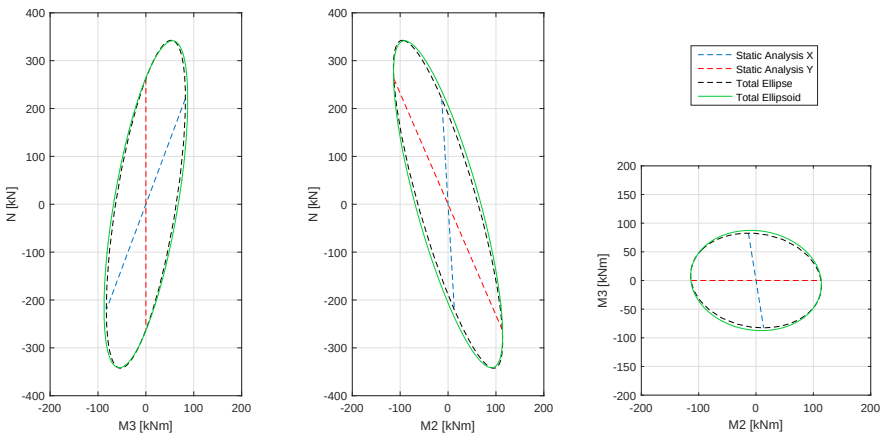

Figure 6.27: Ex3 - Ellipse and Ellipsoid projections for column $C1$.

6.3.3 Columns with Combined Footing

Consider now a different design situation: Combined Foundations.

Keeping in mind the footing will support columns 1 and 2, which are sufficiently close to each other, we evaluate a solution with the following characteristics of the soil and the footing listed in Figure 6.28, which reproduces Figure 5.10 (on page 48) for clarity.

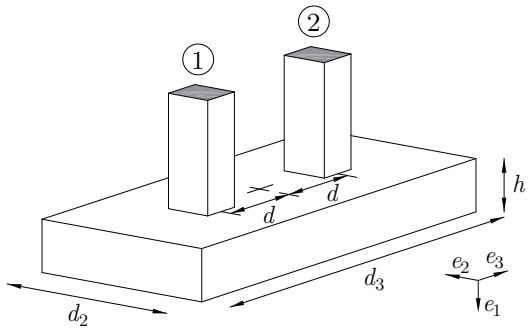

Soil	
σ_{max}	700 kPa
Footing	
d_2	1.5 m
d_3	4.0 m
h	1.5 m
d	1.5 m

Figure 6.28: Ex3 - Characteristics of the Combined Footing.

We first consider only the 2D design, assuming only the N and M_2 values but considering the two earthquake directions. Figure 6.29 plots the individual ellipses at the base sections of the two columns. Observe the different $N - M_2$ correlation in each column. Furthermore, these envelopes are calculated in fictional sections 1.5 m below the soil level to correctly calculate the correlation matrix in the base section of the foundation. It is clear from this figure that column C_1 cannot have a separate footing since the extreme low N value is nearly zero.

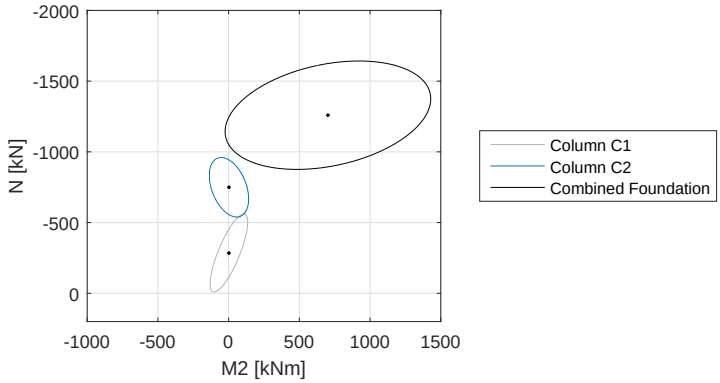

Figure 6.29: Ex3 - Ellipses for individual columns and combined footing.

The total interaction envelope of the combined footing is also plotted. Its shape tends to have a horizontal orientation which can be explained by the opposite correlation of N values in the two columns.

The N coordinate of the center of the combined foundation ellipse is the sum of the values of the individual columns ($N_{C1} = 284.50$ kN and $N_{C2} = 749.60$ kN) plus the weight of the footing (225 kN), resulting in the 1259.1 kN plotted in the Figure. The center of the interaction envelope of the combined footing is split into two components: the static stress-resultants and the footing self-weight which are plotted in Figure 6.30

For the dynamic component we begin by evaluating the response for each mode and earthquake direction by equations (5.17), combine them and finally obtain a matrix $\boldsymbol{X}$ for the footing.

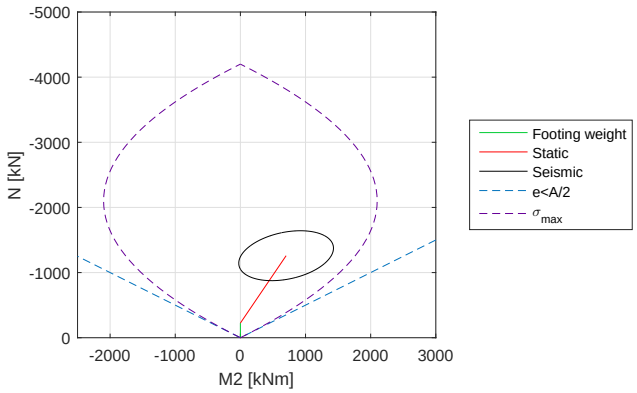

Figure 6.30: Ex3 - Safety Verification for the combined footing.

Also shown in this Figure are two dotted lines that represent design criteria: one limits the soil stress to σ_{max} and the other limits the eccentricity so the center of pressure is within the footing. The second behaves as an asymptote of the first.

For further detail, we can analyze the foundation in 3D, calculating the resistance with the numerical method explained in section 5.2. In Figure 6.31 the action ellipsoid and the resistant surface are plotted, intersected at given values of N. In Figure 6.32 the window is adjusted to values on N that contain the action ellipsoid and is presented as a top view, so it becomes easy to validate its safety.

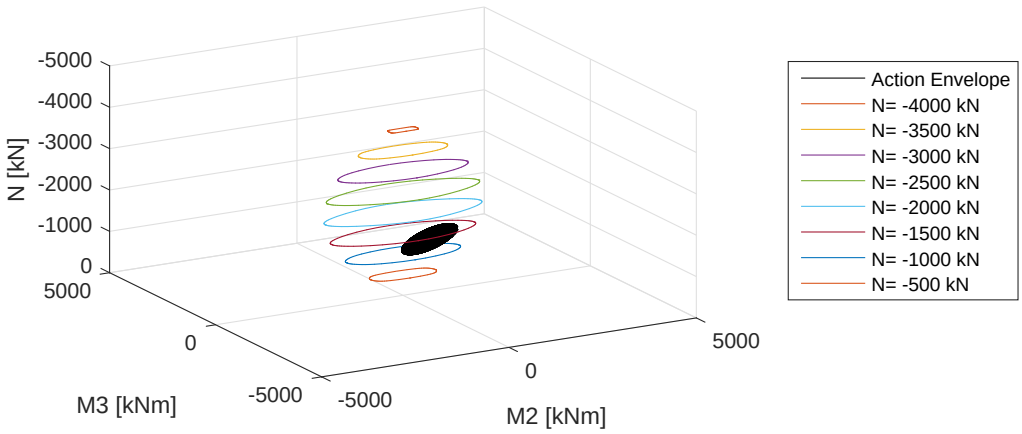

Figure 6.31: Ex3 - 3D Action and resistant interaction surfaces.

If the perspective is to analyze multiple solutions, instead of just one as was done so far, it is possible to create images such as the one in Figure 6.33. It displays three different geometries for the footing and the correspondent resistant interaction envelopes intersect at the maximum and minimum values of the action ellipsoid.

There is also plotted the ellipsoid with an arrow indicating the direction of increasing compression (note this is a 2D plot, were the N scale is omitted).

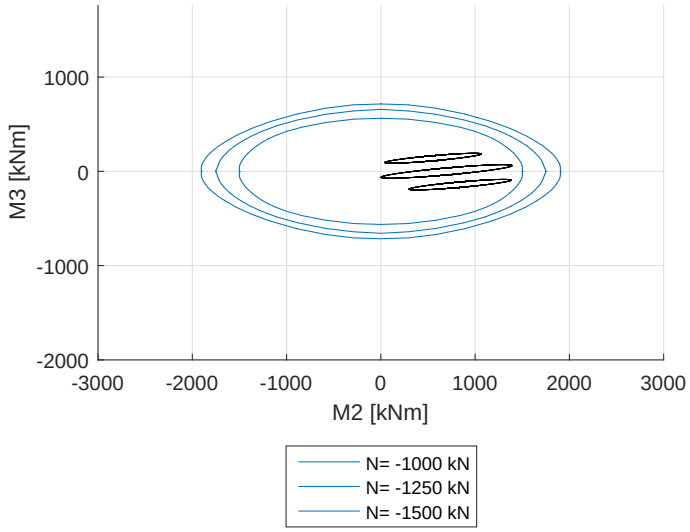

Figure 6.32: Ex3 - Zoomed and top view.

The red footing (3.0×1.5 m^2) does not verify the safety criteria and the blue one (6.0×1.5 m^2) is clearly over conservative. The green solution (4.0×1.5 m^2) is the one previously studied which confirms the safety of the footing that is suggested in this Figure.

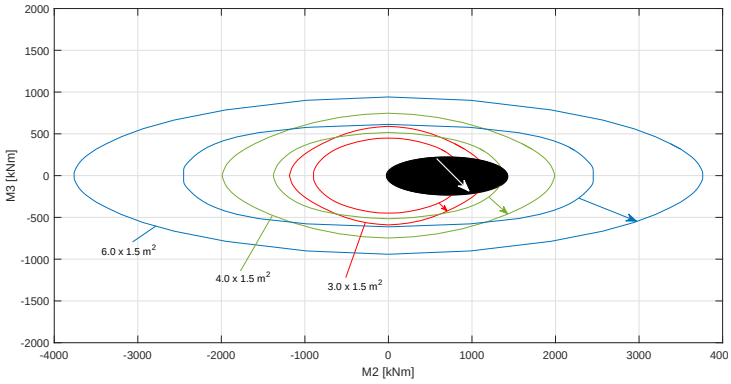

Figure 6.33: Ex3 - Different footing geometries.

This is a unique approach to footing design as it does not need to assume that all maximum values of stress-resultants occur simultaneously in both columns. As was done for the design of a single section we construct a correlation matrix for the stress-resultants, in the footing base, with the information of each mode. Afterward, we use the proper combination of modes and directions and plot the resultant interaction envelope. This geometrical entity can then be used to assist the designer in the safety verifications.

Chapter 7

Conclusions

The present dissertation was elaborated with the main goal of exploring the construction and application of interaction surfaces to the design of structures subjected to seismic actions.

The interaction surfaces replace the common practice of assuming that the multiple stress-resultants maximum values calculated with a response spectrum method can be simultaneous. This can lead to an over-design of a structure since the most unfavorable combinations of all the stress-resultants relevant for the design of each section are picked. The interaction surfaces refine the data used for design by evaluating the correlations between those stress-resultants in each vibration mode and combining them properly. It also presents a geometric representation of points whose coordinates are sets of stress-resultant values (for example: M_2, M_3 and N) that can occur together in a given section.

To support the use of these interaction surfaces we remark that it resorts to the information typically calculated in seismic analysis, based on modal combinations and response spectra. The increase of computational effort to process that information can be compensated by the material savings it allows in the design phase, by being less conservative to describe the effects of the seismic action. Such savings are described by specialized literature and reconfirmed in this dissertation.

Three different methods to construct the interaction envelopes were studied: the intersection, the divider and the equation method. Although all methods present the same outcome when is used an SRSS or CQC modal combination (which is an ellipse), only the intersection method can describe the ABS combination. This allows the comparison of these three modal combinations, not just when applied to one variable but to combinations of two variables (such as $M - N$). As a result, graphical representations of these common combinations in 2D were presented.

When the study was extrapolated to 3D structures, strategies to interpret the geometry of the interaction envelopes were developed. With a CQC modal combination the interaction envelope is an ellipsoid. One strategy is to present the projections of this 3D form in the three coordinate planes and another is to intersect it with horizontal planes at different levels. Following this idea, resistant capacity surfaces of the reinforced concrete sections were constructed, also intersected at given values of the vertical coordinate, the axial force N. Having the action and resistant interaction surfaces, intersected by the same set of horizontal planes and overlaid in the same 3D plot, allows a visual design of the section.

Additionally, a procedure was developed to automatically calculate the necessary steel ratio for a list of desired sections: the top and base sections on columns.

Taking the concept of correlating variables instead of designing with the maximum values of each, we applied it to a different situation: combined footings. In this case, the interaction exists between the stress-resultants of the two columns that share the same footing. Using the modal information, procedures to quantify the action envelope and also the resistant capacity surface were developed, once again to allow its design.

Lastly, we investigated an alternative to the construction of interaction surfaces, avoiding building an interaction matrix and its graphic representation for each individual section. The idea is based on calculating a set of static forces equivalent to the seismic action that is applied once to the structure and originates the design stress-resultants in every desired section. This is developed for both 2D and 3D structures, having the shear forces as the starting point to calculate the equivalent static forces.

The 3D case is more complex as it involves two shear forces and a torsional moment. The calculation of the equivalent forces also resorts to the concept of interaction surfaces of these stress-resultants and to the selection of one of those points. The final output, once the equivalent static forces are applied, is a flat ellipse in a 3D coordinate space which approximates the complete interaction ellipsoid, which in any case seems to be very thin.

These concepts were exemplified with simple and regular structures reason why the domains of validity of these static analyses need further study.

7.1 Future Work

Following the previous idea, we propose to extend the study of interaction matrices and its applications to real structures. These could have irregularities in height, columns with different geometries (even structural walls) or basements. The purpose of such analysis is to assess the relations between the ellipsoid semi-axes, which could not be so apart as the ones calculated for the examples in this dissertation.

It would also be interesting to investigate if the equivalent static analyses can be applied to those irregular structures.

In addition, time-based analyses could be conducted and compared to the elliptical envelopes, both in 2D and 3D.

Finally, the same theoretical basis of correlating variables could be applied to structures whose security verifications are also dependent of displacements, such as the pot bearings in bridges supports.

Bibliography

[1] C. Menun and A. Der Kiureghian. Envelopes for seismic response vectors. I: Theory. *Journal of Structural Engineering*, 126(4):467–473, 2000.

[2] C. Menun and A. Der Kiureghian. Envelopes for seismic response vectors. II: Application. *Journal of Structural Engineering*, 126(4):474–481, 2000.

[3] C. E. De Normalisation. Eurocode 8–Design of structures for earthquake resistance–Part 1: General rules, seismic actions and rules for buildings. *European Standard NF EN*, 1:2005, 1998.

[4] A. Der Kiureghian. Structural response to stationary excitation. *Journal of the Engineering Mechanics Division*, 106(6):1195–1213, 1980.

[5] J. J. Azevedo. Vibrações aleatórias, dinâmica estocástica. Technical report, Instituto Superior Técnico, 1996.

[6] J. Penzien and M. Watabe. Characteristics of 3-dimensional earthquake ground motions. *Earthquake engineering & structural dynamics*, 3(4):365–373, 1974.

[7] E. L. Wilson, I. Suharwardy, and A. Habibullah. A clarification of the orthogonal effects in a three-dimensional seismic analysis. *Earthquake spectra*, 11(4):659–666, 1995.

[8] E. L. Wilson. *Three-dimensional static and dynamic analysis of structures*. Computers ans Structures Inc., 1998.

[9] C. Menun and A. Der Kiureghian. A replacement for the 30%, 40%, and SRSS rules for multicomponent seismic analysis. *Earthquake Spectra*, 14(1):153–163, 1998.

[10] J. J. Hernandez and O. A. Lopez. Discussion of “A replacement for the 30%, 40%, and SRSS rules for multicomponent seismic analysis” by Charles Menun and Armen Der Kiureghian. *Earthquake spectra*, 14(4):713–715, 1998.

[11] C. Menun and A. Der Kiureghian. Response to JJ Hernandez and OA Lopez ‘Discussion of “A replacement for the 30%, 40%, and SRSS rules for multicomponent seismic analysis” by Charles Menun and Armen Der Kiureghian. *Earthquake spectra*, 14(4):717–718, 1998.

[12] S. Sessa, F. Marmo, and L. Rosati. Effective use of seismic response envelopes for reinforced concrete structures. *Earthquake Engineering & Structural Dynamics*, 44(14):2401–2423, 2015.

[13] A. Gupta and M. Singh. Design of column sections subjected to three components of earthquake. *Nuclear Engineering and Design*, 41(1):129–133, 1977.

[14] A. K. Gupta. *Response spectrum method in seismic analysis and design of structures*, chapter 4, pages 51–65. CRC press, 1990.

[15] L. Leblond. Progrès récents concernant les méthodes de calcul sismique des structures en béton armé: Calcul sismique par la méthode modale utilisation des responses pour le dimensionnement. In *Annales de l'Institut Technique du Batiment et des Travaux Publics: Theories et methodes de calcul nº232*, pages 119–127, 1980.

[16] C. Menun. A response-spectrum-based envelope for Mohr's circle. *Earthquake engineering & structural dynamics*, 32(12):1917–1935, 2003.

[17] C. Menun. An envelope for Mohr's circle in seismically excited three-dimensional structures. *Earthquake engineering & structural dynamics*, 33(9):981–998, 2004.

[18] P. Panetsos and K. Anastassiadis. Evaluation of the most unfavorable combinations of simultaneous element forces, for the design of R/C cross section subjected to isotropic seismic excitation. In *Proceedings of the eleventh European Conference on Earthquake Engineering*. AA Balkema, 1998.

[19] P. Panetsos and K. Anastassiadis. Earthquake resitant design of structures under three-component orthotropic seismic excitation. In *Proceedings of the eleventh European Conference on Earthquake Engineering*. AA Balkema, 1998.

[20] S. Erlicher, Q. S. Nguyen, and F. Martin. Seismic design by the response spectrum method: A new interpretation of elliptical response envelopes and a novel equivalent static method based on probable linear combinations of modes. *Nuclear Engineering and Design*, 276:277–294, 2014.

[21] K. Tokoro and C. Menum. Application of the modal pushover procedure to estimate non-linear response envelopes. *Research Summary*, 4, 2003.

[22] E. A. Ferreira. Análise sísmica de estruturas porticadas: Determinação da interacção entre esforços. Master's thesis, Instituto Superior Técnico, 2009.

[23] A. F. Belejo. Análise sísmica de estruturas porticadas tridimensionais: Determinação da interacção entre esforços. Master's thesis, Instituto Superior Técnico, 2010.

[24] R. Clough and J. Penzien. *Dynamics of stuctures*. McGraw-Hill, 4^{th} edition, 1981. ISBN:0-07-011392-0.

[25] J. A. Freitas and C. Tiago. Análise elástica de estruturas reticuladas. Technical report, Instituto Superior Técnico, 2016.

[26] The Mathworks Inc. MATLAB R2015b, Massachusetts, United States of America.

[27] P. Mendes and J. Pedro. Estruturas de edifícios sob acções horizontais - Métodos simplificados de análise. Technical report, Instituto Superior Técnico, 2016.

[28] A. Costa. Estruturas de betão II - Folhas de apoio às aulas. Technical report, Instituto Superior Técnico, 2013/2014.

Appendix A

Matlab Files

A.1 Structure Definition

seccao3D_1px1py4pisos.m

```
%Definicao do Problema

%seccoes de pilares dimx dimy
%seccoes de vigas dimx=b e dimy=h
seccao(1)=struct('E',33*10^6,'dimx',0.3,'dimy',0.3); %em kPa e metros
seccao(2)=struct('E',33*10^6,'dimx',0.3,'dimy',0.6);
seccao(3)=struct('E',33*10^6,'dimx',0.3,'dimy',0.6);

for i=1:length(seccao)
    Sec(i).EI2 = seccao(i).E*seccao(i).dimx*seccao(i).dimy^3/12;
    Sec(i).EI3 = seccao(i).E*seccao(i).dimy*seccao(i).dimx^3/12;
    Sec(i).EA = seccao(i).E*seccao(i).dimx*seccao(i).dimy;
    a=max(seccao(i).dimx,seccao(i).dimy);
    b=min(seccao(i).dimx,seccao(i).dimy);
    kj= 1/3-0.21*(b/a)+0.0176*(b/a)^5;
    Sec(i).GJ = seccao(i).E/(2*(1+0.2))*kj*a*b^3;
end

%Nos: coordenadas, apoios, forcas nodais
%incid => graus de liberdade dos nos: 0 = grau de liber. livre;
%                                    -1 = grau de liber. restringido;
% [desl.x ; desl.y ;rot.z]
Nos(1)=struct('x',[5;0;0],'incid',[-1,-1,-1,-1,-1,-1], 'F',[0;0;0;0;0;0]);
Nos(2)=struct('x',[5;7;0],'incid',[-1,-1,-1,-1,-1,-1], 'F',[0;0;0;0;0;0]);
Nos(3)=struct('x',[0;7;0],'incid',[-1,-1,-1,-1,-1,-1], 'F',[0;0;0;0;0;0]);
Nos(4)=struct('x',[0;0;0],'incid',[-1,-1,-1,-1,-1,-1], 'F',[0;0;0;0;0;0]);
%(...)
```

```
%Barras: seccao, no inicial, no final
    %Pilares
Barras(1)=struct('Sec',1,'ni',1,'nf',5,'e2',[1;0;0]);
Barras(2)=struct('Sec',1,'ni',2,'nf',6,'e2',[1;0;0]);
Barras(3)=struct('Sec',1,'ni',3,'nf',7,'e2',[1;0;0]);
Barras(4)=struct('Sec',1,'ni',4,'nf',8,'e2',[1;0;0]);
%(...)
    %Vigas alinhadas com y
Barras(17)=struct('Sec',2,'ni',5,'nf',6,'e2',[1;0;0]);
Barras(18)=struct('Sec',2,'ni',8,'nf',7,'e2',[1;0;0]);
%(...)
   %Vigas alinhadas com x
Barras(25)=struct('Sec',3,'ni',5,'nf',8,'e2',[0;1;0]);
Barras(26)=struct('Sec',3,'ni',6,'nf',7,'e2',[0;1;0]);
%(...)

%Cargas de vao uniformes
%p:carga vertical -z; momento com o sinal da mao direita
alfa=0.4; rcp=6; psi2=0.3; sob=4;
p1=(25*0.4+rcp+psi2*sob)*(7*5)*(1-alfa)/7  +25*seccao(2).dimx*seccao(2).dimy;  %barra mais comprida
p2=(25*0.4+rcp+psi2*sob)*(7*5)*  alfa  /5  +25*seccao(2).dimx*seccao(2).dimy;
    %Vigas alinhadas com y
CargasU(1)=struct('barra',17,'p',p1,'m',0);
CargasU(2)=struct('barra',18,'p',p1,'m',0);
%(...)
    %Vigas alinhadas com x
CargasU(9)=struct('barra',25,'p',p2,'m',0);
CargasU(10)=struct('barra',26,'p',p2,'m',0);
%(...)

%Definicao do sismo
Sismo(1)=struct('tipo',1,'terreno',2,'zona',1.3,'gamaimp',1); %Lisboa
q=2.5;
%menu para separar o sismo em x do em y. escolher um numero entre 0 e 1.
factorx=1;
factory=1;
%Numero de modos pretendidos
modospretendidos=5;

%Barra generica
% Barras(1)=struct('Sec',2,'ni',1,'nf',2,'e2',[0;0;0]);
%    for ib=1
%        lo = Nos(Barras(ib).nf).x - Nos(Barras(ib).ni).x;
%        L = sqrt(sum(lo(:,1).^2));
%        for i=1:1:3
%            e1(i)=lo(i)/L;
%        end
%        Barras(ib).e2=cross([0;0;1],e1);
%    end
```

A.2 Main Program

estrutura3D.m

```
%Calculo de estruturas 3D elasticos
clear;
close all;

%Declaracao de variaveis
seccao =struct('E',0,'dimx',0,'dimy',0);
Sec = struct('EI',0,'EA',0);
Nos = struct('x', [ 0; 0; 0], 'incid', [0, 0, 0, 0, 0, 0], 'F', [0; 0; 0; 0; 0; 0]);
Barras = struct('Sec',0, 'ni', 0, 'nf', 0,'e2',[0;0;0]);
CargasU = struct('barra',0,'p',0,'m',0);
CargasC = struct('barra',0,'a','0','P',0,'M',0);
Sismo = struct('tipo',0,'terreno',0,'zona',0,'gamaimp',0);
modospretendidos=0;

%Dados do problema
seccao3D_1px1py4pisos;

%Iniciar variaveis de trabalho (work) das Barras
for ib=1:length(Barras)
    BarrasW(ib) = struct('L', 0,'Dn', zeros(12,1),'Ff', zeros(12,1), 'A', zeros(6,6), ...
    'K', zeros(12,12),'M',zeros(12,12), 'e1',zeros(3,1),'e2',zeros(3,1), 'e3',zeros(3,1));
end

%Atribuir deslocamentos aos nos
ndesl = 0;
for in = 1:length(Nos)
    for m = 1:6
        if (Nos(in).incid(m) < 0)
            Nos(in).incid(m) = 0;
        else
            ndesl = ndesl + 1;
            Nos(in).incid(m) = ndesl;
        end
    end
end
Estrutura=struct('Fne',zeros(ndesl,1),'Ff',zeros(ndesl,1),'K',zeros(ndesl,ndesl),'M',zeros(ndesl,ndesl));
vectordos1x=zeros(ndesl,1);
vectordos1y=zeros(ndesl,1);

% Calcular vector das forcas
for in = 1:length(Nos)
    inc = Nos(in).incid;   %graus de liberdade globais deste no
    incl = inc>0;          %identificacao logica daqueles que nao sao apoios
    incr = inc(incl);      %incidencia reduzida
```

```
    Estrutura.Fne(incr) = Nos(in).F(incl);
end

% Calcular Propriedades das Barras, Matriz de Rigidez e de Massas
for ib = 1:length(Barras)
    %incidencias
    inc = [Nos(Barras(ib).ni).incid, Nos(Barras(ib).nf).incid]; %graus de liberdade desta barra
    incl = inc>0; %identificacao logica
    incr = inc(incl); %incidencia reduzida

    %Comprimento da barra e
    %Matriz de transformacao entre os deslocamentos globais e os locais
    lo = Nos(Barras(ib).nf).x - Nos(Barras(ib).ni).x; %comprimento inicial (lo)
    BarrasW(ib).L = sqrt(sum(lo(:,1).^2));
    for i=1:1:3
        BarrasW(ib).e1(i)=lo(i)/BarrasW(ib).L;      %vector paralelo a barra
    end
    BarrasW(ib).e2=Barras(ib).e2;
    BarrasW(ib).e3=cross(BarrasW(ib).e1,BarrasW(ib).e2);

    A=[BarrasW(ib).e1(1),BarrasW(ib).e1(2),BarrasW(ib).e1(3);
       BarrasW(ib).e2(1),BarrasW(ib).e2(2),BarrasW(ib).e2(3);
       BarrasW(ib).e3(1),BarrasW(ib).e3(2),BarrasW(ib).e3(3)];
    BarrasW(ib).A=[A,zeros(3);zeros(3),A];
    BarrasW(ib).vet1 = [BarrasW(ib).A' * incl(1:6)';BarrasW(ib).A' * incl(7:12)'];
    vet2 = [0;0;0;0;0;0;0;0;0;0;0;0];
    vet3 = [0;0;0;0;0;0;0;0;0;0;0;0];
    for i=[1,7]
        if BarrasW(ib).vet1(i)~=0
           vet2(i)=1;
        end
    end
    BarrasW(ib).vet2=vet2;
    vectordos1x(incr) = vet2(incl); %sismo segundo x
    for i=[2,8]
        if BarrasW(ib).vet1(i)~=0
           vet3(i)=1;
        end
    end
    BarrasW(ib).vet3=vet3;
    vectordos1y(incr) = vet3(incl); %sismo segundo y

    %%%%%%%%%%%%%%%%%%%%%%% RIGIDEZ %%%%%%%%%%%%%%%%%%%%%%%

    %matriz de rigidez local
    kEAL=Sec(Barras(ib).Sec).EA/BarrasW(ib).L;
    kGJL=Sec(Barras(ib).Sec).GJ/BarrasW(ib).L;

    kEI2L=Sec(Barras(ib).Sec).EI2/BarrasW(ib).L;
```

```
kEI2L2=Sec(Barras(ib).Sec).EI2/BarrasW(ib).L^2;
kEI2L3=Sec(Barras(ib).Sec).EI2/BarrasW(ib).L^3;

kEI3L=Sec(Barras(ib).Sec).EI3/BarrasW(ib).L;
kEI3L2=Sec(Barras(ib).Sec).EI3/BarrasW(ib).L^2;
kEI3L3=Sec(Barras(ib).Sec).EI3/BarrasW(ib).L^3;

kii=[ kEAL,           0,          0,    0,         0,       0;
         0,   12*kEI3L3,          0,    0,         0,6*kEI3L2;
         0,           0,  12*kEI2L3,   0,-6*kEI2L2,       0;
         0,           0,           0,kGJL,         0,       0;
         0,           0,  -6*kEI2L2,   0,  4*kEI2L,       0;
         0,    6*kEI3L2,           0,   0,         0, 4*kEI3L];

kif=[-kEAL,           0,          0,    0,         0,       0;
         0,  -12*kEI3L3,          0,    0,         0,6*kEI3L2;
         0,           0, -12*kEI2L3,   0,-6*kEI2L2,       0;
         0,           0,           0,-kGJL,        0,       0;
         0,           0,   6*kEI2L2,   0,  2*kEI2L,       0;
         0,   -6*kEI3L2,           0,   0,         0, 2*kEI3L];


kff=[ kEAL,           0,          0,    0,         0,       0;
         0,   12*kEI3L3,          0,    0,         0,-6*kEI3L2;
         0,           0,  12*kEI2L3,   0,6*kEI2L2,         0;
         0,           0,           0,kGJL,         0,       0;
         0,           0,   6*kEI2L2,   0,  4*kEI2L,       0;
         0,   -6*kEI3L2,           0,   0,         0,  4*kEI3L];

BarrasW(ib).K=[kii, kif; kif', kff];
%matriz de rigidez da barra nos deslocamentos globais
A=BarrasW(ib).A;
kb=[ A'*kii*A, A'*kif*A;
    A'*kif'*A, A'*kff*A ];
Estrutura.K(incr,incr) = Estrutura.K(incr,incr) + kb(incl,incl);

%%%%%%%%%%%%%%%%%%%%%%% MASSA %%%%%%%%%%%%%%%%%%%%%%%

for ic=1:length(CargasU)
    massa=BarrasW(CargasU(ic).barra).L*CargasU(ic).p/420/9.8;
    L=BarrasW(ib).L;
    if ib==CargasU(ic).barra
        %matriz de massa local
        mii=massa*[ 140,   0,    0, 0,    0,    0;
                      0, 156,    0, 0,    0, 22*L;
                      0,   0,  156, 0,-22*L,    0;
                      0,   0,    0, 0,    0,    0;
                      0,   0,-22*L, 0,4*L^2,    0;
                      0,22*L,    0, 0,    0,4*L^2];
```

```
            mfi=massa*[  70,    0,    0, 0,     0,    0;
                         0,   54,    0, 0,     0, 13*L;
                         0,    0,   54, 0, -13*L,    0;
                         0,    0,    0, 0,     0,    0;
                         0,    0, 13*L, 0,-3*L^2,    0;
                         0,-13*L,    0, 0,     0,-3*L^2];

            mff=massa*[ 140,    0,    0, 0,    0,     0;
                         0,  156,    0, 0,    0, -22*L;
                         0,    0,  156, 0, 22*L,     0;
                         0,    0,    0, 0,    0,     0;
                         0,    0, 22*L, 0,4*L^2,     0;
                         0,-22*L,    0, 0,    0, 4*L^2];
            BarrasW(ib).M=[mii, mfi'; mfi, mff];
            %matriz de massa da barra nos deslocamentos globais
            A=BarrasW(ib).A;
            mb=[ A'*mii*A, A'*mfi'*A;
                 A'*mfi*A, A'*mff*A ];
            Estrutura.M(incr,incr) = Estrutura.M(incr,incr) + mb(incl,incl);
        end
    end
end

%%%%%%%%%%%%%%%%%%%%%%%%%%%%% ESTATICA %%%%%%%%%%%%%%%%%%%%%%%%%%%%%%%%%%%%

for ib = 1:length(Barras)
    Lb=BarrasW(ib).L;
    for ic = 1:length(CargasU)
        if ib==CargasU(ic).barra
            Ffix=[ 0; 0; -CargasU(ic).p*Lb/2; 0; +CargasU(ic).p*Lb^2/12+CargasU(ic).m*Lb/2; 0;
                   0; 0; -CargasU(ic).p*Lb/2; 0; -CargasU(ic).p*Lb^2/12+CargasU(ic).m*Lb/2; 0];
            BarrasW(ib).Ff=BarrasW(ib).Ff+Ffix;
        end
    end
    %incidencias
    inc = [Nos(Barras(ib).ni).incid, Nos(Barras(ib).nf).incid];
    incl = inc>0;         %identificacao logica daqueles que nao sao apoios
    incr = inc(incl);     %incidencia reduzida
    Ffixglob=[BarrasW(ib).A'*BarrasW(ib).Ff(1:6);BarrasW(ib).A'*BarrasW(ib).Ff(7:12)];
    Estrutura.Ff(incr) = Estrutura.Ff(incr) + Ffixglob(incl);
end

%Deslocamentos Nodais
desl = Estrutura.K\(Estrutura.Fne - Estrutura.Ff);

for ib = 1:length(Barras)
    %incidencias
    inc = [Nos(Barras(ib).ni).incid, Nos(Barras(ib).nf).incid]; %graus de liberdade desta barra
```

```
    incl = inc>0; %identificacao logica
    incr = inc(incl); %incidencia reduzida

    %Forcas Nodais de extremidade nas barras
    deslb=zeros(12,1);
    deslb(incl)=desl(incr);
    BarrasW(ib).Dn=[BarrasW(ib).A*deslb(1:6);BarrasW(ib).A*deslb(7:12)];
    BarrasW(ib).esfb=BarrasW(ib).K*BarrasW(ib).Dn + BarrasW(ib).Ff;
end


%%%%%%%%%%%%%%%%%%%%%%% SISMO %%%%%%%%%%%%%%%%%%%%%%%

agr=[1.1,1.2,1.3,1.4,1.5,1.6 ,2.1,2.2,2.3,2.4,2.5;
     2.5,2.0,1.5,1.0,0.6,0.35,2.5,2.0,1.7,1.1,0.8];

 % 'A',   'B',  'C',  'D',  'E';
 terreno=[   1,   2,  3,  4,  5;
     1.0,1.35,1.6,2.0,1.8;
     0.1, 0.1,0.1,0.1,0.1;
     0.6, 0.6,0.6,0.8,0.6;
     2.0, 2.0,2.0,2.0,2.0];
Sismo.terenumb=2;

for iagr=1:length(agr(1,:))
    if Sismo.zona==agr(1,iagr)
        Sismo.agr=agr(2,iagr); %m/s^2
    end
end

Sismo.ag=Sismo.agr*Sismo.gamaimp; %m/s^2

for iter=1:length(terreno(1,:))
    if Sismo.terenumb==terreno(1,iter)
        Sismo.smax=terreno(2,iter); %m/s^2
        Sismo.TB=terreno(3,iter); %seg
        Sismo.TC=terreno(4,iter); %seg
        Sismo.TD=terreno(5,iter); %seg
    end
end

if Sismo.ag <=1
    Sismo.S=Sismo.smax;
else
    if Sismo.ag <=4
        Sismo.S=Sismo.smax-(Sismo.smax-1)*(Sismo.ag-1)/3;
    else
        Sismo.S=1;
    end
```

```
end

ndeslmod=floor(ndesl/2);
%matriz de vectores pp em coluna, matriz diagonal de valores pp
[Estrutura.Vect,Estrutura.Val] = eigs(Estrutura.K,Estrutura.M,ndeslmod,'sa');
%coluna de valores pp
Estrutura.valores2 =eigs(Estrutura.K,Estrutura.M,ndeslmod,'sa');
Estrutura.valores= sqrt(Estrutura.valores2);              %p [rad/s]
Estrutura.freq = Estrutura.valores/2/pi;                  %f [Hz]
for ifr=1:ndeslmod
    Estrutura.periodo(ifr) = 1/ Estrutura.freq(ifr);      %T [s]
end
for i=1:ndeslmod
    if Estrutura.periodo(i)<Sismo.TB
        Estrutura.Sd(i)=Sismo.ag*Sismo.S+(2/3+Estrutura.periodo(i)*(2.5/q-2/3)/Sismo.TB);
    else if Estrutura.periodo(i)<Sismo.TC
            Estrutura.Sd(i)=Sismo.ag*Sismo.S*2.5/q;
        else if Estrutura.periodo(i)<Sismo.TD
                Estrutura.Sd(i)=Sismo.ag*Sismo.S*2.5/q*Sismo.TC/Estrutura.periodo(i);
            else
                Estrutura.Sd(i)=Sismo.ag*Sismo.S*2.5/q*Sismo.TC*Sismo.TD/Estrutura.periodo(i)^2;
            end
        end
    end
end

%Vectores Normalizados
for i=1:ndeslmod
    a=Estrutura.Vect(:,i)'*Estrutura.M*Estrutura.Vect(:,i);
    Estrutura.fi(:,i)=Estrutura.Vect(:,i)/sqrt(a);
end

%Factor de participacao modal
Estrutura.Px=Estrutura.fi'*Estrutura.M*vectordos1x;
Estrutura.Py=Estrutura.fi'*Estrutura.M*vectordos1y;
Estrutura.Meffx=Estrutura.Px.^2;
Estrutura.Meffy=Estrutura.Py.^2;
Meffcumx=cumsum(Estrutura.Meffx);
Meffcumy=cumsum(Estrutura.Meffy);
modosrelevantesx=1;
modosrelevantesy=1;
for i=1:ndeslmod
    if Meffcumx(i)<0.9*sum(Estrutura.Meffx)
        modosrelevantesx=modosrelevantesx+1;
    end
end
for i=1:ndeslmod
    if Meffcumy(i)<0.9*sum(Estrutura.Meffy)
        modosrelevantesy=modosrelevantesy+1;
```

```
    end
end
% modosrelevantes = num de modos que acumulam 90% da massa effectiva
nmodos=max(modosrelevantesx,modosrelevantesy);
nmodos=max(nmodos,modospretendidos);

%Deslocamentos
for imodo=1:nmodos
    Estrutura.qx(:,imodo)=Estrutura.fi(:,imodo)*Estrutura.Px(imodo)*Estrutura.Sd(imodo)...
                          *factorx/Estrutura.valores2(imodo);
    Estrutura.qy(:,imodo)=Estrutura.fi(:,imodo)*Estrutura.Py(imodo)*Estrutura.Sd(imodo)...
                          *factory/Estrutura.valores2(imodo);
end

for ib=1:length(Barras)
    %incidencias
    inc = [Nos(Barras(ib).ni).incid, Nos(Barras(ib).nf).incid]; %graus de liberdade desta barra
    incl = inc>0; %identificacao logica
    incr = inc(incl); %incidencia reduzida

    deslbx=zeros(12,imodo);
    deslby=zeros(12,imodo);
    deslFi=zeros(12,imodo);
    for imodo=1:nmodos
        %Deslocamentos Nodais de extremidade nas barras
        deslbx(incl,imodo)=Estrutura.qx(incr,imodo);
        deslby(incl,imodo)=Estrutura.qy(incr,imodo);
        deslFi(incl,imodo)= Estrutura.fi(incr,imodo);

        BarrasW(ib).Dsismox(:,imodo)=[BarrasW(ib).A*deslbx(1:6,imodo);BarrasW(ib).A*deslbx(7:12,imodo)];
        BarrasW(ib).esfsismox(:,imodo)=BarrasW(ib).K*BarrasW(ib).Dsismox(:,imodo);
        BarrasW(ib).Dsismoy(:,imodo)=[BarrasW(ib).A*deslby(1:6,imodo);BarrasW(ib).A*deslby(7:12,imodo)];
        BarrasW(ib).esfsismoy(:,imodo)=BarrasW(ib).K*BarrasW(ib).Dsismoy(:,imodo);
    end
end

%%%%%%%%%%%%%%%%%%%%%%%%%% COMBINAcaO %%%%%%%%%%%%%%%%%%%%%%%%%%%%%%%%
%Analise da seccao: base de um pilar -> barra 1 e no com x=0
%Inicializacao de variaveis
ib=1;
x=0;
%Estatica
est_M2=-BarrasW(ib).esfb(5)-BarrasW(ib).esfb(3)*x;
est_M3=-BarrasW(ib).esfb(6)+BarrasW(ib).esfb(2)*x;
est_N=-BarrasW(ib).esfb(1)+0*x;
for ic = 1:length(CargasU)
    if ib==CargasU(ic).barra
        est_M2 =est_M2-CargasU(ic).p*x.^2/2 + CargasU(ic).m*x ;
        est_N=est_N+0;
```

```
    end
end

for isismo=1:2   %Direcao do Sismo 1 = x; Direccao do sismo 2 = y
    DirSis(isismo)=struct('N_2tot',0,'M2_2tot',0,'M3_2tot',0,...
                          'NM2tot',0,'NM3tot', 0,'M2M3tot',0);
end
for i=1:nmodos
    Combx(i)=struct('matriz',zeros(3,3),'matriz_a',zeros(3,3),'V',zeros(3,3),'D',zeros(3,3),...
              'xi',zeros(1,imodo),'yi',zeros(1,imodo),'zi',zeros(1,imodo));
    Comby(i)=struct('matriz',zeros(3,3),'matriz_a',zeros(3,3),'V',zeros(3,3),'D',zeros(3,3),...
              'xi',zeros(1,imodo),'yi',zeros(1,imodo),'zi',zeros(1,imodo));
end
desenhox=zeros(2);
desenhoy=zeros(2);
desenhoz=zeros(2);

%%%%%%%%%%%%%%%%%% Pares (M-N) para cada modo $$$$$$$$$$$$$$$$$$$$
for imodo=1:nmodos
    DirSis(1).N(imodo)=(-BarrasW(ib).esfsismox(1,imodo));
    DirSis(1).M2(imodo)=(-BarrasW(ib).esfsismox(5,imodo)-BarrasW(ib).esfsismox(3,imodo)*x);
    DirSis(1).NM2(imodo)=-BarrasW(ib).esfsismox(1,imodo)*(-BarrasW(ib).esfsismox(5,imodo)-...
                          BarrasW(ib).esfsismox(3,imodo)*x);
    DirSis(1).M3(imodo)=(-BarrasW(ib).esfsismox(6,imodo)+BarrasW(ib).esfsismox(2,imodo)*x);
    DirSis(1).NM3(imodo)=-BarrasW(ib).esfsismox(1,imodo)*(-BarrasW(ib).esfsismox(6,imodo)+...
                          BarrasW(ib).esfsismox(2,imodo)*x);
    DirSis(1).M2M3(imodo)=(-BarrasW(ib).esfsismox(5,imodo)-BarrasW(ib).esfsismox(3,imodo)*x)*...
                         (-BarrasW(ib).esfsismox(6,imodo)+BarrasW(ib).esfsismox(2,imodo)*x);

    DirSis(2).N(imodo)=(-BarrasW(ib).esfsismoy(1,imodo));
    %(...)
end

for imodo=1:nmodos
    Combx(imodo).matriz=[DirSis(1).M2(imodo)^2,DirSis(1).M2M3(imodo),DirSis(1).NM2(imodo);
                         DirSis(1).M2M3(imodo),DirSis(1).M3(imodo)^2,DirSis(1).NM3(imodo);
                         DirSis(1).NM2(imodo),DirSis(1).NM3(imodo),DirSis(1).N(imodo)^2];
    [Combx(imodo).V,Combx(imodo).D]=eigs(Combx(imodo).matriz,3);

    e=[Combx(imodo).V(1,3);Combx(imodo).V(2,3);Combx(imodo).V(3,3)];
    Combx(imodo).xi=e(1)*sqrt(Combx(imodo).D(3,3));
    Combx(imodo).yi=e(2)*sqrt(Combx(imodo).D(3,3));
    Combx(imodo).zi=e(3)*sqrt(Combx(imodo).D(3,3));

    desenhox=[-Combx(imodo).xi;Combx(imodo).xi];
    desenhoy=[-Combx(imodo).yi;Combx(imodo).yi];
    desenhoz=[-Combx(imodo).zi;Combx(imodo).zi];

    plot3(desenhox(:),desenhoy(:),desenhoz(:),'DisplayName',cat(2,'Modo ',num2str(imodo)));hold on;
```

```
end

for imodo=1:nmodos
    Comby(imodo).matriz=[DirSis(2).M2(imodo)^2,DirSis(2).M2M3(imodo),DirSis(2).NM2(imodo);
                         DirSis(2).M2M3(imodo),DirSis(2).M3(imodo)^2,DirSis(2).NM3(imodo);
                          DirSis(2).NM2(imodo),DirSis(2).NM3(imodo),DirSis(2).N(imodo)^2];
    %(...)
end

%%%%%%%%%%%%%%%%%%%%%%% Elipsoide 3D %%%%%%%%%%%%%%%%%%%%%%%%%%%%%

for isismo=1:2

     for imodo=1:nmodos
        for jmodo=1:nmodos
            Pj=Estrutura.valores(jmodo);     %p [rad/s] nao depende so sismo
            Pi=Estrutura.valores(imodo);
            r=Pj/Pi;
            zeta=0.05;
            miu(imodo,jmodo)=(8*zeta^2*(1+r)*r^(3/2))/((1-r^2)^2+4*zeta^2*r*(1+r)^2);

            DirSis(isismo).N_2tot=DirSis(isismo).N_2tot + ...
                                  DirSis(isismo).N(imodo)*DirSis(isismo).N(jmodo)*miu(imodo,jmodo);
            DirSis(isismo).M2_2tot=DirSis(isismo).M2_2tot + ...
                                  DirSis(isismo).M2(imodo)*DirSis(isismo).M2(jmodo)*miu(imodo,jmodo);
            %(...)
        end
    end

    DirSis(isismo).matriz=[DirSis(isismo).M2_2tot,DirSis(isismo).M2M3tot,DirSis(isismo).NM2tot;
                           DirSis(isismo).M2M3tot,DirSis(isismo).M3_2tot,DirSis(isismo).NM3tot;
                           DirSis(isismo).NM2tot,DirSis(isismo).NM3tot,DirSis(isismo).N_2tot];
    [DirSis(isismo).Vtot,DirSis(isismo).Dtot]=eigs(DirSis(isismo).matriz,3);

    e1=[DirSis(isismo).Vtot(1,1),DirSis(isismo).Vtot(2,1),DirSis(isismo).Vtot(3,1)];
    e2=[DirSis(isismo).Vtot(1,2),DirSis(isismo).Vtot(2,2),DirSis(isismo).Vtot(3,2)];
    e3=[DirSis(isismo).Vtot(1,3),DirSis(isismo).Vtot(2,3),DirSis(isismo).Vtot(3,3)];

    n=1;
    for i=1:3
        if abs( DirSis(isismo).Dtot(i,i))< 1e-10
         DirSis(isismo).Dtot(i,i)=0;
        end
    end
    a=sqrt(DirSis(isismo).Dtot(1,1));
    b=sqrt(DirSis(isismo).Dtot(2,2));
    c=sqrt(DirSis(isismo).Dtot(3,3));

    for u=-pi/2:0.005:pi/2
```

```
        for v=0:0.005:2*pi
            x(n)= a*cos(u)*cos(v);
            y(n)= b*cos(u)*sin(v);
            z(n)= c*sin(u);
            n=n+1;
        end
    end

    for i=1:3
        DirSis(isismo).xrodado(i,:)=x(:)*e1(i)+ y(:)*e2(i)+z(:)*e3(i);
    end
       plot3(DirSis(isismo).xrodado(1,:),DirSis(isismo).xrodado(2,:),DirSis(isismo).xrodado(3,:)); hold on;
end

SisFinal=struct('N_2tot',0,'M2_2tot',0,'M3_2tot',0,'NM2tot',0,'NM3tot',0,'M2M3tot',0,'matriz',zeros(3,3),...
          'Vtot',zeros(3,3),'Dtot',zeros(3,3));
for isismo=1:2
    SisFinal.N_2tot=SisFinal.N_2tot +DirSis(isismo).N_2tot;
    SisFinal.M2_2tot=SisFinal.M2_2tot+DirSis(isismo).M2_2tot;
    SisFinal.M3_2tot=SisFinal.M3_2tot+DirSis(isismo).M3_2tot;
    SisFinal.NM2tot=SisFinal.NM2tot+DirSis(isismo).NM2tot;
    SisFinal.NM3tot=SisFinal.NM3tot+DirSis(isismo).NM3tot;
    SisFinal.M2M3tot=SisFinal.M2M3tot+DirSis(isismo).M2M3tot;


end
SisFinal.matriz=[SisFinal.M2_2tot,SisFinal.M2M3tot,SisFinal.NM2tot;
                 SisFinal.M2M3tot,SisFinal.M3_2tot,SisFinal.NM3tot;
                  SisFinal.NM2tot,SisFinal.NM3tot,SisFinal.N_2tot];
[SisFinal.Vtot,SisFinal.Dtot]=eigs(SisFinal.matriz,3);
%(...)

%%%%%%%%%%%%%%%%%%%%%%%% Projeccao do elipsoide %%%%%%%%%%%%%%%%%%%%%%%%%%%%%

for i=1:3
    ProjecaoX(i)=struct('matriz',zeros(2,2),'inversa',zeros(2,2));
    ProjecaoY(i)=struct('matriz',zeros(2,2),'inversa',zeros(2,2));
    ProjecaoT(i)=struct('matriz',zeros(2,2),'inversa',zeros(2,2));
end
ProjecaoX(3).matriz=[DirSis(1).M2_2tot,DirSis(1).M2M3tot;
                     DirSis(1).M2M3tot,DirSis(1).M3_2tot];
ProjecaoX(1).matriz=[DirSis(1).M3_2tot,DirSis(1).NM3tot;
                      DirSis(1).NM3tot,DirSis(1).N_2tot];
ProjecaoX(2).matriz=[DirSis(1).M2_2tot,DirSis(1).NM2tot;
                      DirSis(1).NM2tot,DirSis(1).N_2tot];
%(...)

for i=1:3
    ProjecaoX(i).inversa=inv(ProjecaoX(i).matriz);
```

```
    ax=ProjecaoX(i).inversa(1,1);
    bx=ProjecaoX(i).inversa(1,2);
    cx=ProjecaoX(i).inversa(2,2);
    %(...)
    ndivisoes=350000;
    for iteta=1:1:ndivisoes
    vetorteta(iteta)=(iteta-1)*pi/(ndivisoes-1);
    teta=vetorteta(iteta);
    r1X(iteta)=sqrt(1/(ax*cos(teta)^2+2*bx*sin(teta)*cos(teta) +cx*sin(teta)^2));
    r2X(iteta)=-sqrt(1/(ax*cos(teta)^2+2*bx*sin(teta)*cos(teta) +cx*sin(teta)^2));
    %(...)
    end

    [x1sismoX,y1sismoX] = pol2cart(vetorteta,r1X);
    [x2sismoX,y2sismoX] = pol2cart(vetorteta,r2X);
    xsismoX=cat(2,x1sismoX,x2sismoX);
    ysismoX=cat(2,y1sismoX,y2sismoX);
    %(...)
    plot(xsismoX,ysismoX,'Color',[0.0 0.447 0.741],'DisplayName','Earthquake X');hold on;
end

%%%%%%%%%%%%%%%%%%%%%%%% FATIAS DE ELIPSoIDE %%%%%%%%%%%%%%%%%%%%%%%%%

deltaN1=est_N-deltaN;
deltaN2=est_N+deltaN;
Nmaxfatia=floor(deltaN2/100)*100;
Nminfatia=ceil(deltaN1/100)*100;
nfatias=(Nmaxfatia-Nminfatia)/100+1;
passo=100;

InvFinal=pinv(SisFinal.matriz,e-12);

CMM=[InvFinal(1,1),InvFinal(1,2);
     InvFinal(2,1),InvFinal(2,2)];
CMN=[InvFinal(1,3);InvFinal(2,3)];
CNN=InvFinal(3,3);

for ifatia=1:nfatias
    Nfatia=Nmaxfatia-passo*(ifatia-1);      %N do elipsoide no centro certo - parte estatica
    Nelipse=+Nfatia-est_N;               %N do elipsoide na origem

    Rb2=1-Nelipse*CNN*Nelipse;

    M0=-inv(CMM)*CMN*Nelipse ;
    R02=1+M0'*CMM*M0-Nelipse*CNN*Nelipse;
    CMM_R02=CMM/R02;

    m0(ifatia,1)=M0(1);
    m0(ifatia,2)=M0(2);
```

```
    af=CMM_R02(1,1); %f = fatia
    bf=CMM_R02(1,2);
    cf=CMM_R02(2,2);
    clearvars vetorteta;
    ndivisoes=15000;
    for iteta=1:1:ndivisoes
        vetorteta(iteta)=(iteta-1)*pi/(ndivisoes-1);
        teta=vetorteta(iteta);
        r1f(iteta)=sqrt(1/(af*cos(teta)^2+2*bf*sin(teta)*cos(teta) +cf*sin(teta)^2));
        r2f(iteta)=-sqrt(1/(af*cos(teta)^2+2*bf*sin(teta)*cos(teta) +cf*sin(teta)^2));
        N(iteta)=Nfatia;
    end

    [x1f(ifatia,:),y1f(ifatia,:)] = pol2cart(vetorteta,r1f);
    [x2f(ifatia,:),y2f(ifatia,:)] = pol2cart(vetorteta,r2f);
    plot3(x1f(ifatia,:)+M0(1)+est_M2  ,y1f(ifatia,:)+M0(2)+est_M3, N,...
          x2f(ifatia,:)+M0(1)+est_M2  ,y2f(ifatia,:)+M0(2)+est_M3, N);hold on;

end

%%%%%%%%%%%%%%%%%%%%%%%% CURVAS DE INTERACCaO %%%%%%%%%%%%%%%%%%%%%%%%%

h=seccao(Barras(ib).Sec).dimy; %0.3
b=seccao(Barras(ib).Sec).dimx; %0.3
rec=0.05; %ao centro do varao

%A500
eud=0.01; %Classe de ductilidade C (alta) eud=0.9*0.075
eyd=2.1753e-3;
fyd=435e+3; %kN/m2
Es=200e+6; %kN/m2
%C30/37
ecu2=-0.0035;
ec2=-0.002;
fcd=20e+3; %kN/m2

%Discretizacao do Betao
divy=10; %numero de divisoes em y e z
divz=10;
ndiv_betao=divy*divy;
hdiv=h/divz;   %altura da divisao
bdiv=b/divz;   %largura da divisao
Adiv=hdiv*bdiv;

ybetao=zeros(ndiv_betao,1);
zbetao=zeros(ndiv_betao,1);
%Centro do Referencial e o Centro de Gravidade!
nlinha=1;
```

```
for i=1:1:ndiv_betao
    ncoluna=i-(divy*(nlinha-1));

    ybetao(i)= ncoluna*bdiv -b/2 -bdiv/2;
    zbetao(i)= nlinha*hdiv  -h/2 -hdiv/2;
    if ncoluna==divy
        nlinha=nlinha+1;
    end
end
w=0.6;
verifica=1;
%%Discretizacao do Aco
while verifica ~=0
    wtot=w;
    ndiv_aco=16;
    As=h*b*wtot*fcd/fyd/ndiv_aco;
    nespacos=ndiv_aco/4;
    disty=(b-2*rec)/nespacos;
    distz=(h-2*rec)/nespacos;

    yaco=zeros(ndiv_aco,1);
    zaco=zeros(ndiv_aco,1);
    for i=1:1:ndiv_aco

        if i<(ndiv_aco/4)+2
            yaco(i)= b/2 -rec -(i-1)*disty;
            zaco(i)= h/2-rec;
        else if i<(ndiv_aco/2)+2
                yaco(i)= -b/2 + rec;
                zaco(i)= h/2 -rec -(i-5)*distz;
            else if i<(3*ndiv_aco/4)+2
                    yaco(i)= -b/2 +rec +(i-9)*disty;
                    zaco(i)= -h/2+rec;
                else
                    yaco(i)= b/2 - rec;
                    zaco(i)= -h/2 +rec +(i-13)*distz;
                end
            end
        end
    end
    n=0;
    eg=0;
    delta_eg=1;
    for iN=1:1:nfatias
        Npretendido=Nmaxfatia-passo*(iN-1);
        for iteta=1:1:19
            teta=(iteta-1)*5*pi/180;
            erro=100;
            n=0;
```

```
while abs(erro)>1
    for i=1:1:ndiv_betao
        hbetao(i)=-zbetao(i)*cos(teta)+ ybetao(i)*sin(teta);
        curvbetao(i)=(ecu2-eg)/hbetao(i);
        if curvbetao(i)<=0
            curvbetao(i)=100;
        end
    end
    curvbetao_max=min(curvbetao(:));
    for i=1:1:ndiv_aco
        haco(i)=-zaco(i)*cos(teta)+ yaco(i)*sin(teta);
        curvaco(i)=(eud-eg)/haco(i);
        if curvaco(i)<=0
            curvaco(i)=100;
        end
    end
    curvaco_max=min(curvaco(:));
    cur_max=min(curvaco_max,curvbetao_max);
    Ncalc=0;
    Mycalc=0;
    Mzcalc=0;
    EA=0;
    for i=1:1:ndiv_aco
        eaco(i)=eg+cur_max*haco(i);
        if eaco(i)==0
            sinal(i)=1;
        else
            sinal(i)=eaco(i)/abs(eaco(i));
        end
        F_aco(i)= min(abs(eaco(i)*Es),fyd) * As * sinal(i);

        Ncalc=Ncalc +F_aco(i);
        Mycalc=Mycalc + F_aco(i)*zaco(i);
        Mzcalc=Mzcalc + F_aco(i)*(-yaco(i));

        if min(abs(eaco(i)*Es),fyd)==fyd
            Eaco(i)=0.1*Es;
        else Eaco(i)=Es;
        end
        EA=EA+Eaco(i)*As;
    end
    for i=1:1:ndiv_betao
        ebetao(i)=eg+cur_max*hbetao(i);
        if ebetao(i)>-ec2
            F_betao(i)=0;
            Ebetao(i)=0;
        else if ebetao(i)>0
                F_betao(i)=0;
                Ebetao(i)=2*fcd*(-ec2)/ec2^2;
```

```
                    else if ebetao(i)>ec2
                            F_betao(i)=-fcd*(1-(1-ebetao(i)/ec2)^2)*Adiv;
                            Ebetao(i)=2*fcd*(-ec2+ebetao(i))/ec2^2;
                        else
                            F_betao(i)=-fcd*Adiv;
                            Ebetao(i)=0;
                        end
                    end
                end
                Ncalc=Ncalc+F_betao(i);
                Mycalc=Mycalc+F_betao(i)*zbetao(i);
                Mzcalc=Mzcalc+F_betao(i)*(-ybetao(i));
                EA=EA+Ebetao(i)*Adiv;
            end
            erro=Ncalc-Npretendido;
            delta_eg = -erro/EA;
            eg=eg+delta_eg;
            n=n+1;
        end
        Ncurva(iN,iteta)=Npretendido;
        My(iN,iteta)=Mycalc;
        Mz(iN,iteta)=Mzcalc;
    end
end

%%%%%%%%%%%%%%%%%%%%%% verificacao de w %%%%%%%%%%%%%%%%%%%%%%%%%%%%%%
%Descrever a accao e a resistencia em vectores (teta, raio)

for iN=1:1:nfatias
    Npretendido=Nmaxfatia-passo*(iN-1);
    curvintMy(iN,:)= cat(2,My(iN,:),-1*fliplr(My(iN,:)),-My(iN,:),fliplr(My(iN,:)));
    curvintMz(iN,:)= cat(2,Mz(iN,:),fliplr(Mz(iN,:)),-Mz(iN,:),-1*fliplr(Mz(iN,:)));
    curvintN(iN,:)= cat(2,Ncurva(iN,:),Ncurva(iN,:),Ncurva(iN,:),Ncurva(iN,:));
    [curvintteta(iN,:),curvintraio(iN,:)] = cart2pol(curvintMy(iN,:),curvintMz(iN,:));

    accaoMy(iN,:)= cat(2,x1f(iN,:)+m0(iN,1)+est_M2,x2f(iN,:)+m0(iN,1)+est_M2);
    accaoMz(iN,:)= cat(2,y1f(iN,:)+m0(iN,2)+est_M3,y2f(iN,:)+m0(iN,2)+est_M3);
    [accaoteta(iN,:),accaoraio(iN,:)] = cart2pol(accaoMy(iN,:),accaoMz(iN,:));
end

numteta1=length(curvintteta(1,:));
numteta2=length(accaoteta(1,:));
deltateta=2.5*pi/180;
verifica=0;
for iN=1:1:nfatias
    if verifica==1
        break
    else
        Npretendido=Nmaxfatia-passo*(iN-1);
```

```
            for iteta1=1:numteta1
                if verifica==1
                    break
                else
                    teta=(iteta1-1)*5*pi/180;
                    teta1=teta-deltateta;
                    teta2=teta+deltateta;
                    n=1;
                    for iteta2=1:numteta2
                        if accaoteta(iN,iteta2)>teta1 || accaoteta(iN,iteta2)<teta2
                            accaoraioteste(iN,n)=accaoraio(iN,iteta2);
                            n=n+1;
                        end
                    end
                    if n==1  %Se n=1 nao existem pontos da accao nessa divisao
                    else
                        for iteste=1:(n-1)
                            if accaoraioteste(iN,iteste)<curvintraio(iN,iteta1)
                                verifica=verifica+0;
                            else
                                verifica=verifica+1;
                                break
                            end
                        end
                    end
                end
            end
        end
    end
    w=w+0.05
end
```